Phenomenological Studies on Nonequilibrium Dynamics of Interfaces and Polymers

by

Mehmet Deniz Ertaş

Submitted to the Department of Physics
in partial fulfillment of the requirements for the degree of

Doctor of Philosophy

at the

MASSACHUSETTS INSTITUTE OF TECHNOLOGY

June 1995

Author .....
Department of Physics
May 18, 1995

Certified by .....
Mehran Kardar
Professor of Physics
Thesis Supervisor

Accepted by .....
George F. Koster
Chairman, Departmental Graduate Committee

to my wonderful family

Phenomenological Studies on Nonequilibrium Dynamics of Interfaces and Polymers

by

Mehmet Deniz Ertaş

Submitted to the Department of Physics
on May 19, 1995, in partial fulfillment of the
requirements for the degree of
Doctor of Philosophy

Abstract

This thesis discusses several phenomenological evolution equations derived from general symmetry arguments, which are believed to model nonequilibrium processes in interface growth and polymer drift. Universality classes associated with kinetic roughening and the depinning transition are determined by dynamic renormalization group calculations and numerical simulations.

The first model describes nonequilibrium dynamic fluctuations of a polymer in a dilute solution, subject to a uniform external force. In most physically relevant cases, the fluctuations are superdiffusive, governed by a swelling exponent $\nu = 1/2$ and a dynamic exponent $z = 3$. The polymer exhibits "kinetic" form birefringence as it is stretched by the flow. The crossover to anisotropy occurs at a velocity inversely proportional to the squareroot of the polymer length. Numerical simulations show that strong crossover behavior may produce larger swelling exponents along the force direction at intermediate length scales, potentially giving rise to a stretching transition. Next, the effect of quenched disorder is explored through a model describing a Flux Line in a Type-II superconductor, driven by a bulk current $\vec{J}$ near the depinning threshold. In the absence of transverse fluctuations, the system reduces to recently studied models of interface depinning. In most cases, the presence of transverse fluctuations don't influence the critical exponents that describe longitudinal fluctuations. For a manifold with $d = 4 - \epsilon$ internal dimensions *in an isotropic medium*, longitudinal fluctuations are described by a roughness exponent $\zeta_{\|} = \epsilon/3$ to all orders in ϵ, and a dynamical exponent $z_{\|} = 2 - 2\epsilon/9 + O(\epsilon^2)$. Transverse fluctuations have a smaller roughness exponent $\zeta_{\perp} = \zeta_{\|} - d/2$ and relax more slowly, with a dynamical exponent $z_{\perp} = z_{\|} + 1/\nu$. [$\nu = 1/(2 - \zeta_{\|})$ is the correlation length exponent.] There is good agreement with numerical results. Anisotropy and a nonzero Hall angle lead to additional universality classes. Finally, the effect of nonlocal interactions on the depinning transition is studied in a contact line. The only important change is the reduction of the upper critical dimension from $d_c = 4$ for the elastic interface to $d_c = 2$, giving $\zeta = 1/3$. The dynamical exponent $z = 1 - 2\epsilon/9 + O(\epsilon^2) < 1$ suggests unusual dynamical properties.

Thesis Supervisor: Mehran Kardar
Title: Professor of Physics

Acknowledgments

First of all, I would like to thank Mehran Kardar for his invaluable guidance throughout my years in graduate school. He has been a constant inspiration to me, especially with regard to his unsurpassable teaching and research skills. I shall consider myself extremely lucky if I managed to gain a bit of his physical insight and intuition, and his talent to express questions and ideas in a crystal clear manner. With his admirable generosity, he has always been there for me and anybody else that needed his help, keeping his office door open at all times. Without his help and criticism, much of this work would not have been possible. I especially appreciate his utmost confidence in me, in both academical and other matters, which he amply demonstrated by letting me work at my own pace, putting me in charge of a $20K computer purchase (twice!), and most importantly, by letting me choose the wine during group dinners.

I would also like to thank Patrick Lee and Wolfgang Ketterle for agreeing to be in my thesis committee, and accepting a short review period.

I acknowledge the financial support of MIT (through a Teaching Assistantship), the NSF (through Grant Nos. DMR-93-03667, PYI/DMR-89-58061, and DMR-94-00334), and the MIT/INTEVEP collaborative program.

I would like to take this opportunity to thank all that have provided invaluable help, guidance and inspiration throughout my physics education. They are (in chronological order) İsmet Özkaya, Nevzat Önsöz, Ordal Demokan, Salim Çıracı, Atilla Erçelebi, Nihat Berker, and Yacov Kantor. Among others, I have benefited from discussions with Terence Hwa, Susan Coppersmith, Ernesto Medina, Onuttom Narayan, Jean–Philippe and Elizabeth Bouchaud, and Mark Robbins. Many thanks to Mark Sherwin, Mehran Kardar, Ayşe Erzan, Önder Pekcan, William Bialek and James Langer for organizing schools/workshops that helped shape my career path. Of course, many thanks to all former and current graduate students and postdocs in the Condensed Matter Theory corridor for valuable discussions and general fellowship, in particular to Alkan Kabakçıoğlu, Claudio Chamon, Alexis Falicov, Daniel Aalberts and Manfred Sigrist.

My years at MIT were brightened by the support and community spirit of the MIT Folk Dance Club. Besides fulfilling my need for physical exercise and making a fine dancer out of me, the club helped me meet many wonderful people, and most importantly, my wife.

I cannot overemphasize the support and influence of my family on every aspect of my life, including this thesis. In particular, my aunt İnci Eroğlu has always been very supportive as a loving family member and a mentor, especially in my formative years during college. My parents have been a constant source of love, affection and encouragement throughout my life. And finally, I do not have the words to thank Kim, whose love and companionship means so much to me. She will be in my heart, and in every aspect of my life, even long after this thesis has gathered considerable dust on the shelves. I dedicate this thesis to my wonderful family, for which I am very fortunate and eternally grateful.

Contents

List of Figures

List of Tables

Chapter 1

Introduction

This chapter is an attempt to place this thesis in its proper context.

1.1 Phenomenology

Humanity has been in a constant struggle with Nature from earliest times of its history, in order to survive and thrive on Planet Earth. Early on, it became clear that a better understanding of *how* Nature works can be a very important means to accomplish many of the desired goals. As the inner workings of objects around us have been slowly revealed over time, many technological advances have greatly aided our comfort and prosperity – although at an arguable cost.

The present picture we have of the world around us is markedly different from what it was a century ago. Two big revolutions in physics, the Theories of Relativity and Quantum Mechanics, have created a very different picture of reality, enabling an immense advancement of knowledge and technology, at the same time leaving behind a number of very important philosophical issues to be resolved. Yet it is clear that the understanding of relativity and quantum mechanics was by no means necessary to build huge structures such as towers and bridges, to invent the steam engine and to utilize electricity. Natural sciences had already reached a certain maturity in the late nineteenth century, and it was even believed that all secrets of Nature were soon to be revealed by scientists. We now know that matter behaves in a profoundly different way at the microscopic level, yet these discoveries were not of much direct consequence to the geophysicist studying rock formations, or the mechanical engineer building a combustion engine. These and many other disciplines focus on systems that are of macroscopic size, and phenomenological parameters such as the density of the rock or the vapor pressure of the fuel are all that are needed to study them. Even the modern discipline of atomic physics can be considered phenomenological: The masses of atomic nuclei and electrons are just parameters that can be measured experimentally. Their origins are not known to the discipline; nor would such a knowledge alter the understanding of the subject matter a great deal.

Although an ontological understanding of Nature is a very important intellectual challenge, the power of phenomenology should not be undermined: After all, exper-

iments and observations are the only connections between the human mind and the reality perceived by it. In this thesis, I address a number of current problems in open nonequilibrium systems from a phenomenological point of view. A brief review leading to the topics discussed in this thesis is in order.

1.2 Thermodynamics

Thermodynamics is "the theory of the relations between heat and mechanical energy, and of the conversion of either into the other"[1]. More precisely, it is a phenomenological description of thermal properties of *macroscopic* systems *in equilibrium.* It only concerns itself with a few macroscopic observables of the system under study, such as the temperature and pressure of a gas, and provides an account of how such systems interact with each other at this macroscopic level, without trying to give an explanation or cause. The "laws" of thermodynamics were originally deduced from observation, not by mathematical proof. In spite of this, it is tremendously successful: One does not need to know the detailed internal structure of the water molecule to build a steam engine.

1.3 Statistical Mechanics

The gap between microscopic theories that obey the laws of molecular dynamics and the properties of systems that are well described by thermodynamics is bridged by *Statistical Mechanics.* It aims to derive not only the general laws of thermodynamics but also thermodynamic quantities (such as entropy, pressure, free energy, and chemical potential) from the microscopic model[2]. The idea is to start from an energy functional, a *Hamiltonian* $\mathcal{H}[\mu]$, which gives the total energy of the system in terms of its *microstate* μ described by the positions and momenta of a very large number [1] of particles. The microstate contains a huge quantity of information about the system, most of which is not needed if one is concerned only with macroscopic quantities such as the pressure of a gas, or the magnetization of a crystal. Statistical Mechanics reaches its goal by a simple idea: In equilibrium, each microstate of an isolated system that is consistent with a given set of macroscopic parameters is assumed to be as equally likely to occur as any other. This assumption of *equal a priori probabilities* is very successful in describing a wide variety of macroscopic phenomena. It implies that the probability of observing a particular macrostate is directly proportional to its corresponding volume in the *phase space* (which contains all microstates).

Assume that we are interested in the thermodynamic properties of a system in thermal equilibrium at temperature T. We start by considering the system (with microstates $\{\mu\}$ and Hamiltonian $\mathcal{H}$) and a much larger heat reservoir (with microstates $\{\mu_R\}$ and Hamiltonian $\mathcal{H}_R$)in thermal contact with it. The assembly is then isolated from the environment, so that its total energy $E = \mathcal{H} + \mathcal{H}_R$ does not change with time. Since we are only interested in the microstates of the system and not the

[1] approx. 10^{23}

reservoir, we can eliminate $\{\mu_R\}$ simply by summing over these degrees of freedom. This summation yields the well-known Boltzmann distribution for the probability of a microstate:

$$\mathcal{P}[\mu] = Q^{-1} e^{-\mathcal{H}[\mu]/k_B T}, \tag{1.1}$$

where k_B is the Boltzmann constant and Q is the normalization factor, also called the *partition function*:

$$Q = \sum_{\mu} e^{-\mathcal{H}[\mu]/k_B T}. \tag{1.2}$$

The expectation value of any macroscopic observable $O[\mu]$, which is what experiments measure, is then given by its weighted average over the probability distribution:

$$\langle O \rangle = \sum_{\mu} O[\mu]\mathcal{P}[\mu] = Q^{-1} \sum_{\mu} \mathcal{O}[\mu] e^{-\mathcal{H}[\mu]/k_B T}. \tag{1.3}$$

Of course, the experimental measurements will be meaningful and reproducible only if the fluctuations of the actually observed values around the expected value are very small, i. e.

$$\left\langle (O - \langle O \rangle)^2 \right\rangle \ll \langle O \rangle^2. \tag{1.4}$$

The law of large numbers guarantees this condition in almost all cases, except when the system is near a *critical point*, which I shall describe later.

The partition function has all the information necessary to calculate thermodynamic functions. For example, the *Gibbs free energy* is given by $G = -k_B T \ln Q$. Statistical Mechanics is thus mostly concerned about calculating Q from a given microscopic model. For most systems, this is a very difficult task to do exactly, and approximation schemes are necessary.

1.4 The Ising Model

In order to demonstrate these ideas, let us consider a prototype toy model that attempts to describe a uniaxial ferromagnet: The Ising Model[3]. Consider a square lattice, with L sites on a side and a lattice constant a, where each of the $N = L^2$ lattice sites is occupied by a particle which can be magnetized either in the "up" $(+1)$ or "down" (-1) direction, without any other degrees of freedom. Then, a microstate is completely described by the enumeration of the "spins" $\sigma = \pm 1$ of each particle:

$$\mu = \{\sigma_i\}. \tag{1.5}$$

The 2^N possible values of μ constitute the phase space Ω of the system. Since we would like to describe a ferromagnet, assume that there is an energy gain of J whenever two neighboring particles are aligned. Also, there is an external magnetic field H which tends to align the spins along its direction, causing an additional energy cost of $-H\sigma_i$ at each site. Thus, the Hamiltonian is given by

$$\mathcal{H}[\{\sigma_i\}] = -J \sum_{\langle ij \rangle} \sigma_i \sigma_j - H \sum_i \sigma_i, \tag{1.6}$$

where $\langle ij \rangle$ denotes a summation over nearest neighbor pairs. (Periodic boundary conditions are imposed to insure that every site has equivalent surroundings.) The partition function is

$$Q = \sum_{\{\sigma_i\}} \exp\left\{ \frac{J}{k_B T} \sum_{\langle ij \rangle} \sigma_i \sigma_j + \frac{H}{k_B T} \sum_i \sigma_i \right\}. \tag{1.7}$$

The physical quantity of interest is the total magnetization, which is simply the sum of all spins:

$$M[\{\sigma_i\}] = \sum_i \sigma_i. \tag{1.8}$$

In thermal equilibrium, the expected value of the magnetization is

$$\begin{aligned} M(T,H) &= Q^{-1} \sum_{\{\sigma_i\}} \left(\sum_i \sigma_i \right) \exp\left\{ \frac{J}{k_B T} \sum_{\langle ij \rangle} \sigma_i \sigma_j + \frac{H}{k_B T} \sum_i \sigma_i \right\} \\ &= k_B T \frac{\partial \ln Q}{\partial H} = -\frac{\partial G}{\partial H}. \end{aligned} \tag{1.9}$$

The magnetization per site for an infinite system $m(T,H) = \lim_{N\to\infty} M(T,H)/N$ is plotted in Figure 1.4. In thermal equilibrium, the infinite system gives rise to a paramagnet at high temperatures ($m \propto H$) and a ferromagnet at low temperatures [$m = \pm m_0(T)$ for $H \to 0^{\pm}$], causing a discontinuity in the magnetization as the magnetic field changes sign. The transition from a smoothly varying m to the discontinuity occurs at the critical temperature T_c, where the Gibbs free energy G acquires a singular part. This non-analytic behavior is a consequence of taking the $N \to \infty$ limit. Thermodynamic response functions, such as the magnetic susceptibility $\chi = \partial m/\partial H$ and the heat capacity $C = \partial \langle \mathcal{H} \rangle / dT = k_B T^2 \partial^2 G / \partial T^2$ diverge with associated power laws as a function of the *reduced temperature* $t = (T - T_c)/T_c$:

$$C \sim |t|^{-\alpha}, \quad \chi \sim |t|^{-\gamma}, \tag{1.10}$$

valid for small t and $H = 0$. The magnetization also has non-analytic behavior as a function of t and H:

$$m \sim |t|^{\beta} \text{ (for } H = 0), \quad m \sim H^{-1/\delta} \text{ (for } t = 0). \tag{1.11}$$

Being the quantity that distinguishes the two phases, the magnetization is usually called the *order parameter* of the system. The exponents $\alpha, \beta, \gamma, \delta$ are called *critical exponents*, and they have rather remarkable properties: First of all, they are not independent, related to each other by a number of *scaling laws* which can be derived from dimensional arguments using the *scaling hypothesis*. (See below.) Furthermore, physical systems seem to fall into a relatively small number of groups called *universality classes*, within which the critical exponents are identical. For example, critical exponents near the liquid-gas critical point are not only the same across a wide variety of materials, but they are also very close to the values found for the three-dimensional Ising Model[4], which is hardly an accurate model to describe a liquid-gas system.

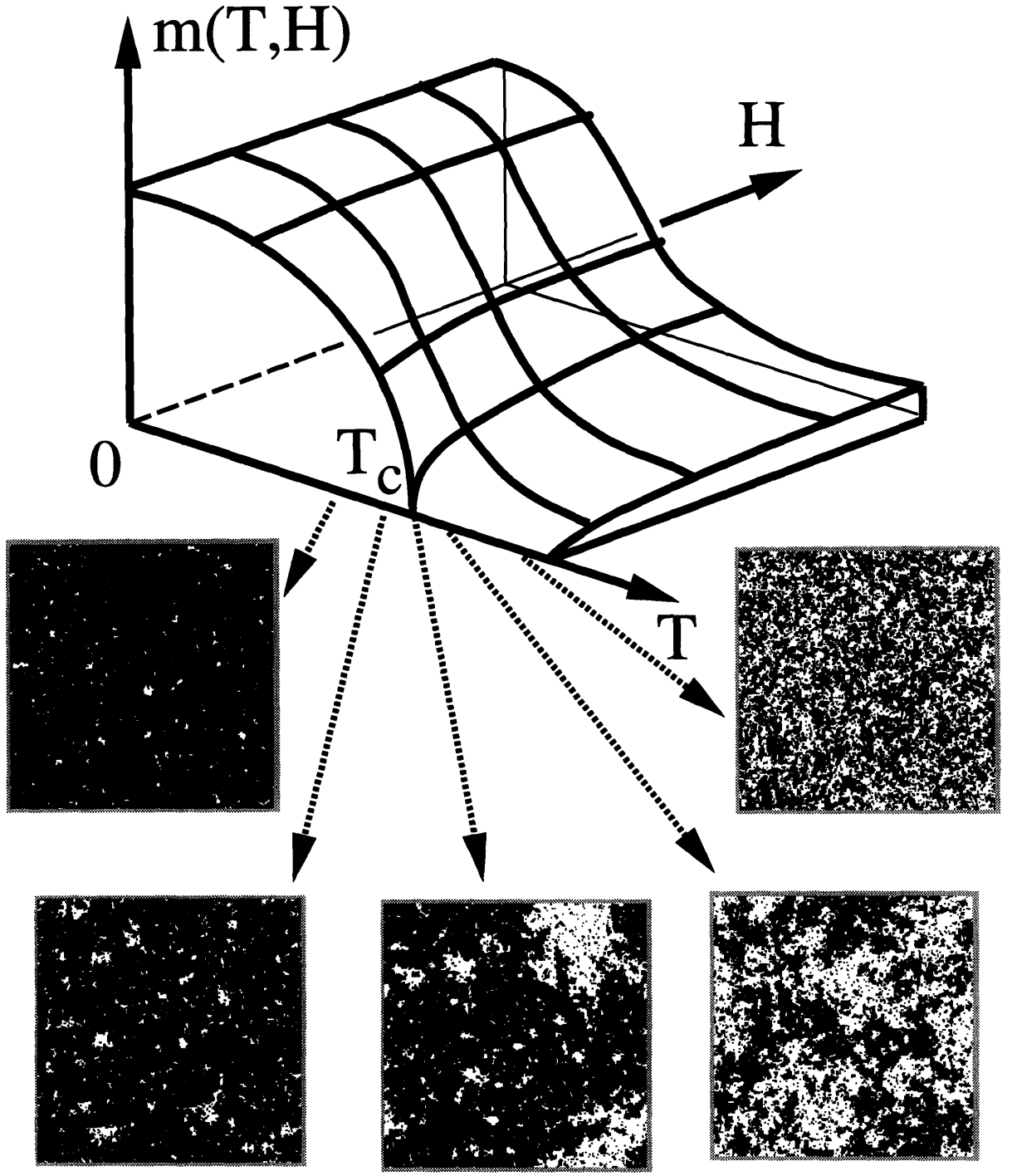

Figure 1-1: Qualitative phase diagram of the two dimensional Ising Model, along with typical configurations on the $H = 0$ line near the critical temperature T_c.

The modern theory of critical phenomena[5] aims to explain this insensitivity to microscopic parameters and to derive the critical exponents. To achieve this goal, a very powerful mathematical tool called the *Renormalization Group* (RG), first used by Wilson[6] in this context, is employed. In order to motivate this tool, we should first look at the connection between fluctuations in a system and its thermodynamic response functions.

1.5 Correlations and Scaling

If the original "macroscopic" system is broken into smaller and smaller subsystems, a size will eventually be reached when the subsystems cannot be considered macroscopic, since Eq.(1.4) breaks down. How large does a subsystem have to be in order be still considered as macroscopic? The answer depends on the nature of fluctuations in the system. Assume that there is a device which can measure the average magnetization of spins within a distance b of its center, i. e.

$$m(\mathbf{r}) = \sum_i \sigma_i f_b(\mathbf{r} - \mathbf{r}_i), \tag{1.12}$$

where $\mathbf{r}_i$ is the location of spin i and f_b is a suitable and properly normalized window function. (For a device that measures total magnetization, b would be equal to the system size.) Since features that are smaller in size than b cannot be resolved, it becomes desirable to describe the system in terms of these *coarse-grained* variables $m(\mathbf{r})$ instead of the original spins $\{\sigma_i\}$. This can be done by a partial summation over all microstates that give rise to the same coarse-grained observables in the partition function. This process is called *coarse-graining.*

Due to the nearest-neighbor coupling J, the spins in two nearby sites are not entirely independent of each other. This dependence is measured by the *correlation function* $\Gamma_{ij} = \langle \sigma_i \sigma_j \rangle - \langle \sigma_i \rangle \langle \sigma_j \rangle$, which would equal to zero if the sites were independent. In terms of the coarse-grained variables,

$$\Gamma(\mathbf{r}) = \langle m(\mathbf{r}) m(\mathbf{0}) \rangle - \langle m(\mathbf{0}) \rangle^2. \tag{1.13}$$

Typically, the correlation function decays exponentially as a function of the distance between the spins, with a characteristic length ξ, called the *correlation length*:

$$\Gamma(\mathbf{r}) \sim e^{-r/\xi}, \quad (r \ll \xi). \tag{1.14}$$

The magnetic susceptibility is intimately related to the spin correlation function through the relation

$$\chi = \frac{1}{k_B T} \int d\mathbf{r}\, \Gamma(\mathbf{r}). \tag{1.15}$$

Thus, the divergence of χ implies that the correlation length ξ becomes arbitrarily large near a critical point. Typically, $\xi \sim |t|^{-\nu}$, defining the correlation length exponent ν. At the critical point, $\Gamma(\mathbf{r})$ decays as a power law instead of an exponential, giving rise to a *self similar* structure.

1.6 Critical Phenomena

Large-scale fluctuations play an important role in the properties of the system at criticality. It is plausible to expect that ξ becomes the only important length scale in the system, in terms of which all other terms must be measured. (This assumption is often called the *scaling hypothesis.*[2]) Thus, the appearance of power laws near a critical point is not accidental, but a consequence of the loss of length scale in the correlations. Power laws have the important property of retaining their original form (up to an overall constant) upon a transformation of length scales. This scale-invariance lies in the heart of the RG treatment. The RG is essentially a mapping in parameter space that connects two systems at different length scales. Near criticality, the system looks self similar over a range of scales, which indicates that the parameters of the system are close to a fixed point of the RG transformation. By examining the flow of parameters near this fixed point, it is possible to derive critical exponents of the model. The universality of critical exponents becomes clearer in this approach: Two different systems will have identical critical exponents if they are influenced by the same fixed point of the RG transformation near criticality.

Computations on many different systems suggest that there are a small number of attributes that influence the observed critical exponents of a system under study. First of all, the dimensionality d of the embedding space is very important: The Ising Model has different exponents in two and three dimensions. In fact, many systems have trivial critical behavior in dimensions $d > 4$. The reason is that at high spatial dimensionality, each site has many nearest neighbors and fluctuations from each of these sites tend to cancel out. In this case, mean-field theories usually give the correct critical exponents. The second important attribute is the degrees of freedom each site has: For example, if the spin at each site is allowed to point in any direction rather than just "up" or "down", the critical exponents will be different. In the coarse-grained description, this corresponds to replacing m with an n-component vector $\vec{m}$. ($n = 3$ in the example above.) Once again, the determination of the critical exponents become usually easier for some models when n is large. Since exact results for the critical exponents are difficult to obtain for physical values of d and n (The two dimensional Ising Model is still the only case where exponents are known exactly), useful controlled approximations have been developed. They estimate critical exponents by analytical continuation down from $d = 4$ (ϵ-expansion) and $n = \infty$ ($1/n$ expansion), where exact results are known. Such methods have been successfully employed to determine critical exponents to a high accuracy. (A few percent for the d=3 Ising Model.)

[2]See Chapter 4 of Ref. [5] for an elegant introduction to the scaling hypothesis, and further chapters for an introduction to the RG and its application to critical phenomena. See Ref. [7] for a more recent and very readable treatment. A detailed discussion of these concepts is beyond the scope of this thesis.

1.7 A Note On Disorder

So far, I have only discussed "pure" systems: In the Ising Model, the nearest-neighbor coupling J and the external field H does not vary from site to site. Most materials we encounter in real life are not so homogenous: Even the cleanest systems may have impurities, dislocations or vacancies. Such effects can be incorporated into the Ising Model by allowing the couplings and external fields to vary slightly at each lattice point: $J \to J + \delta J_{ij}$, $H \to H + \delta H_i$. Since the system is very sensitive near a critical point (as evidenced by diverging susceptibilities), and disorder usually has a profound effect on the critical properties of the system: It may change the critical exponents, or even eliminate the phase transition altogether. For example, the Random Field Ising Model (RFIM) with fluctuating local fields is in a different universality class than its pure counterpart. Thus, the nature of disorder in the system has to be carefully considered when dealing with critical phenomena.

1.8 Generic Scale Invariance

The critical point is very special: It is necessary to fine-tune some parameter to a specific value (e. g. the temperature to T_c) in order to observe fluctuations at all length scales, with power law correlation functions. However, as particularly emphasized by B. Mandelbrot [8], many occurences in nature such as mountains, clouds and coast lines exhibit statistical scale invariance over a wide range of lengths, without any apparent "tuning" of external parameters. This kind of generic scale invariance has spurred considerable interest among physicists, and several mechanisms have been suggested. The "sandpile model" of Bak, Tang and Wiesenfeld (BTW)[9] has become the prototype of numerous *dynamical* models, described by time evolution rules rather than a Hamiltonian. These systems operate far from thermodynamic equilibrium, and the scale invariance is believed to arise from the self-organization of the system to a critical state due to the particular dynamical rules that are involved, hence the overly popular term "self-organized criticality" (SOC). There are also field theories that give a coarse-grained picture of a system, such as the configuration of a domain wall or interface, where scale invariance appears naturally as a result of symmetries and/or conservation laws. To illustrate how symmetries give rise to scale-invariance, let us consider a line with line tension τ, which is confined to the xy-plane and is on the average oriented along the x-direction, but free to move along the y direction. (See Fig. 1-2.) Its configurations (microstates) can be described by the height profile $y(x)$, assumed to retain single-valuedness. The energy of the line is proportional to its length:

$$\mathcal{H} = \tau \int_0^L dx \sqrt{1 + (dy/dx)^2} \approx \tau L + \frac{\tau}{2} \int_0^L dx \, (dy/dx)^2, \tag{1.16}$$

where L is the length of the completely flat line. The final approximation is valid when $|dy/dx| \ll 1$, which I'll show later to hold at large length scales. The first term creates a constant prefactor in the partition function, it can be safely ignored. One

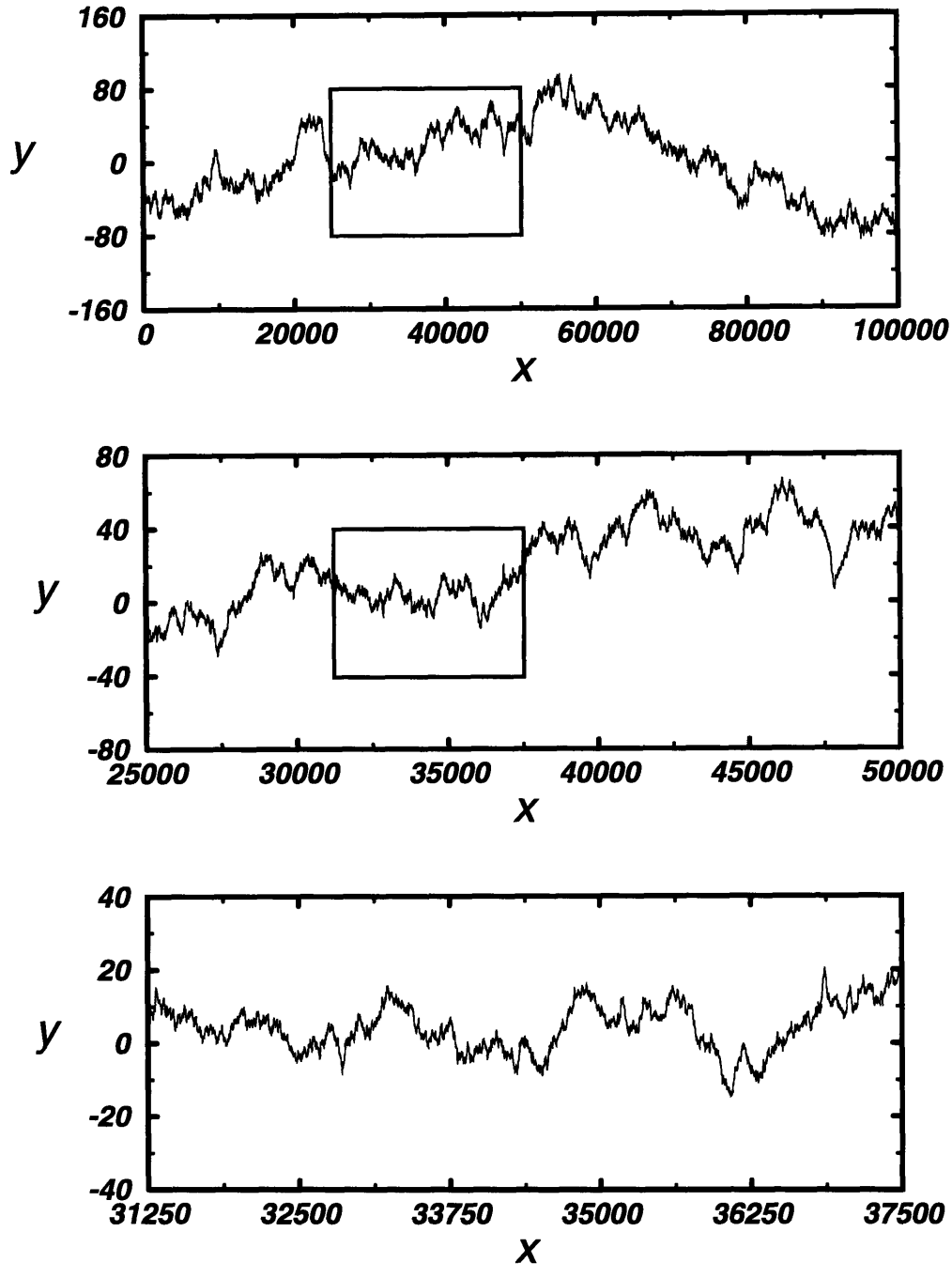

Figure 1-2: A fluctuating line in two dimensions. Successive rescalings by 4 along the x-axis and by $\sqrt{4} = 2$ along the y-axis gives statistically similar pictures, demonstrating the self affinity of the line.

very important property of this Hamiltonian is that it involves only derivatives of y. This follows naturally from the observation that a uniform shift $\tilde{y}(x) = y(x) + c$ of the line along the y-axis has no energy cost. No matter how complicated the Hamiltonian is (the line could have a bending rigidity, for example) this feature will persist as long as the translational symmetry along the y-axis is preserved. Our system actually has another symmetry: The energy of the mirror image of a configuration with respect to the $y = 0$ line is also identical to the original. This requires that $\mathcal{H}$ can not change when $y(x)$ is substituted by $-y(x)$. Thus, y can appear in only even powers in the Hamiltonian. Clearly, symmetry considerations alone strongly restrict the possible Hamiltonians one can write down for a given system. The absence of terms proportional to $y(x)$ in Eq.(1.16) gives rise to a scale-invariant profile. The simplest way to see this is to notice that the Hamiltonian remains unchanged under a scale transformation $x \to bx, y \to b^{1/2}y$. Although the line remains parallel to the x axis on the average, the magnitude of the deviation scales as the square-root of the x-distance between two points on the line, i. e.

$$\langle |y(x) - y(0)|^2 \rangle \sim |x|. \tag{1.17}$$

A typical configuration of the line will have the same statistical properties when shrunk by different amounts in the x and y directions. Such configurations are called *self-affine* as opposed to *self-similar*, a term used for systems that remain statistically invariant under an isotropic scale transformation. Self-affine systems are characterized by the *roughness exponent* ζ, defined through the scaling relation

$$\langle |y(x) - y(0)|^2 \rangle \sim |x|^{2\zeta}. \tag{1.18}$$

Thus, the elastic line has a roughness exponent $\zeta = 1/2$. The typical magnitude of the average slope at lateral resolution b scales as $b^{\zeta-1} \sim 1/\sqrt{b}$, therefore the approximation $|dy/dx| \ll 1$ is justified after sufficient coarse-graining.

Similarly, the self-organization in the sandpile model of BTW[9] can be traced to the conservation of sand particles by the dynamics: Sand particles which enter the pile at random locations can only leave it through the open boundaries at the edge. Criticality is lost as soon as random sinks are placed in the sandpile. Clearly, dynamics plays a very important role in determining the scaling properties of these systems, and will be the next point of focus.

1.9 Approach to Equilibrium: Dynamics

Standard Statistical Mechanics is successful at describing equilibrium properties, but in many cases the *approach* to equilibrium is very important in understanding dynamical phenomena such as transport properties. In order to study dynamical properties of a system, it is necessary to investigate correlations in time as well as in space. In order to obtain such statistical averages, the concept of phase space is expanded from static configurations $\{m(\mathbf{r})\}$ of a system to complete *histories* of configurations $\{m(\mathbf{r}, t)\}$. The assumption of equal a priori probabilities is then applied to all histories that are consistent with the evolution equations of the system. If the system

under study is near equilibrium, the time evolution of the order parameter $m(\mathbf{r},t)$ is usually approximated by a *Langevin Equation* of the form

$$\frac{\partial m(\mathbf{r},t)}{\partial t} = -\mu \frac{\delta \mathcal{H}[\{m\}]}{\delta m(\mathbf{r},t)} + \eta(\mathbf{r},t). \tag{1.19}$$

The first term on the right ensures that m relaxes towards the minimum of the Hamiltonian. μ determines the speed of this relaxation and is called the *kinetic coefficient.* The second term mimics the thermal agitation from the heat bath and spreads out the distribution of m such that the Boltzmann distribution is recovered when equilibrium is reached. [η is a Gaussian white noise with zero mean and correlations $\langle \eta(\mathbf{r},t)\eta(\mathbf{r}',t')\rangle = k_B T \mu \delta(\mathbf{r}-\mathbf{r}')\delta(t-t')$.] When the system is near a critical point, the divergence of the susceptibility and/or the singular behavior in kinetic coefficients cause the relaxation rates of certain modes to go to zero. This *critical slowing down* can then lead to observable anomalies in other transport coefficients and dynamic properties[10]. In many cases, the resulting critical behavior can be successfully described by extending the scaling hypothesis to relaxation rates and introducing a *dynamical exponent* z which relates relaxation rates of "slow" modes to their wavelength. The scaling form of the response functions can then be used to relate the dynamical exponent to the static critical exponents. Depending on the type of dynamics, z may assume different values even if the equilibrium distributions of two systems are identical. For example, in the Ising Model, if relaxation to equilibrium occurs through spin exchange processes, the magnetization (which is the order parameter) is locally conserved by the dynamics. If the relaxational process is spin flip, magnetization is not conserved. The relaxation is found to be much slower if the order parameter is conserved, characterized by a larger dynamical exponent. Even if the order parameter is not conserved, the dynamical exponent is increased if the order parameter is coupled to some conserved field, such as the local energy density. Thus, there are a number of distinct *dynamical universality classes* that have the same static critical exponents, and dynamical critical phenomena are in general richer than their static counterparts. Dynamical RG methods have been successfully used to justify the dynamic scaling hypothesis and to investigate the dynamical critical exponent and associated universality classes[10].

1.10 Systems Far From Equilibrium

There are many examples of open systems which are driven far from equilibrium by external forces. Examples include polymers that are in an external flow field, surface growth due to deposition processes such as sputtering and Molecular Beam Epitaxy, and fluid invasion in porous media. When the system of interest is far from equilibrium, many well established methods based on a Hamiltonian and the notion of equilibrium become useless, and a different approach is needed. There are still a number of ways to attack the problem, such as the formalism of Martin, Siggia and Rose[11]. One possibility is to treat the *evolution equations* as more fundamental, and to consider the most general equation of motion consistent with the symmetries and

conservation laws of the system under study[12]. The idea is similar to the Landau-Ginzburg approach for obtaining the effective coarse-grained Hamiltonian through symmetry considerations: The parameters that are introduced are phenomenological, and in principle derivable from a more precise microscopic description of the system. Hydrodynamics is a good example of such a phenomenological approach: The evolution of large-scale structure in a fluid is described in terms of a few measurable parameters, whose derivation from first principles can be very difficult and not particularly necessary to understand the studied phenomena. Once such evolution equations are constructed, their critical properties can be studied by numerical and analytical tools.

1.11 Scope of This Thesis

The principal common goal of the research described in this thesis is to identify and investigate the generic and/or critical dynamic scaling of fluctuations in simple prototype models that describe a wide variety of nonequilibrium phenomena related to interface and polymer dynamics. The focus is on overdamped systems, and the goal is to determine how the dynamical scaling behaviors of these systems are influenced by of thermal and quenched (static in time) disorder, dimensionality of the embedding space and the embedded structure, and local vs. nonlocal interactions. General symmetry considerations are employed to construct phenomenological evolution equations, whose parameters are linked to experimentally observable quantities when possible.

Figure 1-3 shows the physical realizations that are studied in particular, although very similar equations can be used to describe a wide variety of other systems, such as the convection of a passive scalar[13], propagation of crack fronts[14], and dynamics of interfaces coupled to diffusive fields[15].

The first system investigated is a polymer in a dilute solution, drifting due to a uniform external force. A good experimental realization is DNA Electrophoresis[16]. The time evolution of the polymer is described by the equation

$$\partial_t r_{\|} = D_{\|}\partial_x^2 r_{\|} + \frac{\lambda_{\|}}{2}(\partial_x r_{\|})^2 + \frac{\lambda_{\times}}{2}\sum_{i=1}^{2}(\partial_x r_{\perp i})^2 + \eta_{\|}(x,t), \tag{1.20a}$$

$$\partial_t r_{\perp i} = D_{\perp}\partial_x^2 r_{\perp i} + \lambda_{\perp}\partial_x r_{\|}\partial_x r_{\perp i} + \eta_{\perp i}(x,t) \qquad (i=1,2), \tag{1.20b}$$

where $\mathbf{r}(x,t)$ denotes the position of monomer x with respect to the center of mass, and $\eta(x,t)$ represents the disorder (thermal or quenched), with zero mean and correlations of the form

$$\langle \eta_{\|}(x,t)\eta_{\|}(x',t')\rangle = 2T_{\|}\delta(x-x')\delta(t-t'), \tag{1.20c}$$

$$\langle \eta_{\perp i}(x,t)\eta_{\perp j}(x',t')\rangle = 2T_{\perp}\delta_{i,j}\delta(x-x')\delta(t-t')\ . \tag{1.20d}$$

These equations give rise to a self-affine configuration, due to the translationally invariant dynamics of the system.

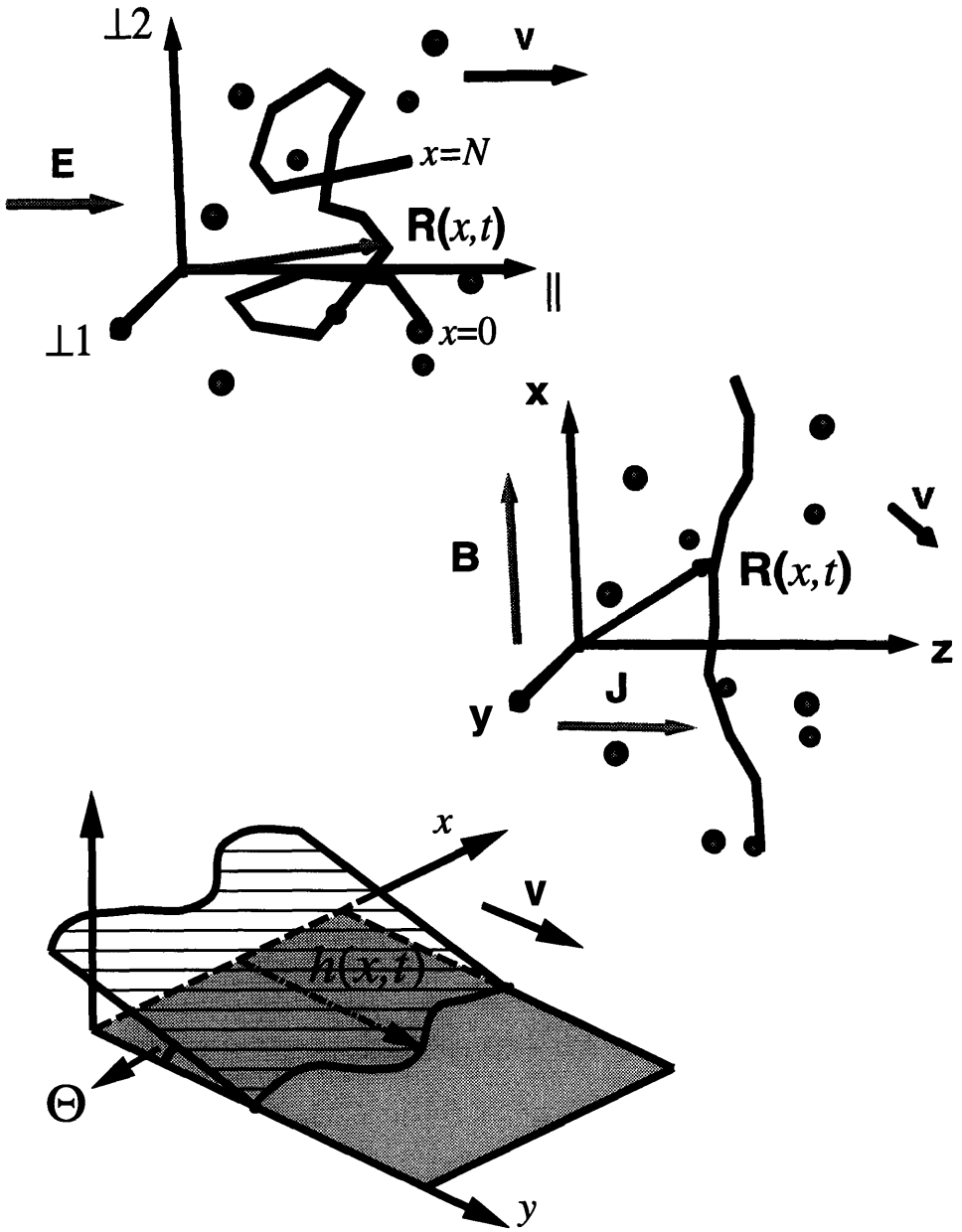

Figure 1-3: Three systems studied in detail. From top to bottom: A uniformly charged polymer in a dilute solution driven by an external electric field **E** (Chapter 2); A Flux Line in a type-II superconductor driven by a bulk supercurrent **J** (Chapters 2 and 3); Contact line of a partially wetting liquid, advancing on a surface (Chapter 4).

The second system is a single flux line in a Type-II superconductor. The effect of quenched disorder and the resulting critical behavior near depinning are investigated. The equations of motion are

$$\eta\partial_t r_{\|} = K_{11}\partial_x^2 r_{\|} + K_{12}\partial_x^2 r_{\perp} + F + \tilde{f}_{\|}(x, \mathbf{r}(\mathbf{x}, t)), \tag{1.21a}$$

$$\eta\partial_t r_{\perp} = K_{21}\partial_x^2 r_{\|} + K_{22}\partial_x^2 r_{\perp} + \tilde{f}_{\perp}(x, \mathbf{r}(x, t)), \tag{1.21b}$$

where $r_{\|}(x,t)$ and $r_{\perp}(x,t)$ denote fluctuations from a straight line along and transverse to the drift direction, respectively. The disorder is short-range in space, but quenched in time:

$$\langle \tilde{f}_{\alpha}(x, \mathbf{r}) \tilde{f}_{\gamma}(x', \mathbf{r}') \rangle = \delta(x - x') \tilde{\Delta}_{\alpha\gamma}(\mathbf{r} - \mathbf{r}'), \tag{1.21c}$$

where $\tilde{\Delta}$ is a function that decays rapidly for large values of its argument. As the depinning threshold is approached, the FL shows distinct scaling properties reminiscent of a second order phase transition; with a diverging correlation length and scaling exponents distinct from those obtained at large drift velocities.

Finally, the third system is the contact line of a partially wetting liquid on a heterogenous surface. When the contact line moves quasi-statically, the capillary modes on the liquid-vapor interface create an effective nonlocal interaction between different points on the contact line[17]. Thus, the dynamics near the depinning transition is described by the equation of motion

$$\mu^{-1}\left(\frac{\partial h(x,t)}{\partial t}\right) = -\frac{\gamma\Theta^2}{\pi} \int\limits_{a<|x-x'|} dx' \frac{h(x,t) - h(x',t)}{(x-x')^2} + f[x, h(x,t)] + F, \tag{1.22a}$$

where the disorder is again assumed to be short-range in space, but quenched in time:

$$\langle f(x,y) f(x',y') \rangle = \Delta(r/a). \tag{1.22b}$$

In the above, $r^2 = (x-x')^2 + (y-y')^2$, a is the characteristic size of defects, and Δ is a function that decays rapidly for large values of its argument.

1.12 A Warning on Notation

The assignment of greek letters to scaling exponents has been far from standardized, and major discrepancies exist across disciplines. I have tried to follow as much as possible the convention used by the modern theory of critical phenomena and the widely accepted notation in interface science. However, the notation is very different in polymer science for historical reasons. Such conflict is inevitable when dealing with a very general set of equations applicable to a number of disciplines. In order to make the chapters more readable to people familiar with the particular system discussed, the exponents are defined explicitly in each chapter, and the scope of their definition is strictly within that chapter. Therefore, I urge the readers to go through the definitions carefully in each chapter before interpreting the results. A chart of equivalence across chapters is given in Table 1.1.

Quantity	Chapter 2	Chapter 3	Chapter 4
Fluctuation	$r_\alpha(x,t)$	$r_\alpha(x,t)$	$h(x,t)$
Correlation length exp.	–	ν	ν
Velocity exp.	–	β	β
Roughening/swelling exp.	ν_α	ζ_α	ζ
Dynamic exp. (interface)	$\zeta_\alpha = \nu_\alpha z_\alpha$	z_α	z
Dynamic exp. (polymer)	z_α	z_α/ζ_α	z/ζ

Table 1.1: The correspondence of the fluctuating field and scaling exponents across chapters. The subscript α refers to $\{\|, \perp\}$ components.

Chapter 2

Dynamic Relaxation of Drifting Polymers

This chapter is a slightly edited reprint of Ref.[18].

2.1 Introduction and Summary

The dynamics of polymers in fluids is of much technological interest and has been extensively studied[19, 20]. The combination of polymer flexibility, interactions, and hydrodynamics make a first principles approach to the problem quite difficult. There are, however, a number of phenomenological studies that describe various aspects of this problem[21]. One of the simplest is the Rouse model[22]: The configuration of the polymer at time t is described by a vector $\mathbf{R}(x,t)$, where $x \in [0,N]$ is a continuous variable replacing the discrete monomer index. (See Fig. 2-1.) Ignoring inertial effects, the relaxation of the polymer in a viscous medium is approximated by

$$\partial_t \mathbf{R}(x,t) = \mu \mathbf{F}(\mathbf{R}(x,t)) = D\partial_x^2 \mathbf{R} + \eta(x,t), \tag{2.1}$$

where μ is the mobility. The force $\mathbf{F}$ has a contribution from interactions with near neighbors that are treated as springs. (In a coarse-grained formulation the origin of this term is entropic.) Steric and other interactions are ignored. The effect of the medium is represented by the random forces η with zero mean. The Rouse model is a linear Langevin equation that is easily solved. It predicts that the mean square radius of gyration $R_g^2 = \langle |\mathbf{R} - \langle \mathbf{R} \rangle|^2 \rangle$ is proportional to the polymer size N and the largest relaxation times scale as the fourth power of the wavenumber, i.e. in scattering experiments, the half width at half maximum of the scattering amplitude scales as the fourth power of the scattering wave vector $\mathbf{q}$. These results can be summarized as $R_g \sim N^\nu$ and $\Gamma_\mathbf{q} \sim q^z$ where ν and z are called the *swelling* and *dynamic* exponents, respectively. Thus, for the Rouse model, $\nu = 1/2$ and $z = 4$.

The Rouse model ignores hydrodynamic interactions mediated by the fluid. These effects were originally considered by Kirkwood and Risemann[23], and later on by Zimm[24]. The basic idea is that the motion of each monomer modifies the flow field

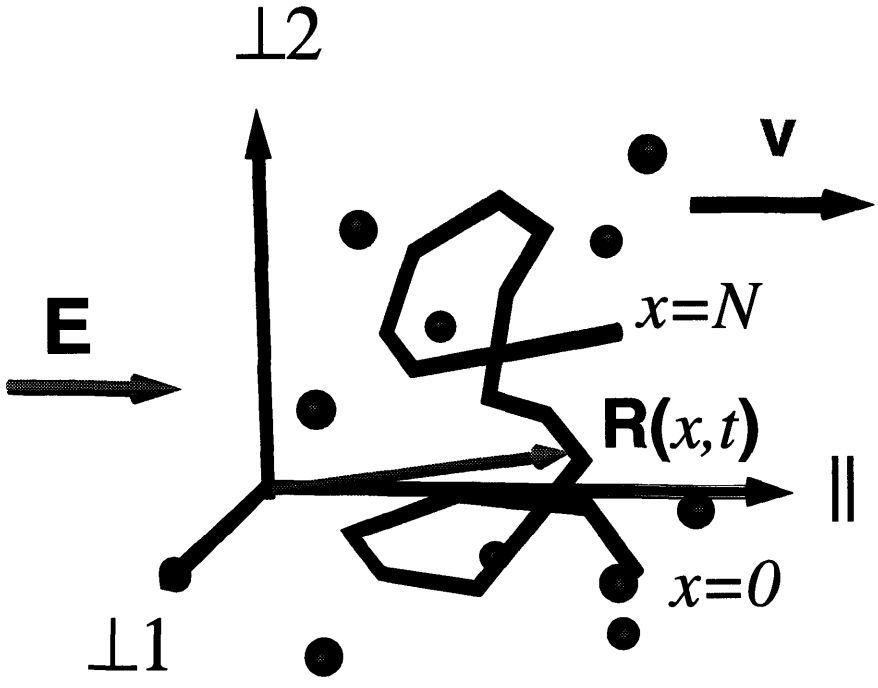

Figure 2-1: Configurations of the polymer at time t are described by $\mathbf{R}(x,t)$, where x labels the monomer index.

at large distances. Consequently each monomer experiences an additional velocity

$$\begin{aligned}\delta_H \partial_t \mathbf{R}(x,t) &= \frac{1}{8\pi\eta_s}\int dx' \frac{\mathbf{F}(x')r_{xx'}^2 + (\mathbf{F}(x')\cdot\mathbf{r}_{xx'})\mathbf{r}_{xx'}}{|\mathbf{r}_{xx'}|^3} \\ &\approx \int dx' \frac{\gamma}{|x-x'|^\nu}\partial_x^2\mathbf{R}, \end{aligned} \tag{2.2}$$

where $\mathbf{r}_{xx'} = \mathbf{R}(x) - \mathbf{R}(x')$, η_s is the viscosity of the solvent and the final approximation is obtained by replacing the actual distance between two monomers by their average value. The modified equation is still linear in $\mathbf{R}$ and easily solved. The main result is the speeding up of the relaxation dynamics as the exponent z changes from 4 to 3. Most experiments on polymer dynamics indeed measure exponents close to 3[25]. Rouse dynamics is still important in other circumstances, such as diffusion of a polymer in a solid matrix, stress and viscoelasticity in concentrated polymer solutions, and is also applicable to relaxation times in Monte Carlo simulations[19].

There are also many studies of the morphology of polymers in shear flows. The approach is usually to follow the evolution of a probability distribution for the shape of the polymer under the combined action of shear and elastic forces[26]. Under some circumstances the shear force may cause a coil to rod transition[27]. In this chapter I consider the dynamics of a polymer drifting through the fluid *at a constant velocity* U, due to a uniform external force $\mathbf{E}$, and in the absence of any external velocity gradients. Specific examples include *sedimentation* of polymers, in which case $\mathbf{E}$ is the acceleration due to gravity, $\mathbf{g}$, and *gel electrophoresis*[16] where $\mathbf{E}$ is the electric field.

At first sight it may appear that there should be no difference in the relaxation dynamics of a polymer at rest and one moving at a uniform velocity. This conclusion is in fact not correct due to the interactions with the surrounding fluid. For example, the drift velocity of a rod pulled through a viscous fluid depends on its orientation relative to the force[21]. (In principle the force acting on a linear object can be calculated from the equations of "slender body theory"[28].) Therefore, the motion of a monomer, more accurately modeled as a cylindrical rod along the chain rather than a spherical bead, in general depends on its orientation relative to the driving force. Thus, as $\mathbf{E}$ (and consequently U) is increased, there should be a cross over to a regime where the anisotropy is no longer negligible. The scale of this crossover can be estimated from dimensional analysis alone: For physical quantities that involve the whole polymer, like form birefringence, the natural length scale is the radius of gyration, $R_g = b_0 N^\nu$. The parameter D, appearing in Eq.(2.1) has dimensions of (length)^2/(time). We can thus construct a dimensionless parameter $y = UR_g/D = UN^\nu/U^*$, where $U^* = D/b_0 = b_0/\tau_0$ is a characteristic velocity. Here b_0 and τ_0 are microscopic length and time scales for the monomers. For *both* the Rouse and Zimm Models, this quantity is given roughly by $U^* \approx kT/(\pi\eta_s b_0^2)$. For a dilute solution of polystyrene in benzene (after Adam and Delsanti[25]), $U^* \approx 10$ m/s. For a polymer with $M_W = 10^6$, $y \approx 1$ when $U \approx 4$ cm/s. Another calculation, using the relaxation time data from Farrell *et al.*[25] yields $U^* \approx 20$ m/s, about the same order of magnitude. (Not surprisingly, y is proportional to the Reynolds number, $\mathcal{R}e = UR_g/\eta_s$, corresponding to the polymer

size, i.e., the same variable also controls the crossover to hydrodynamic instabilities[1].) Yet another scaling argument considers energetics: The energy scale associated with monomer orientation is roughly Eb_0, where b_0 is the monomer length. This should be compared to the energy of thermal fluctuations, which scales as kT. For a polymer with N monomers, the thermal fluctuations add up as independent random variables unlike orientational energies, thus comparing these two total energy scales, we once again obtain the scaling variable

$$y \approx \frac{NEb_0}{N^{1/2}kT} \approx \frac{UN^{1/2}}{kT/6\pi\eta_s b_0^2} \approx \frac{UN^{1/2}}{U^*}, \tag{2.3}$$

where the Rouse mobility relation $E = 6\pi\eta_s b_0 U$ was used in the second identity.

We are primarily interested in understanding the static and dynamical scaling properties of the nonlinear and anisotropic regime for $U \gtrsim U^*$. A first principles approach to the problem is quite difficult due to the complexity of the system and the non-equilibrium nature of the problem. I shall instead take a phenomenological route and construct the equations of motion based on symmetry considerations. Such an approach has been successful in describing other non-equilibrium problems[12].

As in the case of the Rouse model, let us neglect inertial effects and write the velocity of a point on the polymer (Fig. 2-1) as

$$\partial_t \mathbf{R}(x,t) = \mu \mathbf{F}(\partial_x \mathbf{R}(x,t), \partial_x^2 \mathbf{R}(x,t), \cdots; \mathbf{e}(x,t)). \tag{2.4}$$

I shall restrict the discussion to forces $\mathbf{F}$ that are *local*, but that can be expanded in powers of gradients of $\mathbf{R}$. (Due to the translational symmetry $\mathbf{R} \mapsto \mathbf{R} + \mathbf{c}$, $\mathbf{R}$ cannot appear in the equations of motion.) The effects of steric interactions, and nonlocal hydrodynamic forces as in Eq.(2.2) will be discussed later. Non-equilibrium effects enter through the external force $\mathbf{e} = \mathbf{E} + \delta\mathbf{e}$, with a *non-zero average* value of $\mathbf{E}$, and fluctuations $\delta\mathbf{e}(x,t)$ due to thermal stochasticity and other sources of disorder in the solvent. I also assume that any barriers to motion in the medium are isotropic, and sufficiently weak that the polymer reaches a *steady state* where its "center of mass", $\mathbf{R}_0(t)$, is *depinned* and moves with a uniform velocity. The leading terms in the expansion of Eq.(2.4) yield (see Appendix 2A) the evolution of relative monomer positions, $\mathbf{r}(x,t) = \mathbf{R}(x,t) - \mathbf{R}_0(t)$, as

$$\partial_t r_{\|} = D_{\|}\partial_x^2 r_{\|} + \frac{\lambda_{\|}}{2}(\partial_x r_{\|})^2 + \frac{\lambda_\times}{2}\sum_{i=1}^{n}(\partial_x r_{\perp i})^2 + \eta_{\|}(x,t), \tag{2.5a}$$

$$\partial_t r_{\perp i} = D_\perp \partial_x^2 r_{\perp i} + \lambda_\perp \partial_x r_{\|}\partial_x r_{\perp i} + \eta_{\perp i}(x,t), \qquad (i = 1, \cdots, n). \tag{2.5b}$$

In the above equation, and henceforth, I shall use the symbols $\|$ and $\{\perp\, i\}$ to indicate the components parallel (longitudinal) or perpendicular (transverse) to the force field. For the general case of a polymer embedded in a d-dimensional space,

[1] For the given examples, the Reynolds number is $\mathcal{R}e \approx 0.005y$. Therefore, there is a velocity range where the dynamical effects are important *and* low Reynolds Number hydrodynamics is applicable. However, the derivation of Eqs.(2.5) is solely based on symmetry arguments and not limited to the low Reynolds number regime.

there are $n = d - 1$ transverse coordinates $\{\perp i\}$. The noise, η_α, has zero mean, but unlike thermal noise need not be isotropic, and its second cumulants[2] satisfy

$$\langle \eta_\parallel(x,t)\eta_\parallel(x',t')\rangle = 2T_\parallel \delta(x-x')\delta(t-t'), \tag{2.6a}$$

$$\langle \eta_{\perp i}(x,t)\eta_{\perp j}(x',t')\rangle = 2T_\perp \delta_{i,j}\delta(x-x')\delta(t-t') \; . \tag{2.6b}$$

The equations of motion (2.5-2.6) are already "coarse-grained" in both space and time, i.e., faster modes associated with the motion of the fluid around the polymer have been integrated out. The resulting noise correlations may have long range correlations; this possibility will be discussed later. The nonlinear coefficients $\left\{\lambda_\parallel, \lambda_\times, \lambda_\perp\right\}$ must vanish in equilibrium due to invariance of the equations under $\mathbf{r} \mapsto -\mathbf{r}$. As shown in Appendix 2A, the external field breaks this symmetry, and hence these coefficients are proportional to E, for small fields. One source of such nonlinearity is the hydrodynamic interactions of the polymer with the solvent. They can be estimated by starting from the Rouse model, but regarding each monomer as a slender rod[28], oriented along $\partial_x \mathbf{r}$, rather than a spherical bead. The mobility of each rod is then a function of its *orientation*[19], and a brief calculation of the resulting nonlinear effects is given in Appendix 2B. The results show that to lowest order in the applied field, all three nonlinear coefficients are positive. However, symmetry considerations alone do not restrict their signs. Without loss of generality I shall assume that $\lambda_\parallel$ is positive and finite (its sign can be changed by $r_\parallel \to -r_\parallel$), and focus on the behavior of the polymer as a function of the ratios $\lambda_\perp/\lambda_\parallel$ and $\lambda_\times/\lambda_\parallel$, as in Fig. 2-2. (The vertical axis is actually chosen as $\lambda_\times T_\perp D_\parallel/\lambda_\parallel T_\parallel D_\perp$ for the convenience of demonstrating renormalization group trajectories.)

In the absence of transverse fluctuations, i.e. $n = 0$, Eqs.(2.5) reduce to the KPZ equation[31] that describes a growing surface in two dimensions. Thus the transverse components can also be interpreted as scalar fields that couple locally to the profile of the growing interface[15]. For example, the special case of $\lambda_\perp = 0$ corresponds to n diffusive scalar fields coupled nonlinearly to an order parameter $r_\parallel$. The case $n = 1$ represents a directed polymer, such as a flux line in a type-II superconductor, and will be discussed in more detail in Chapter 3, close to the depinning transition. In this chapter, I shall investigate the more general problem with the emphasis on $n = 2$, describing polymers in three dimensional space.

The noise-averaged correlation functions of Eqs.(2.5) satisfy the dynamic scaling form

$$\langle [r_\alpha(x,t) - r_\alpha(x',t')]^2\rangle = |x-x'|^{2\nu_\alpha} f_\alpha\left(\frac{|x-x'|^{\zeta_\alpha}}{|t-t'|}\right), \tag{2.7}$$

where f_α are scaling functions, ν_α and $z_\alpha = \zeta_\alpha/\nu_\alpha$ are the *swelling* and *dynamic* exponents, respectively. (The exponent ζ is introduced for convenience in the renormalization group (RG) procedure. The index α refers to either the longitudinal, or to any of the n transverse components.) In the absence of nonlinearities, the independent diffusion equations can be solved *exactly* to give $\nu_\parallel = \nu_{\perp i} = 1/2$ and $z_\parallel = z_{\perp i} = 4$. A renormalization group (RG) treatment, perturbative in the nonlinearities, indicates

[2]Non-trivial correlations or non-gaussian distributions of the noise, which may potentially alter the scaling behavior[29, 30], require a more general treatment and are not considered here.

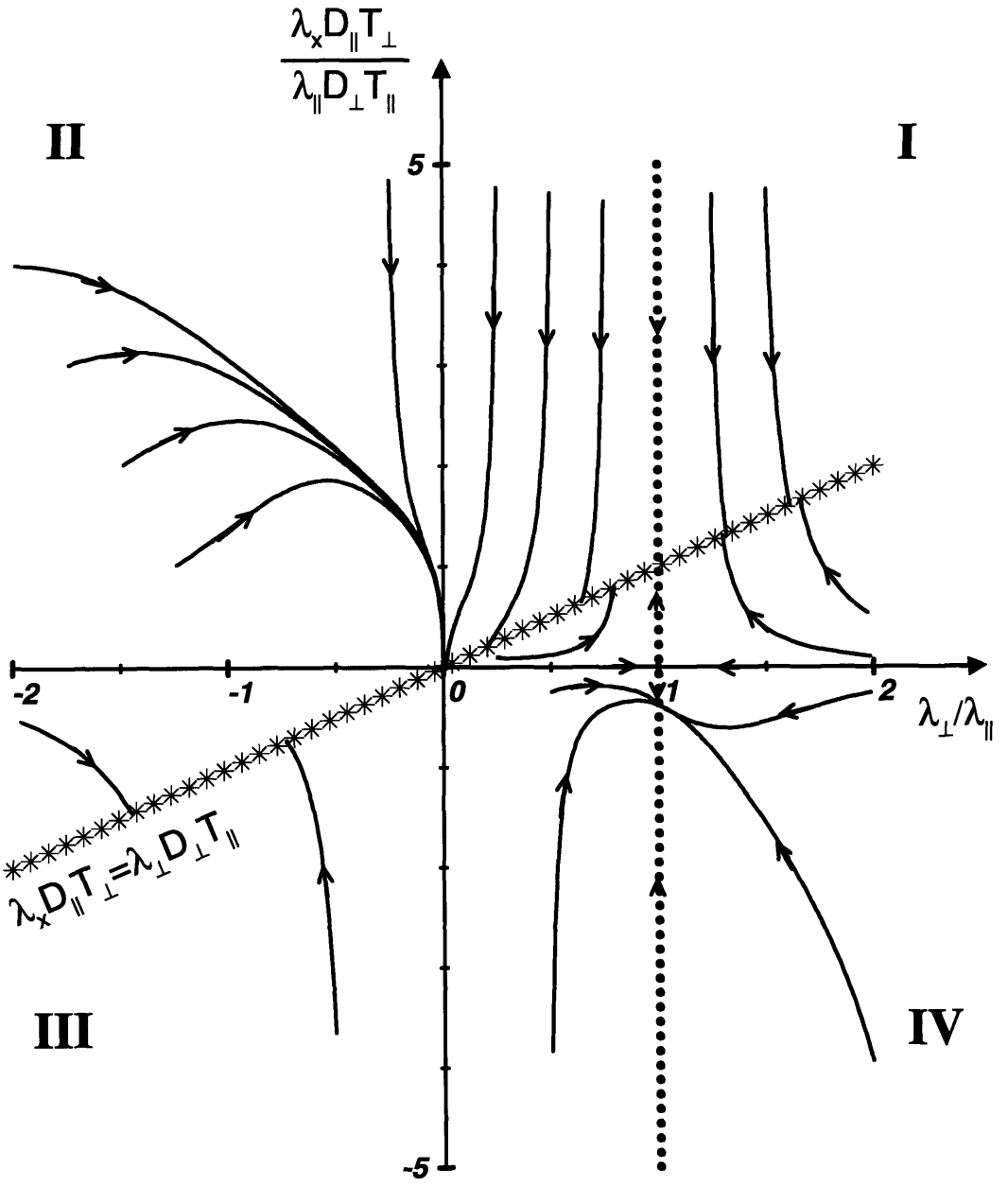

Figure 2-2: A projection of the RG flows in Eqs.(2.26) for $n = 2$. The quadrants mentioned in the text are shown in roman numerals. The conditions necessary for Galilean invariance and Fluctuation-Dissipation are indicated by dotted and starred lines respectively. The projected RG flows are constrained by these lines.

that all the nonlinear terms in Eqs.(2.5) are relevant and may modify the exponents in Eq.(2.7). Recent studies of related stochastic equations[32, 33] indicate that interesting dynamic phase diagrams may emerge from the competition between nonlinearities. Surprisingly, in most cases the nonlinearities reduce the exponent z to 3, the value obtained from the Zimm model in Eq.(2.2). (This is a coincidence, but indicates that the nonlinearities can mimic some of the effects of hydrodynamic interactions.) Furthermore, the model parameters in Eqs. (2.5) and (2.6) become anisotropic in general under RG, which implies the existence of a kinetically induced form birefringence *even in the absence of an external velocity gradient.* This change in scaling from Rouse dynamics is controlled by the dimensionless parameters $\lambda^2 T/D^3$, not surprisingly scaling as $(U\ell^{1/2}/U^*)^2$, where ℓ is the coarse-grained length scale. Thus, all the effects discussed in subsequent sections become important when $y \geq 1$.

In order to justify the applicability of Eqs.(2.5) to real polymers, we have to address the importance of terms left out of the local description. Since the Zimm model is the correct starting point for polymers at rest, paramount among these is the long-range hydrodynamic interactions appearing in Eq.(2.2). However, while the hydrodynamic interactions are strongly relevant at the Rouse fixed point, they are only marginal at the nonlinear fixed point of Eqs.(2.5). (This is because z is already 3 at this fixed point.) In fact even self-avoiding interactions, usually left out of the Zimm treatment are also marginal, indicating the robustness of this behavior. The remaining source of difficulty is a nonlinear *and* non-local term described in Section 2.5. The magnitude of this term is likely to be small, but if it becomes relevant, it could signal yet another scaling regime, possibly one in which the polymer completely unravels and becomes stretched.

The rest of the chapter is organized as follows.

In Section 2.2, I address a number of nonperturbative properties of Eqs.(2.5), that will be a helpful in interpreting the RG recursion relations (2.26). One such property is a *galilean invariance (GI)* that, for the case $\lambda_{\|} = \lambda_{\perp}$, implies an exact exponent identity $\nu_{\|} + \nu_{\|} z_{\|} = 2$. This identity holds as long as the noise has only short-time correlations. The *Cole-Hopf (CH) transformation* is an important method for the exact study of solutions to the one component nonlinear diffusion equation[34]. I present a generalization that extends the applicability of this method to arbitrary n. This enables an analytic solution to the *deterministic* equation and is a useful tool in studying the full stochastic equation by path integral methods. In particular for $n = 1$, the exact exponents $z_{\|} = 3, \nu_{\|} = 1/2$ are obtained. Finally, I investigate special cases where a *fluctuation-dissipation (FD) theorem* can be written for the system, which leads to the exact exponent values $\nu_{\|} = \nu_{\perp} = 1/2$. The regions in parameter space, where these properties are applicable, are indicated in Fig. 2-2.

In Section 2.3, I present a one-loop dynamical RG calculation, perturbatively in the nonlinear couplings, which determines the scaling exponents ν_α, and ζ_α. At the point $\lambda_{\|} > 0$, $\lambda_{\perp} = \lambda_{\times} = 0$ the equations for $r_{\|}$ and $r_{\perp i}$ decouple, and $\zeta_{\perp} = 2$ while $\zeta_{\|} = 3/2$. However, in general we expect $\zeta_{\|} = \zeta_{\perp} = \zeta$ unless the effective $\lambda_{\perp}$ is zero. For example at the intersection of the subspaces with GI and FD (see Section 2.2) the exact exponents $\nu_{\|} = \nu_{\perp} = 1/2$ and $\zeta_{\|} = \zeta_{\perp} = 3/2$ are obtained by utilizing the exponent identities. To construct the RG equations, we use only one value of

ζ and check for consistency by requiring that $\lambda_\perp$ renormalizes to a finite nonzero value. (The perturbative RG treatment breaks down when $\zeta_\perp \neq \zeta_\parallel$, this limits the usefulness of this method.) Under a change of scale, $x \to e^\ell x$, $t \to e^{\zeta\ell} t$, $r_\parallel \to e^{\nu_\parallel \ell} r_\parallel$, and $r_{\perp i} \to e^{\nu_\perp \ell} r_{\perp i}$, the renormalization of the parameters in Eqs.(2.5), computed to one loop order by standard methods of dynamic RG[13, 29], is given in Eqs.(2.26). The projections of the RG flows on the two parameter subspace of Fig. 2-2 are also indicated in this diagram. The resulting exponents are discussed below in conjunction with those of numerical integrations.

Section 2.4 describes details of the direct numerical integrations of Eqs.(2.5), used to determine the exponents numerically. The scaling behavior in the various regions, obtained by combining nonperturbative, RG, and numerical results, is as follows:

$1 \leq n < 4$: In this case, the recursion relations give rise to the flow in parameter space like the one shown in Fig. 2-2. When all three nonlinear terms have *the same sign* (Quadrant I in Fig. 2-2), the RG flows terminate on the fixed line where FD conditions apply, and the exponents assume fixed point values $\nu_\alpha = 1/2$, and $\zeta_\alpha = 3/2$ ($z_\alpha = 3$). The equilibrium polymer shape in this case is an ellipsoid, with an aspect ratio that depends on $D_\parallel T_\perp / D_\perp T_\parallel$ which varies continuously along the fixed FD line. In three dimensions ($n = 2$), starting from the $\{\lambda\}$ values calculated in Appendix 2B, The RG flow can be followed to determine the fixed-point anisotropy, yielding $\langle r_\parallel^2 \rangle / \langle r_\perp^2 \rangle \approx 6$. However, the fixed point value is reached only for very long polymers ($\approx 10^7$ persistence lengths) unless the external force is large, in which case the assumptions in Appendix 2B are inappropriate. When $\lambda_\perp = 0$, transverse and longitudinal components decouple, resulting in a simple diffusion equation for $r_{\perp i}$, with $\zeta_\perp = 2$. Since $\lambda_\times \neq 0$, the transverse components act as a strongly correlated (both in space and time) noise[29] on the longitudinal component. There is no finite scale-invariant fixed point and the RG is inconclusive. A naive application of the results in Ref. [29], treating this coupling as a noise correlated in space only, gives $\nu_\parallel = 2/3$ and $\zeta_\parallel = 4/3$ ($z_\parallel = 2$). Numerical results give an even larger swelling exponent $\nu_\parallel$ (see Table 2.1), which seems to increase with system size, suggesting a change in the scaling properties of the system[3]. A polymer with swelling exponents $\nu_\parallel > \nu_\perp$ is elongated and cigar shaped. On the other hand, when $\lambda_\times = 0$, the longitudinal displacement satisfies the KPZ equation, i.e. $\nu_\parallel = 1/2$, $\zeta_\parallel = 3/2$ ($z_\parallel = 3$). Its coupling to the transverse components, however, changes the scaling exponents to $\nu_\perp = 0.75$, $\zeta_\perp = 3/2$ ($z_\perp = 2$). With swelling exponents $\nu_\perp > \nu_\parallel$, the polymer assumes a pancake shape. This increased value of $\nu_\perp$ is verified by the numerical results as well, as seen in Table 2.1. In the light of these results, different scaling behaviors are anticipated when the nonlinearities have *different relative signs*. The recursion relations (2.26) indicate that the flows do not terminate at a finite fixed point in quadrants II and IV of Fig. 2-2. It is possible that there is no steady state

[3]It is interesting to note that such coupling to a diffusive field leads to a larger exponent. A number of recent experiments, from immiscible displacement in porous media[35, 36] to evolution of bacterial colonies[37] observe interfaces in 1+1 dimensions with a roughness exponent near 0.8. Various other fields (e.g. fluid pressure, nutrient concentration) are certainly present in such experiments. The given example indicates that coupling to such fields may indeed lead to larger roughness exponents[38].

$\lambda_{\parallel}$	$\lambda_{\times}$	$\lambda_{\perp}$	$\nu_{\parallel}$	$z_{\parallel}$	$\nu_{\perp}$	$z_{\perp}$
20	20	20	0.48	3.0	0.48	3.0
			(1/2)	(3)	(1/2)	(3)
20	20	2.5	0.75	1.7	0.50	3.7
20	5	25	0.51	3.4	0.56	2.9
5	5	-5	0.83	unstable	0.44	3.6
				(No fixed point for finite ν, ζ)		
20	-20	-20	0.50	3.1	0.50	2.9
			(1/2)	(3)	(1/2)	(3)
5	-5	5	0.52	3.3	0.57	3.4
			(1/2)	(3)	(Strong coupling)	
20	0	20	0.49	3.1	0.72	2.2
			(1/2)	(3)	(0.75)	(2)
20	0	-20	0.48	3.0	0.65	3.1
			(1/2)	(3)	($\zeta_{\perp} > \zeta_{\parallel}$)	
20	20	0	0.84	1.4	0.50	4.0
				($\zeta_{\parallel} < \zeta_{\perp}$)	(1/2)	(4)
20	-20	0	0.55	2.9	0.51	4.0
				($\zeta_{\parallel} < \zeta_{\perp}$)	(1/2)	(4)

Table 2.1: Numerical estimates of the scaling exponents, for various values of model parameters for $n = 1$. In all cases, $D_{\parallel} = D_{\perp} = 1$ and $T_{\parallel} = T_{\perp} = 0.01$, unless indicated otherwise. Typical error bars are ± 0.05 for ν, ± 0.1 for z. Entries in parantheses are theoretical results. Exact values are given in fractional form.

n	$\nu_\parallel$	$z_\parallel$	$\zeta_\parallel$	$\nu_\perp$	$z_\perp$	$\zeta_\perp$
1	0.48	3.0	1.46	0.48	3.0	1.46
2	0.49	3.1	1.53	0.48	3.1	1.50
3	0.54	2.8	1.52	0.49	3.1	1.55
4	0.50	2.6	1.33	0.50	3.3	1.64
5	0.51	2.8	1.42	0.50	3.2	1.62
6	0.49	2.6	1.27	0.50	3.2	1.61

Table 2.2: Numerical estimates of scaling exponents for the parameter values $D_\parallel = D_\perp = 1$, $\lambda_\parallel = \lambda_\times = \lambda_\perp = 20$, and $T_\parallel = T_\perp = 0.01$, for different number of transverse components n.

in this region, and the numerical integration procedure indeed suffers instabilities caused by discretization. The exponents quoted in this regime are obtained from examining the correlation functions over short times before the instabilities take over. As such they are not reliable, at most reflecting the qualitative changes in these regions of parameter space. For the case $\lambda_\perp > 0$ and $\lambda_\times < 0$ (quadrant IV), the RG flows converge to a subspace where the CH transformation, discussed in Section 2.2, is applicable, suggesting $\nu_\parallel = 1/2$, $\zeta_\parallel = 3/2$. Since $\lambda_\perp$ remains finite, we expect $\zeta_\perp = \zeta_\parallel = 3/2$, but there is no information on $\nu_\perp$. For the case $\lambda_\perp < 0$ and $\lambda_\times > 0$, none of the methods employed give a definite result. RG exponents diverge as $\ell \to \infty$, and there are no applicable nonperturbative arguments. Numerical results show the trend towards a large $\nu_\parallel$, but fail to give a definite result due to instabilities in the discretized integration. It is possible that higher order terms in the equation of motion are necessary to determine the correct behavior of the system. When both $\lambda_\perp$ and $\lambda_\times$ have signs opposite to that of $\lambda_\parallel$, the system settles back to the scaling behavior $\nu_\alpha = 1/2$, $\zeta_\alpha = 3/2$, the RG flows terminating at the FD fixed line.

$n \geq 4$: The perturbative RG now breaks down as the expansion parameters diverge. (Specifically, $D_\perp/D_\parallel \to 0$ in quadrant I.) However, nonperturbative, i.e. exact, results still hold. In order to see the effect of increasing n, I have numerically integrated the system at the point where both the GI and FD conditions are satisfied. The measured exponents for up to $n = 6$ are given in Table 2.2. The exact swelling exponents $\nu_\parallel = \nu_\perp = 1/2$ are recovered, in compliance with the FDT condition, but the dynamical exponents seem to depart from $\zeta = 3/2$. This behavior does not conflict with the GI condition, which implies $d(\ln \lambda_\parallel)/d\ell = \nu_\parallel + \zeta - 2$, since it is possible that $\nu_\parallel + \zeta_\parallel < 2$ and $\lambda_\parallel$ is *irrelevant*. Thus there is a possibility that for large n, the system goes to a regime where the dynamical exponents are different. This region therefore needs further attention and analysis.

Finally, in Section 2.5, I discuss several generalizations of the model to directed flux lines and to drifting membranes. I also examine the relevance of long-range correlated noise, hydrodynamic interactions, and steric constraints. Surprisingly, both effects

appear to be much less important in the presence of nonlinearities.

2.2 Nonperturbative Properties

For special choices of their parameters, Eqs.(2.5) satisfy some important properties, which are addressed in this section.

2.2.1 Galilean Invariance

For $\lambda_{\|} = \lambda_{\perp}$, Eqs.(2.5) are unchanged by the infinitesimal transformation

$$\begin{cases} x' = x - \lambda_{\|}\epsilon t \ , \ t' = t \ , \\ r'_{\|} = r_{\|} + \epsilon x \ , \ r'_{\perp i} = r_{\perp i} \ , \quad (i = 1, n). \end{cases} \tag{2.8}$$

This result can be established by noting that under the change of coordinates, the derivatives transform as

$$\begin{cases} \partial_x = \partial_{x'} \ , \\ \partial_t = \partial_{t'} - \epsilon\lambda_{\|}\partial_{x'} \ . \end{cases} \tag{2.9}$$

In particular, in terms of the transformed distortions, $\partial_x r_{\|} = (\partial_{x'} r'_{\|} - \epsilon)$, while $\partial_x r_{\perp i} = \partial_{x'} r_{\perp i}$. Using this information we can rewrite Eqs.(2.5) as

$$\begin{aligned} (\partial_{t'} - \epsilon\lambda_{\|}\partial_{x'})(r'_{\|} - \epsilon x) &= D_{\|}\partial^2_{x'} r'_{\|} + \frac{\lambda_{\|}}{2}(\partial_{x'} r'_{\|} - \epsilon)^2 + \sum_{i=1}^{n} \frac{\lambda_{\times}}{2}(\partial_{x'} r'_{\perp i})^2 \\ &\quad + \eta_{\|}(x' - \lambda_{\|}\epsilon t', t'), \end{aligned} \tag{2.10}$$

$$\begin{aligned} (\partial_{t'} - \epsilon\lambda_{\|}\partial_{x'})(r'_{\perp i}) &= D_{\perp}\partial^2_{x'} r'_{\perp i} + \lambda_{\perp}(\partial_{x'} r'_{\|} - \epsilon)\partial_{x'} r'_{\perp i} \\ &\quad + \eta_{\perp i}(x' - \lambda_{\|}\epsilon t', t') \ . \end{aligned} \tag{2.11}$$

Keeping terms to order of ϵ, we see that the deterministic parts of the above equations become identical to Eqs.(2.5) for $\lambda_{\|} = \lambda_{\perp}$. The transformed noise is evaluated at a different point, but it is easy to see that its correlations still satisfy Eqs.(2.6). In fact this invariance holds even for noise that has spatial (but not temporal) correlations[29]. The significance of this invariance lies in the fact that $\lambda_{\|}$ appears both in the transformation and the equations of motion (2.5). Consequently it cannot be changed by any rescaling of the equation that preserves this invariance[13, 29]. This implies the exact exponent identity $\nu_{\|} + \zeta_{\|} = 2$, for the special case $\lambda_{\|} = \lambda_{\perp}$.

2.2.2 Generalized Cole-Hopf (CH) Transformation

The CH transformation is a useful tool in studying the exact solutions to the one component ($n = 0$) nonlinear diffusion equation[34]. Here, I extend this transformation to $n = 1$, for a specific subset in parameter space.

Consider the nonlinear complex transformation (for $\lambda_\times < 0$),

$$W(x,t) = \exp\left\{\frac{\lambda_\parallel r_\parallel(x,t) + i\sqrt{-\lambda_\parallel\lambda_\times}\, r_\perp(x,t)}{2D}\right\}. \tag{2.12}$$

Under this transformation, the linear diffusion equation

$$\partial_t W = D\partial_x^2 W + \mu(x,t)W, \tag{2.13}$$

leads to Eqs.(2.5) with $D_\parallel = D_\perp = D$ and $\lambda_\parallel = \lambda_\perp$. (Here $\mathrm{Re}(\mu) = \lambda_\parallel\eta_\parallel/2D$ and $\mathrm{Im}(\mu) = \sqrt{-\lambda_\parallel\lambda_\times}\,\eta_\perp/2D$.) This transformation enables us to solve the *deterministic* equations exactly, for any given initial conditions $r_\alpha(x,0)$. The solution to the *stochastic* equation can be written as the path integral

$$W(x,t) = \int_{(0,0)}^{(x,t)} \mathcal{D}x'(\tau)\exp\left\{-\int_0^t d\tau\left[\frac{\dot{x}'^2}{2D} + \mu(x',\tau)\right]\right\}. \tag{2.14}$$

Eq.(2.14) has been extensively studied in connection with quantum tunneling in a disordered medium[40], with W representing the wave-function. In particular, results for the tunneling probability $|W|^2$ suggest $\nu_\parallel = 1/2$ and $z_\parallel = 3$. The transverse fluctuations correspond to the phase in the quantum problem which is not an observable. Hence this mapping does not provide any information on $\nu_\perp$ and $z_\perp$ which are in fact observable in the directed polymer problem. Unfortunately, this generalization does not apply to the $n = 2$ case, therefore the arguments are not applicable to non-directed polymers.[4]

2.2.3 Fluctuation-Dissipation (FD) Condition

From the Langevin Eqs.(2.5), we can also construct a Fokker-Planck equation for the time evolution of the joint probability $\mathcal{P}\left[r_\parallel(x), r_{\perp i}(x)\right]$ for the case of uncorrelated (white) noise as

$$\partial_t\mathcal{P} = \int dx \sum_\alpha \left(\frac{\delta\mathcal{P}}{\delta r_\alpha(x)}\cdot\partial_t r_\alpha + T_\alpha\frac{\delta^2\mathcal{P}}{\delta r_\alpha^2(x)}\right). \tag{2.15}$$

Since Eqs.(2.5) are not generated from a Hamiltonian, it is not a priori clear that the above equation has a stationary solution. Nevertheless, the probability distribution

$$\mathcal{P}_0 = \exp\left(-\int dx\left[\frac{D_\parallel}{2T_\parallel}(\partial_x r_\parallel)^2 + \frac{D_\perp}{2T_\perp}\sum_i(\partial_x r_{\perp i})^2\right]\right), \tag{2.16}$$

[4]The construction in Ref.[18] for general n and its conclusions are incorrect if the matrices $\{A_\alpha\}$ of the Jordan Algebra don't commute. For $n > 1$, there are no Jordan Algebras that satisfy all the required conditions.

upon substituting in Eq.(2.15), satisfies

$$\frac{1}{\mathcal{P}_0}\frac{\partial \mathcal{P}_0}{\partial t} = -\int dx \left\{ \frac{D_\parallel \lambda_\parallel}{2T_\parallel}(\partial_x^2 r_\parallel)(\partial_x r_\parallel)^2 + \sum_i \left[\frac{D_\parallel \lambda_\times}{2T_\parallel}(\partial_x^2 r_\parallel)(\partial_x r_{\perp i})^2 + \frac{D_\perp \lambda_\perp}{T_\perp}(\partial_x^2 r_{\perp i})(\partial_x r_\parallel)(\partial_x r_{\perp i}) \right] \right\}. \tag{2.17}$$

The first term in the integrand is a complete derivative,

$$(\partial_x^2 r_\parallel)(\partial_x r_\parallel)^2 = \partial_x \left[\frac{1}{3}(\partial_x r_\parallel)^3 \right], \tag{2.18}$$

and gives no contribution to the integral, since boundary terms vanish (only profiles with $\lim_{x\to\pm\infty} \partial_x r_\alpha = 0$ have nonzero probability[41].) The remaining terms can also be combined into a complete derivative,

$$\partial_x[(\partial_x r_\parallel)(\partial_x r_{\perp i})^2] = (\partial_x^2 r_\parallel)(\partial_x r_{\perp i})^2 + 2(\partial_x r_\parallel)(\partial_x r_{\perp i})(\partial_x^2 r_{\perp i}) \tag{2.19}$$

provided that $\lambda_\times D_\parallel T_\perp = \lambda_\perp D_\perp T_\parallel$. Thus for this special choice of parameters, depicted by a starred line in Fig. 2-2, the probability distribution of Eq.(2.16) is a stationary solution of the Fokker-Planck equation. If $\mathcal{P}$ converges to this solution, the response functions of the full system are related to this stationary solution through a FDT[29, 42]. This implies a nonrenormalization of the "bare" parameters $T_\parallel/D_\parallel$ and $T_\perp/D_\perp$, which appear both in the original equation of motion (2.5) and the full response functions (2.7). Thus the long-time behavior of the correlation functions in Eq.(2.7) can be directly read off from the naive scaling of these ratios, giving $\nu_\parallel = \nu_\perp = 1/2$. For $D_\parallel = D_\perp$ and $T_\parallel = T_\perp$, the stationary distribution is identical to that of the Rouse model. However, when $D_\parallel T_\perp \neq D_\perp T_\parallel$, the average stationary shape will be a ellipsoid with $\langle r_\parallel^2\rangle/\langle r_\perp^2\rangle = D_\perp T_\parallel/D_\parallel T_\perp = \lambda_\times/\lambda_\perp$. This quantity varies continuously along the FDT subspace. The non-spherical shape results in a form birefringence that originates from the nonlinearities.

As we shall see in the following sections, the large N behavior is controlled by this subspace, at least in the low field limit. It is therefore possible to determine the nonlinearities $\{\lambda\}$ by macroscopic measurements. In order to do this, consider the situation where a stretching force $\mathbf{f}$ is applied to the two ends of the polymer. This will alter $\mathcal{P}_0$ only by the change

$$\partial_x r_\parallel \mapsto (\partial_x r_\parallel - s f_\parallel),\ \partial_x r_{\perp i} \mapsto (\partial_x r_{\perp i} - s f_{\perp i}).$$

(s is a constant describing the amount of stretching.) This modified distribution describes a rod of length proportional to sN with transverse fluctuations that scale as $\sqrt{N}$. Thus, the polymer behaves as a slender rod, and the nonlinear terms can be obtained by measuring the orientational dependence of the mobility.

2.3 Renormalization Group (RG) Analysis

The information on exponents, and the dynamic universality class, is contained in the $(k,\omega) \to 0$ limit of the noise-averaged correlations in Eq.(2.7), which after Fourier

transforming in space and time read

$$\langle r_\alpha(k,\omega) r_\alpha(k',\omega')\rangle = \delta(k+k')\delta(\omega+\omega')|k|^{\zeta_\alpha - 1 - 2\nu_\alpha} f\left(\frac{\omega}{|k|^{\zeta_\alpha}}\right). \tag{2.20}$$

Following a change of scale to $x \to bx$, accompanied by $t \to b^\zeta t$ and $r_\alpha \to b^{\nu_\alpha} r_\alpha$, Eqs.(2.5) transform into

$$b^{\nu_\parallel - \zeta}\partial_t r_\parallel = D_\parallel b^{\nu_\parallel - 2}\partial_x^2 r_\parallel + \frac{\lambda_\parallel}{2} b^{2\nu_\parallel - 2}(\partial_x r_\parallel)^2 + \frac{\lambda_\times}{2} b^{2\nu_\perp - 2}\sum_{i=1}^{n}(\partial_x r_{\perp i})^2 + b^{-(1+\zeta)/2}\eta_\parallel(x,t), \tag{2.21a}$$

$$b^{\nu_\perp - \zeta}\partial_t r_{\perp i} = D_\perp b^{\nu_\perp - 2}\partial_x^2 r_{\perp i} + \lambda_\perp b^{\nu_\parallel + \nu_\perp - 2}\partial_x r_\parallel \partial_x r_{\perp i} + b^{-(1+\zeta)/2}\eta_{\perp i}(x,t). \tag{2.21b}$$

Eq.(2.6) is used to determine the scaling of noise. We conclude that the parameters of the equations transform to

$$\begin{aligned} D_\alpha &\to b^{\zeta-2} D_\alpha, \\ T_\alpha &\to b^{\zeta - 2\nu_\alpha - 1} T_\alpha, \\ \lambda_\parallel &\to b^{\nu_\parallel + \zeta - 2}\lambda_\parallel, \\ \lambda_\perp &\to b^{\nu_\parallel + \zeta - 2}\lambda_\perp, \\ \lambda_\times &\to b^{2\nu_\perp - \nu_\parallel + \zeta - 2}\lambda_\times. \end{aligned} \tag{2.22}$$

When all three nonlinear terms are absent, the equations become scale invariant upon the choice of $\zeta = 2,\ \nu_\parallel = \nu_\perp = 1/2$. However, all three nonlinearity parameters grow under rescaling. They are therefore *relevant* and may change the scaling exponents. For example, when $\lambda_\parallel > 0,\ \lambda_\perp = \lambda_\times = 0$, Eqs.(2.5) decouple and reduce to a KPZ equation (for $r_\parallel$) and n diffusion equations (for $r_{\perp i}$), with the exponents

$$\zeta_\parallel = 3/2,\ \zeta_\perp = 2,\ \nu_\parallel = \nu_\perp = 1/2. \tag{2.23}$$

In order to calculate the exponents in the presence of nonlinearities, we can reorganize Eqs.(2.5) into a form suitable for a perturbative calculation of $\mathbf{r}(k,\omega)$ in powers of the nonlinearities $\{\lambda\}$. Fourier transforming Eqs.(2.5) in space and time, after some rearrangement, yields

$$\begin{aligned} r_\parallel(k,\omega) &\equiv G_\parallel(k,\omega)\eta_\parallel(k,\omega) \\ &= G_{0\parallel}(k,\omega)\eta_\parallel(k,\omega) - \frac{\lambda_\parallel}{2}\int\frac{d\Omega}{2\pi}\int^{\Lambda}\frac{dq}{2\pi} q(k-q) r_\parallel(q,\Omega) r_\parallel(k-q,\omega-\Omega) \\ &\quad - \frac{\lambda_\times}{2}\sum_i \int\frac{d\Omega}{2\pi}\int^{\Lambda}\frac{dq}{2\pi}\, q(k-q)\, r_{\perp i}(q,\Omega) r_{\perp i}(k-q,\omega-\Omega), \end{aligned} \tag{2.24a}$$

$$\begin{aligned} r_{\perp i}(k,\omega) &\equiv G_\perp(k,\omega)\eta_{\perp i}(k,\omega) \\ &= G_{0\perp}(k,\omega)\eta_{\perp i}(k,\omega) - \lambda_\perp \int\frac{d\Omega}{2\pi}\int^{\Lambda}\frac{dq}{2\pi}\, q(k-q)\, r_{\perp i}(q,\Omega) r_\parallel(k-q,\omega-\Omega). \end{aligned} \tag{2.24b}$$

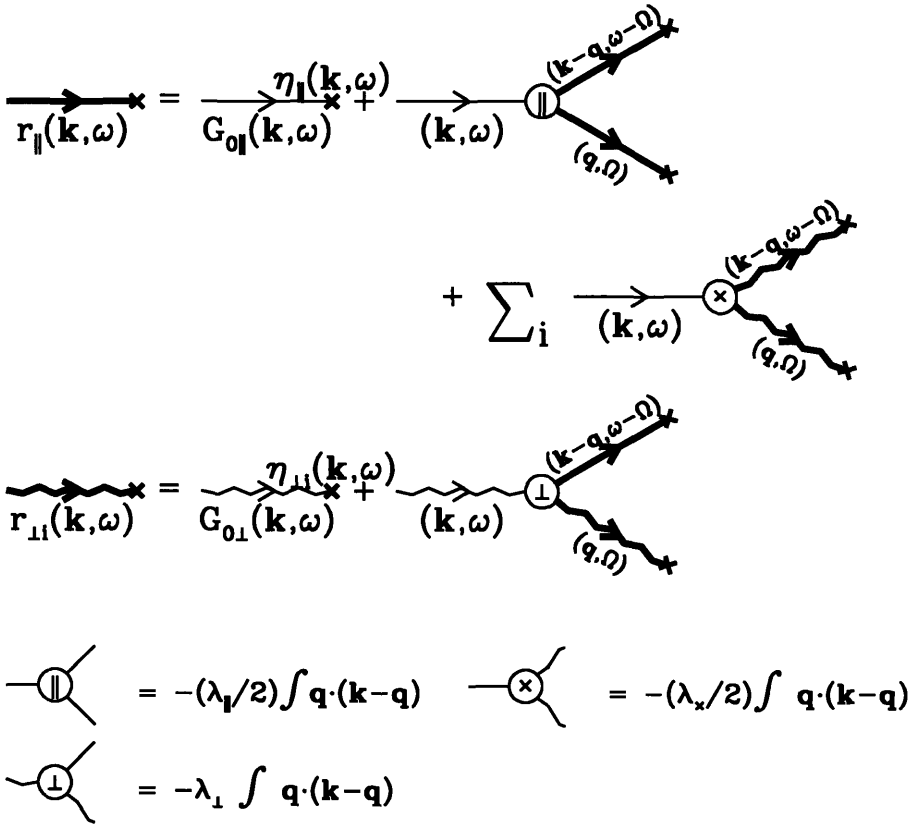

Figure 2-3: Diagrammatic representation of the nonlinear integral equations (2.24).

Here, $G_{0\alpha}$'s are bare propagators $(D_\alpha k^2 - i\omega)^{-1}$, in the absence of nonlinearities, and Λ is a suitable short distance cutoff. This set of nonlinear integral equations is indicated diagrammatically in Fig. 2-3. The averaging is done using the Fourier transform of Eqs.(2.6), which reads

$$\langle \eta_\alpha(k,\omega)\eta_\beta(k',\omega')\rangle = 2T_\alpha \delta_{\alpha,\beta}\delta(k+k')\delta(\omega+\omega'). \tag{2.25}$$

The perturbative expressions for the effective response functions $G_\parallel, G_\perp$ are represented diagrammatically in Fig. 2-4. (The combinatorial factor for each diagram is found by counting all possible noise contractions that give rise to it.) Actually, the dimensionless perturbative parameters are of the form $\lambda^2 T/D^3$. Since $G_0(k,0) = 1/Dk^2$, one can define an effective tension $\tilde{D}$ from $G(k,0) = 1/\tilde{D}k^2$. Similarly, an effective spectral density function $\tilde{T}(k,\omega)$ is defined by

$$\langle r^*_\alpha(k,\omega) r_\alpha(k,\omega)\rangle = 2\tilde{T}_\alpha(k,\omega) G_\alpha(k,w) G_\alpha(-k,-w),$$

and calculated perturbatively by the series shown in Fig. 2-5. Effective vertex functions are similarly computed perturbatively by the series shown in Fig. 2-6. The corrections to the bare parameters diverge at small loop momenta. I therefore reorganize the summation of these corrections in order to avoid singularities. The RG procedure works as follows: We average noise over a momentum shell $\Lambda e^{-\ell} < |k| < \Lambda$ and find the contribution of this averaging to the parameters, after which we make a change of scale $x \to e^\ell x$, $t \to e^{\zeta\ell} t$, $r_\parallel \to e^{\nu_\parallel \ell} r_\parallel$, $r_{\perp i} \to e^{\nu_\perp \ell} r_{\perp i}$. This procedure gives rise to recursion relations for the effective parameters in Eqs.(2.5). The calculations are lengthy and not particularly instructive as straightforward generalization of those in ref.[29]. Details of the calculation are given in Appendices 2C, 2D and 2E. The resulting recursion relations are

$$\frac{dD_\parallel}{d\ell} = D_\parallel \left[\zeta - 2 + K_1 \frac{\lambda_\parallel^2 T_\parallel}{4D_\parallel^3} + nK_1 \frac{\lambda_\perp \lambda_\times T_\perp}{4D_\parallel D_\perp^2} \right], \tag{2.26a}$$

$$\frac{dD_\perp}{d\ell} = D_\perp \left[\zeta - 2 + K_1 \frac{\lambda_\perp[(\lambda_\times T_\perp/D_\perp) + (\lambda_\perp T_\parallel/D_\parallel)]}{2D_\perp(D_\perp + D_\parallel)} + K_1 \frac{D_\perp - D_\parallel}{D_\perp + D_\parallel} \frac{\lambda_\perp[(\lambda_\times T_\perp/D_\perp) - (\lambda_\perp T_\parallel/D_\parallel)]}{D_\perp(D_\perp + D_\parallel)} \right], \tag{2.26b}$$

$$\frac{dT_\parallel}{d\ell} = T_\parallel \left[\zeta - 2\nu_\parallel - 1 + K_1 \frac{\lambda_\parallel^2 T_\parallel}{4D_\parallel^3} \right] + nK_1 \frac{\lambda_\times^2 T_\perp^2}{4D_\perp^3}, \tag{2.26c}$$

$$\frac{dT_\perp}{d\ell} = T_\perp \left[\zeta - 2\nu_\perp - 1 + K_1 \frac{\lambda_\perp^2 T_\parallel}{D_\perp D_\parallel (D_\perp + D_\parallel)} \right], \tag{2.26d}$$

$$\frac{d\lambda_\parallel}{d\ell} = \lambda_\parallel \left[\nu_\parallel + \zeta - 2 \right], \tag{2.26e}$$

$$\frac{d\lambda_\perp}{d\ell} = \lambda_\perp \left[\nu_\parallel + \zeta - 2 - K_1 \frac{\lambda_\parallel - \lambda_\perp}{(D_\perp + D_\parallel)^2} [(\lambda_\times T_\perp/D_\perp) - (\lambda_\perp T_\parallel/D_\parallel)] \right], \tag{2.26f}$$

$$\frac{d\lambda_\times}{d\ell} = \lambda_\times \left[2\nu_\perp - \nu_\parallel + \zeta - 2 + K_1 \frac{\lambda_\parallel D_\perp - \lambda_\perp D_\parallel}{D_\perp D_\parallel (D_\perp + D_\parallel)} [(\lambda_\times T_\perp/D_\perp) - (\lambda_\perp T_\parallel/D_\parallel)] \right]. \tag{2.26g}$$

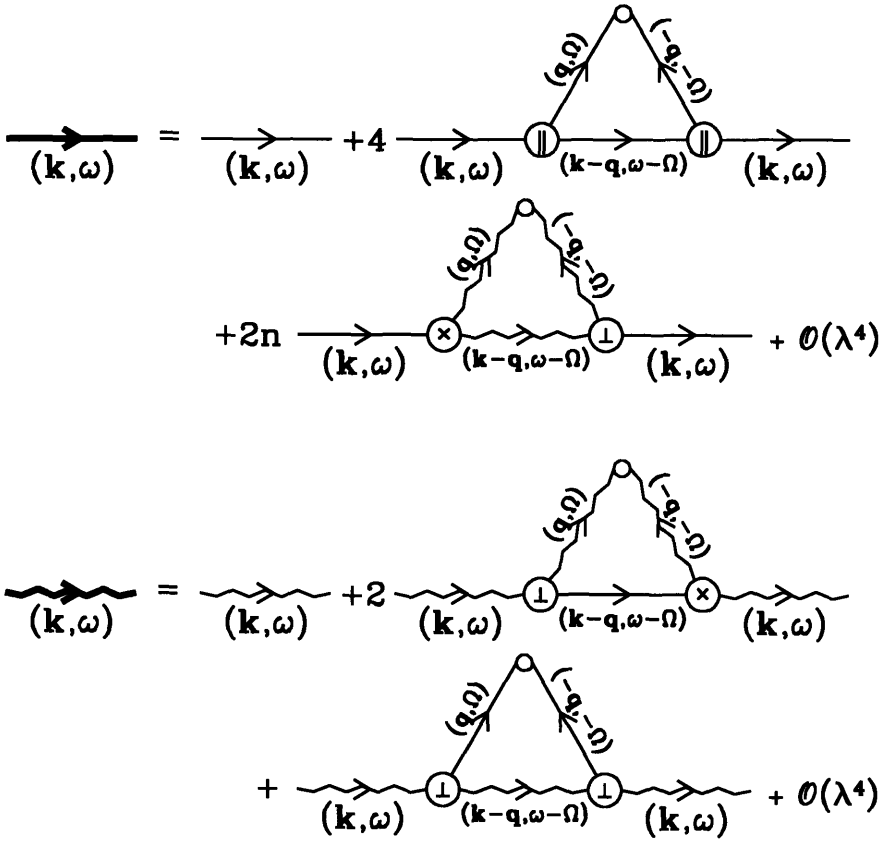

Figure 2-4: Leading corrections to the longitudinal and transverse propagators $G_{\|}, G_{\perp}$ in the perturbative expansion of Fig. 2-3, after averaging over noise.

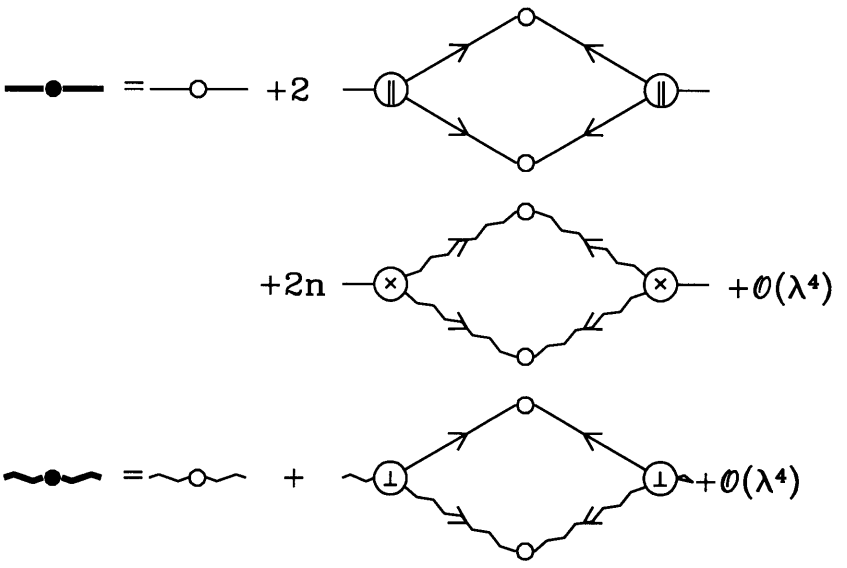

Figure 2-5: Leading corrections to the spectral density functions $T_{\|}, T_{\perp}$.

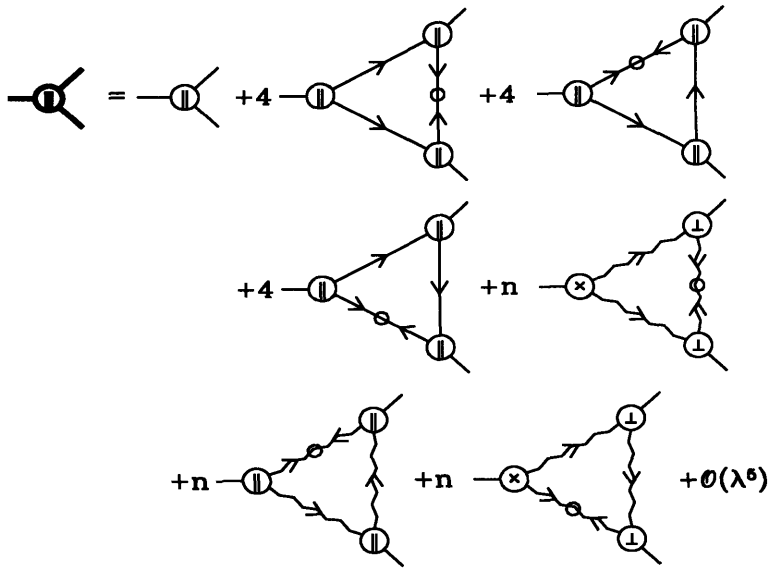

$$\Gamma_{\|} = \Gamma_{0\|}+\Gamma_{\|a}+\Gamma_{\|b}+\Gamma_{\|c}+\Gamma_{\|d}+\Gamma_{\|e}+\Gamma_{\|f}+\mathcal{O}(\lambda^5)$$

(a)

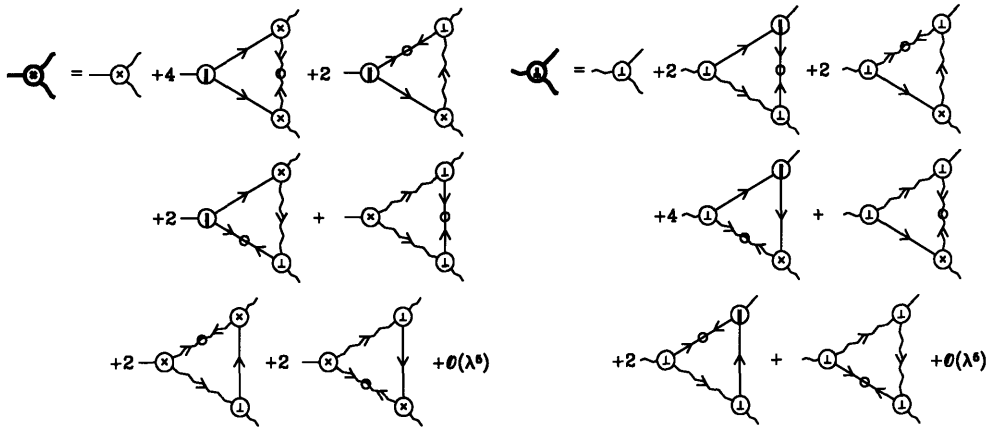

(b) (c)

Figure 2-6: Leading corrections to the vertex functions (a) $\Gamma_{\|}$, (b) $\Gamma_{\times}$, and (c) $\Gamma_{\perp}$.

Starting from a given set of "bare" parameters, the RG flows are generated by integrating these differential equations, corresponding to a repeated application of an infinitesimal renormalization of the system. The exponents $\zeta(\ell)$ and $\nu_{\|}(\ell)$ are chosen such that $D_{\|}$ and $\lambda_{\|}$ remain scale invariant, i.e.

$$\frac{dD_{\|}}{d\ell} = \frac{d\lambda_{\|}}{d\ell} = 0.$$

The exponent $\nu_{\perp}$ can actually be eliminated from the recursion relations by considering the renormalization of $\lambda_{\times}T_{\perp}$ since only this combination appears in the recursion relations. The value of this exponent can later be determined by demanding scale invariance for each of the parameters $\lambda_{\times}, T_{\perp}$ separately. This way, the flow of all the parameters is determined, along with the scaling exponents. The RG flows and resulting exponents are indicated in Fig. 2-2 and Table 2.1, respectively. The resulting flows naturally satisfy the constraints imposed by the non-perturbative results: the subspace of GI is closed under RG, while the FD condition appears as a *fixed line.*

Different dynamical exponents

With the above RG procedure it is difficult to address circumstances when the different components have *distinct* dynamical scaling. As long as the "fixed point equations" are coupled, it is natural to choose $\zeta_{\|} = \zeta_{\perp}$. However, when $\zeta_{\|} \neq \zeta_{\perp}$, the RG flows terminate at a region of parameter space that is not perturbatively accessible. In order to demonstrate this, let us examine a simpler set of equations:

$$\partial_t h_1 = D_1 \partial_x^2 h_1,$$
$$\partial_t h_2 = D_2 \partial_x^4 h_2.$$

These equations can be solved exactly; the dynamical exponents are $\zeta_1 = 2$, $\zeta_2 = 4$. However, when we rescale them together and choose ζ to keep D_1 fixed, we see that $D_2 \to 0$. As long as the equations are decoupled, one can still recover ζ_2 by examining how D_2 flows to the fixed point. But Eqs.(2.26) involve parameters that diverge at such a fixed point. Since the whole RG treatment is only perturbative, a divergence of any perturbative parameter invalidates its results. A different RG treatment or a self-consistent approach[43, 44] may eliminate such problems and enable a systematic analysis of the whole parameter space. I have investigated such regions numerically in order to determine what kinds of properties one might expect. It is also not clear whether such regions of parameter space are accessible to physical systems.

Fixed points and scaling

The scaling behaviors for the different regions in Fig. 2-2 are determined by the values of the exponents at the attracting fixed point(s). The results are presented below:

$\lambda_{\perp} > 0$ *and* $\lambda_{\times} > 0$: In this quadrant (I), for $n < 4$, the RG flows terminate on the fixed line where FD conditions apply, hence $\nu_{\|} = \nu_{\perp} = 1/2$. All along this line, the one loop RG exponent is $\zeta = 3/2$. When $n \geq 4$, the flows indicate that $D_{\perp} \to 0$, even though $\lambda_{\perp}$ remains finite, and RG is inconclusive. The reason for the breakdown

of RG is again the non-perturbative nature of the fixed point. A different scheme is needed when the perturbative parameters diverge[43, 44].

$\lambda_\perp < 0$ *and* $\lambda_\times > 0$: The analysis of this region (II) is the most difficult in that the RG flows do not converge upon a finite fixed point *and* $\lambda_\perp \to 0$. Hence we expect $\zeta_\parallel \neq \zeta_\perp$, and a different RG scheme is necessary.

$\lambda_\perp < 0$ *and* $\lambda_\times < 0$: The FD condition again provides a stable fixed line in this quadrant (III), hence $\nu_\parallel = \nu_\perp = 1/2$ and for $n < 4$, the one-loop RG gives $\zeta = 3/2$. For $n \geq 4$, the RG is once again inconclusive.

$\lambda_\perp > 0$ *and* $\lambda_\times < 0$: For $n = 1$, the *projected* RG flows in this quadrant (IV) converge to the point $\lambda_\perp/\lambda_\parallel = 1$ and $\lambda_\times T_\perp D_\parallel/\lambda_\parallel T_\parallel D_\perp \approx -0.386$. However, this is not a fixed point, as the noise parameters $T_\parallel$ and $T_\perp$ scale to infinity. Therefore, it is not possible to determine the exponents. Fortunately, the CH transformation is applicable to this point, this suggests $\zeta_\parallel = 3/2$ and $\nu_\parallel = 1/2$.

$\lambda_\times = 0$: In this case the equation for $r_\parallel$ is identical to that of an interface in 1+1 dimensions, and $\nu_\parallel = 1/2$, with $\zeta_\parallel = \zeta_\perp = 3/2$ (since $\lambda_\perp \neq 0$). The fluctuations in $r_\parallel$ act as a strong (multiplicative and correlated) noise on $r_{\perp i}$. The one-loop RG yields an exponent $\nu_\perp = 0.75$ for $\lambda_\perp > 0$, while for $\lambda_\perp < 0$, $\lambda_\perp$ scales to 0 and hence the RG is inconclusive except for implying $\zeta_\perp > \zeta_\parallel$. This result is independent of n.

$\lambda_\perp = 0$: The transverse fluctuations satisfy a simple diffusion equation with $\nu_\perp = 1/2$ and $\zeta_\perp = 2$. Through the term $\lambda_\times(\partial_x r_{\perp i})^2/2$, these fluctuations act as a correlated noise[29] for the longitudinal mode. Since $\zeta_\parallel \neq \zeta_\perp$, the RG is once again inconclusive. Simulations (Table 2.1) indicate different behavior depending on the sign of $\lambda_\times$. This dependence on the sign of $\lambda_\times$ is not too surprising in view of the fundamental difference between behaviors in quadrants II and IV of Fig. 2-2.

2.4 Numerical Simulations

In this section, I discuss the numerical integration of Eqs.(2.5), for various parameter values, to provide a comparison to the RG results. Such simulations have been quite successful in obtaining the scaling properties of the interface growth equation[45]. I use the following discretized equations:

$$\begin{aligned} r_\parallel(x,t+dt) &= r_\parallel(x,t) + D_\parallel[r_\parallel(x+1,t) - 2r_\parallel(x,t) + r_\parallel(x-1,t)]dt \\ &\quad + \frac{\lambda_\parallel}{8}[r_\parallel(x+1,t) - r_\parallel(x-1,t)]^2 dt \\ &\quad + \frac{\lambda_\times}{8}\sum_i [r_{\perp i}(x+1,t) - r_{\perp i}(x-1,t)]^2 dt + \sqrt{2T_\parallel dt}\ \psi_\parallel(x,t), \end{aligned} \tag{2.27}$$

$$\begin{aligned} r_{\perp i}(x,t+dt) &= r_{\perp i}(x,t) + D_\perp[r_{\perp i}(x+1,t) - 2r_{\perp i}(x,t) + r_{\perp i}(x-1,t)]dt \\ &\quad + \frac{\lambda_\perp}{4}[r_{\perp i}(x+1,t) - r_{\perp i}(x-1,t)]^2 dt + \sqrt{2T_\perp\ dt}\ \psi_{\perp i}(x,t). \end{aligned} \tag{2.28}$$

Here, ψ_α are random variables with zero mean and standard deviation of unity, independently chosen for each time step and each site.

Simulations were carried out starting from a point initial state, with periodic boundary conditions. The time step was chosen small enough to avoid short range

instabilities, typically 0.005 to 0.05. At every step, the center of mass motion of the polymer was subtracted off, so that $\overline{r}_\alpha(t) = 0$. The scaling exponents were extracted as follows: The mean squared radii $\langle R_\alpha(t,N)\rangle = \langle (N^{-1}\sum_{j=1}^{N}[r_\alpha(j,t)]^2)^{1/2}\rangle$ have the dynamical scaling form

$$\langle R_\alpha(t,N)\rangle = N^{\nu_\alpha} f_\alpha^R\left(\frac{N^{\zeta_\alpha}}{t}\right), \tag{2.29}$$

where the scaling functions f_α^R have the asymptotic behaviors

$$\lim_{u\to\infty} f_\alpha^R(u) = A_\alpha u^{-1/z_\alpha}, \text{ and } \lim_{u\to 0} f_\alpha^R(u) = B_\alpha, \tag{2.30}$$

with A_α, B_α being constants. Therefore, the large t, i.e. steady state, behavior of R_α scales as N^{ν_α}, whereas the large N, small t behavior grows as t^{1/z_α}. For the steady state analysis, time averages (instead of ensemble averages, for computational convenience) of $R_\alpha(t,N)$ were calculated for system sizes $N = 16,\ 32,\ 64,\ 128$ and 256 after the system reached steady state. For the dynamic analysis, system width was calculated as a function of time for $N = 10000$ to 60000, up to $t = 300$. Numerical integrations were performed for different sets of parameters and for different values of n in Eqs.(2.5), with emphasis on $n = 1$. A sample result for the parameters $D_\parallel = D_\perp = 1$, $\lambda_\parallel = \lambda_\times = \lambda_\perp = 20$, $T_\parallel = T_\perp = 0.01$ is shown in Fig. 2-7. Not all exponents correspond to the true asymptotic values, due to finite size effects. The results of the integrations can be summarized as follows:

The exponents for $n = 1$, along with theoretical predictions, are indicated in Table 2.1. Most of the theoretical predictions are supported by these simulations. At the point where GI and FD conditions hold, the exponents match well with the theoretical values. We also see the change in scaling behavior when $\lambda_\times$ or $\lambda_\perp$ approach zero, as predicted by Eqs.(2.26). The values for swelling exponents for small but positive values of $\lambda_\times$ or $\lambda_\perp$ signify a large crossover regime, with enhanced effective swelling exponents. The exponents are expected to approach $1/2$ at larger length scales. This crossover is also evident in the RG equations (2.26), and the flows in Fig. 2-2. In all cases where the RG method was inconclusive, simulations have either suggested $\zeta_\parallel \neq \zeta_\perp$ or the integration scheme has been unstable in the fully nonlinear regime. A more reliable (and computationally demanding) integration scheme must be used to determine the true asymptotic behavior of these regimes.

It is interesting that even though the nonperturbative properties apply to all n, the perturbative RG breaks down for $n \geq 4$. I therefore integrated the equations for different n at the point where GI and FD conditions were satisfied, in order to search for a potential change in scaling properties. Although the results (Table 2.2) are not completely conclusive, there is strong evidence that $\zeta_\parallel < 3/2 < \zeta_\perp$ for $n > 3$, which is consistent with the RG prediction $D_\perp(\ell)/D_\parallel(\ell) \to 0$. It will be interesting to study the large n behavior of this system, where it might be possible to obtain a $1/n$ expansion that becomes exact for $n \to \infty$.

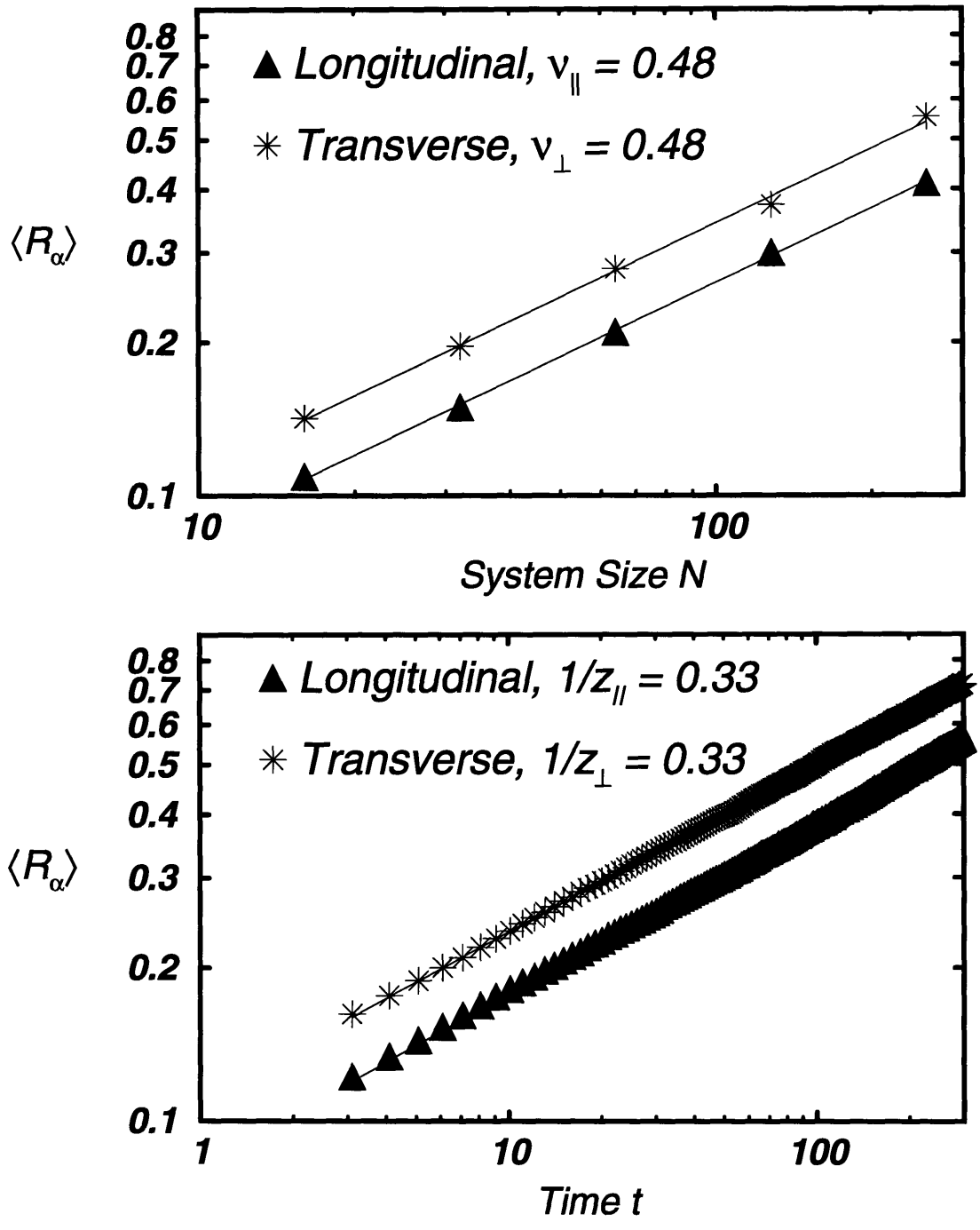

Figure 2-7: *Top*: The longitudinal and transverse sizes of the polymer as a function of its length N. *Bottom*: Same quantities as a function of time t. The straight lines indicate fits to scaling forms $R \propto N^{\nu}$ and $R \propto t^{1/z}$. Points corresponding to transverse size are shifted up by 30% to avoid data overlap.

2.5 Discussion and Conclusions

In this work I studied, on the basis of symmetry considerations, a phenomenological model for the relaxation of a polymer drifting due to an external force. In a *local* description nonlinear terms are proposed to describe the dependence of the velocity on the orientation and extension of the polymer. The nonlinearities are relevant, and (for most values of parameters) lead to faster relaxation with a dynamic exponent $z = 3$. The structure factor of the polymer becomes anisotropic as a function of the driving force, and it is even possible for the polymer to undergo a stretching transition. These results could potentially be probed by diffraction and birefringence experiments on sedimenting polymers, or by examining conformations of polymers during electrophoresis. There are other potential applications of the results to defect lines in liquid crystals or flux lines in superconductors. However, this description leaves out a number of potentially important interactions and constraints, such as noise correlations, self-avoidance and hydrodynamic interactions, reparametrization invariance or arc length conservation[46]. A number of possible extensions and generalizations are discussed below.

2.5.1 Flux Lines

A flux line (FL) is stretched parallel to the direction of the external magnetic field. In the presence of a bulk current, the FL moves due to the Lorentz force. The fluctuations of such a directed line are also described[47] by Eqs.(2.5), with $n = 1$. In this case $r_{\|}$ denotes fluctuations along the direction of average motion, and $r_{\perp i}$ are the fluctuations in the remaining $n = d - 2$ directions. Thus, all of the calculated exponents apply to the drifting FL as well. The dynamics of a FL in three dimensions close to depinning is discussed in much greater detail in Chapter 3.

2.5.2 Drifting Manifolds

We can similarly consider the fluctuations of a membrane drifting with an average velocity. In this case two coordinates are needed to describe a point on the membrane. More generally we can consider a d_s dimensional manifold embedded in a d dimensional space. (Yet another realization is the coupling of a growing interface to a set of scalar fields.) Except for the change in the dimensionality of the argument $\mathbf{x} = (x_1, \cdots, x_{d_s})$, there is no change in Eqs.(2.5). The only changes in the recursion relations (2.26) come from the rescaling of noise and from angular averages in k-space, which appear as overall constants in the correction terms. In the absence of nonlinearities, the Langevin equations are scale invariant with $\zeta_\alpha = 2$, $\nu_\alpha = (2-d_s)/2$. This swelling exponent is characteristic of tethered manifolds[48]. Thus, for $d_s > 2$, small nonlinearities rescale to zero and are *irrelevant*. In such cases, there is also typically a strong coupling ($\lambda \neq 0$) region that is not accessible by perturbative methods. For $d_s < 2$, which includes the case extensively discussed, the nonlinearities are relevant, changing the exponents. Perturbation theory breaks down at $d_s = 2$, and more careful analysis is necessary to obtain correct results. Furthermore, the nonperturbative

properties discussed, other than GI, no longer hold for $d_s \neq 1$, limiting our knowledge of the problem.

2.5.3 Noise Correlations

Starting from a microscopic point of view, Eqs.(2.5) are obtained by removing the "fast" degrees of freedom associated with the surrounding fluid. The resulting noise, η, may acquire long-range correlations in both space and time as a result of this coarse graining. The effects of such correlations have been studied extensively in ref.[29], for the case $n = 0$. It is straightforward, though somewhat lengthy, to extend the analysis to $n > 0$. Consider noise-noise correlations that asymptotically behave as

$$\langle \eta(k,\omega)\eta(k',\omega') \rangle \sim k^{-2\rho}\omega^{-2\theta}\delta(k+k')\delta(\omega+\omega'). \tag{2.31}$$

The effects of these correlations on scaling exponents depend on the relative signs of nonlinearities, as in the case of uncorrelated noise. For example, For $\theta = 0$, (spatial correlations *only*) it can be shown that when all three nonlinearities have the same sign (quadrant I in Fig. 2-2), the *renormalized* spectrum is white noise as long as $2\rho < 2\rho_c = 3\nu - 1 = 1/2$. There are no corrections to the scaling exponents calculated without any correlations. The fluctuation-dissipation condition for *uncorrelated noise*, suggests an effective "mean-field" noise spectrum characterized by $\rho = \rho_c$. It is precisely for this reason that all correlations decaying more (or equally) rapidly are irrelevant. For $\rho > \rho_c$, the noise spectrum is unrenormalized, except for acquiring a white noise part, i.e. $T(k) = T_0 + T_\rho k^{-2\rho}$. This results in modified exponents, *exactly* given by the reduced $z = (5-2\rho)/(1+2\rho)$, and the increased $\nu = (1+2\rho)/3$ as in ref.[29]. On the other hand, when $\lambda_\perp = 0$ and $\lambda_\times \neq 0$, the scaling exponents change for $\rho > 0$, as the transverse noise spectrum is unrenormalized (except for acquiring a white noise part) while the longitudinal correlations are irrelevant for all $\rho \geq 0$. The resulting RG exponents are

$$\begin{aligned} z_\parallel &= (4-4\rho)/(2+4\rho),\ \nu_\parallel = (2+4\rho)/3, \\ z_\perp &= 4/(1+2\rho),\ \nu_\perp = (1+2\rho)/2. \end{aligned}$$

The continuum description naturally breaks down when the chain is fully stretched at $\nu \geq 1$. Temporal correlations, $\theta \neq 0$, complicate the situation by breaking Galilean invariance.

2.5.4 Hydrodynamic Interactions

In constructing equations (2.5), we only allowed for local effects, and ignored the nonlocalities that are the hallmark of hydrodynamics. I shall now demonstrate that (somewhat surprisingly) non-local terms are less important at our nonlinear fixed point that at the corresponding Rouse fixed point. One consequence of hydrodynamic interactions is the *back-flow* velocity in Eq.(2.2) that can be added to the evolution equations (2.5). The approximations leading to Eq.(2.2) make this term linear and its main effect is changing the long wavelength behavior of the bare propagator from

$1/q^2$ to $1/q^{3/2}$. Also for the linear Zimm equation to satisfy a fluctuation-dissipation condition, the noise spectrum must be correlated with $2\rho = 1 - \nu$ and $\theta = 0$ in Eq.(2.31). Since our non-linear fixed point also satisfies a fluctuation-dissipation condition, as demonstrated in the previous section, such noise correlations are not relevant, and do not modify the exponents obtained from uncorrelated (local) noise. As for the modified propagator, in d-dimensional space, it acquires an additional term proportional to $q^{d/2}$, with scaling dimension $y_H = \zeta - d/2$. Thus for $d > 3$ the long-range hydrodynamic interactions can be ignored and the scaling exponent $\zeta = 3/2$ is imposed by the nonlinearities. In dimensions $d < 3$ the hydrodynamic interactions are the most relevant, setting $\zeta = d/2$, and the nonlinear terms are irrelevant. In $d = 3$ both terms are equally relevant, and fixed points most likely occur at finite values of both parameters. A more rigorous RG treatment is required to confirm this picture, and establish the behavior when both effects are present. In any case it is clear that due to their marginal relevance, the interactions of Eq.(2.2) will not substantially modify previous results. However, once non-local terms are included there is no reason to rule out the non-local nonlinearity obtained by replacing $\partial_x^2\mathbf{R}$ is Eq.(2.2) by $(\partial_x\mathbf{R})^2$. This nonlinearity also becomes important at the same point when the $\{\lambda\}$ terms become important. It could have important consequences which are left for future studies.

2.5.5 Steric Interactions

Self-avoidance and entanglement effects are important in low dimensions. The latter are difficult to incorporate and have not been satisfactorily explained. 'Soft'-core repulsions can be incorporated in a Hamiltonian and the corresponding equations of motion as an additional term proportional to $b\int dx'\mathcal{V}(\mathbf{r}(x) - \mathbf{r}(x'))$. The relevance of this term is controlled by the scaling dimension $y_{SA} = \zeta - d/2$. This is a rather surprising result, in that the enhanced relaxation actually makes self-avoidance less relevant. If this conclusion is indeed correct, the added constraints should not significantly modify the results in $d = 3$.

Appendix

2A Derivation of the Equation of Motion

In this appendix, I present the derivation of Eqs.(2.5) from Eq.(2.4). This is accomplished by a Taylor expansion of $\mathbf{F}$ around $\partial_x R_\alpha = \partial_x^2 R_\alpha = 0$, up to second order and ignoring higher order gradients. Eliminating terms inconsistent with symmetries, we obtain

$$\partial_t R_\alpha = v_\alpha + Q_\alpha^\beta \partial_x^2 R_\beta + \frac{1}{2} T_\alpha^{\beta\gamma} \partial_x R_\beta \partial_x R_\gamma + h.o.t., \tag{2.32}$$

where v, Q, T are tensors of first, second and third rank, determined only by $\mathbf{e}(x,t)$. Terms proportional to R_α and $\partial_x R_\alpha$ are excluded because of the symmetries $\mathbf{R} \mapsto \mathbf{R} + \mathbf{c}$ and $x \mapsto -x$, respectively. The remaining terms are of higher order in the

derivatives. Since the external field $\mathbf{E}$ is the only source of breaking isotropy, it appears in these tensors as

$$\begin{aligned} v_\alpha &= a_1 E_\alpha + (a_2\delta_\alpha^\beta + a_3 E_\alpha E_\beta)\delta e_\beta + \mathcal{O}(||\delta\mathbf{e}||^2), \\ Q_\alpha^\beta &= b_1\delta_\alpha^\beta + b_2 E_\alpha E_\beta + \mathcal{O}(||\delta\mathbf{e}||), \\ T_\alpha^{\beta\gamma} &= c_1(\delta_\alpha^\beta E_\gamma + \delta_\alpha^\gamma E_\beta) \\ &\quad + c_2\delta_\beta^\gamma E_\alpha + c_3 E_\alpha E_\beta E_\gamma + \mathcal{O}(||\delta\mathbf{e}||). \end{aligned} \tag{2.33}$$

Here a_j, b_j and c_j are constants, and we have neglected (irrelevant) higher order effects of fluctuations.

The first term in the expansion of v_α is a constant and can be absorbed by defining

$$\mathbf{r}(x,t) = \mathbf{R}(x,t) - a_1\mathbf{E}t.$$

Choosing the coordinate axes such that $E_\parallel = E$, $E_{\perp i} = 0$; and defining

$$\begin{aligned} D_\parallel &= b_1 + b_2 E^2, \\ D_\perp &= b_1, \\ \lambda_\parallel &= (2c_1 + c_2)E + c_3 E^3, \\ \lambda_\times &= c_2 E, \\ \lambda_\perp &= c_1 E, \\ \eta_\parallel &= (a_2 + a_3 E^2)\delta e_\parallel, \\ \eta_\perp &= a_2\delta e_\perp, \end{aligned} \tag{2.34}$$

we immediately arrive at Eqs.(2.5) and (2.6) with

$$\begin{aligned} 2T_\parallel &= d^{-1}(a_2 + a_3E^2)^2\langle||\delta\mathbf{e}||^2\rangle, \\ 2T_\perp &= d^{-1}a_2^2\langle||\delta\mathbf{e}||^2\rangle. \end{aligned} \tag{2.35}$$

2B Derivation of Leading Nonlinear Terms from Slender Body Hydrodynamics

In this appendix, I will derive the leading order *local* nonlinearities in the equation of motion (2.5) in the low Reynolds number limit. In order to do this, consider a rodlike conformation of the polymer with monomer length b_0 where $\partial_x r_\alpha = b_0 t_\alpha$ everywhere on the polymer, so that the elastic (Rouse) force vanishes. If a uniform force $\mathbf{E}$ per monomer acts on this rod, the velocity of the rod can be solved using Kirkwood Theory, and the result is (Chapter 8 in Ref. [19])

$$\mathbf{v} = \frac{(-\ln\kappa)}{4\pi\eta_s b_0}\mathbf{E}\cdot[\mathbf{I} + \mathbf{tt}]. \tag{2.36}$$

In the above equation, η_s is the solvent viscosity, $\mathbf{t}$ is the unit tangent vector, $\kappa = 2b/b_0N$ is the ratio of the width b to the half length $b_0N/2$ of the polymer. Direct comparison with Eqs.(2.32) and (2.33) gives

$$a_1 + \frac{c_2}{2} = C,\ c_1 = C,\ c_3 = 0,$$

where $C = (-\ln\kappa)/4\pi\eta_s b_0$. A more detailed calculation of the force in the more general case of an arbitrarily shaped slender body by Khayat and Cox[28] shows that *nonlocal* contributions to the force, which depend on the whole shape of the polymer rather than the local orientation, are $\mathcal{O}(1/(\ln\kappa)^2)$. Therefore, corrections to Eq.(2.36) are small when $N \gg b/b_0$. However, the calculation in [28] assumes that the radius of curvature at every point is $\mathcal{O}(Nb_0)$, therefore one may argue that nonlocal corrections are small only if the persistence length is much larger than the polymer width. This analysis does not give the value for a_1, but an approximate expression can be found by using the Rouse Model, which is essentially the $\lambda = 0$ limit. In that case, the friction coefficient for a monomer of diameter b_0 is $3\pi\eta_s b_0$, i.e.

$$\mathbf{v} = \frac{1}{3\pi\eta_s b_0}\mathbf{E},$$

which gives

$$a_1 = \frac{1}{3\pi\eta_s b_0}.$$

Therefore, $a_1 \ll C$ if $|\ln\kappa| \gg 1$. We can now use Eq.(2.34) to calculate the nonlinearity parameters:

$$\lambda_{\parallel} = 4(C - a_1/2)E,\ \lambda_{\times} = 2(C - a_1)E,\ \lambda_{\perp} = CE.$$

All three nonlinearities are positive in this low-field limit.

2C Propagator Renormalization

In the following appendices, the details of the RG procedure is given for an arbitrary manifold dimension d_s, as mentioned in Section 2.5. (The discussion in Sections 2.1 to 2.4 involves the case $d_s = 1$ only.) I start from the symmetrized versions of the one-loop expressions depicted in Fig. 2-4. Thus, to leading order in the nonlinearity, the propagators are given as

$$\begin{aligned} G_{\parallel}(\mathbf{k},\omega) \;=\; & G_{0\parallel}(\mathbf{k},\omega) \\ & + G_{0\parallel}^2(\mathbf{k},\omega)\left\{4\left(-\frac{\lambda_{\parallel}}{2}\right)^2 \int_{\mathbf{q}}\int_{\Omega} \left(\mathbf{q}+\tfrac{\mathbf{k}}{2}\right)\cdot\left(\mathbf{q}-\tfrac{\mathbf{k}}{2}\right)\ \mathbf{k}\cdot\left(\mathbf{q}+\tfrac{\mathbf{k}}{2}\right)\right. \\ & \quad \times 2T_{\parallel} G_{0\parallel}\left(\mathbf{q}-\frac{\mathbf{k}}{2},\frac{\omega}{2}-\Omega\right)\left|G_{0\parallel}\left(\mathbf{q}+\frac{\mathbf{k}}{2},\frac{\omega}{2}+\Omega\right)\right|^2 \\ & + 2n\left(-\frac{\lambda_{\times}}{2}\right)(-\lambda_{\perp})\int_{\mathbf{q}}\int_{\Omega} \left(\mathbf{q}+\tfrac{\mathbf{k}}{2}\right)\cdot\left(\mathbf{q}-\tfrac{\mathbf{k}}{2}\right)\ \mathbf{k}\cdot\left(\mathbf{q}+\tfrac{\mathbf{k}}{2}\right) \\ & \quad \left.\times 2T_{\perp} G_{0\perp}\left(\mathbf{q}-\frac{\mathbf{k}}{2},\frac{\omega}{2}-\Omega\right)\left|G_{0\perp}\left(\mathbf{q}+\frac{\mathbf{k}}{2},\frac{\omega}{2}+\Omega\right)\right|^2\right\}, \end{aligned} \tag{2.37a}$$

$$
\begin{aligned}
G_\perp(\mathbf{k},\omega) &= G_{0\perp}(\mathbf{k},\omega) \\
&\quad + G_{0\perp}^2(\mathbf{k},\omega)\left\{2\left(-\frac{\lambda_\times}{2}\right)(-\lambda_\perp)\int_{\mathbf{q}}\int_{\Omega}\left(\mathbf{q}+\tfrac{\mathbf{k}}{2}\right)\cdot\left(\mathbf{q}-\tfrac{\mathbf{k}}{2}\right)\ \mathbf{k}\cdot\left(\mathbf{q}+\tfrac{\mathbf{k}}{2}\right)\right. \\
&\qquad \times 2T_\perp G_{0\|}\left(\mathbf{q}-\frac{\mathbf{k}}{2},\frac{\omega}{2}-\Omega\right)\left|G_{0\perp}\left(\mathbf{q}+\frac{\mathbf{k}}{2},\frac{\omega}{2}+\Omega\right)\right|^2 \\
&\quad + (-\lambda_\perp)^2\int_{\mathbf{q}}\int_{\Omega}\left(\mathbf{q}+\tfrac{\mathbf{k}}{2}\right)\cdot\left(\mathbf{q}-\tfrac{\mathbf{k}}{2}\right)\ \mathbf{k}\cdot\left(\mathbf{q}+\tfrac{\mathbf{k}}{2}\right) \\
&\qquad \left.\times 2T_\| G_{0\perp}\left(\mathbf{q}-\frac{\mathbf{k}}{2},\frac{\omega}{2}-\Omega\right)\left|G_{0\|}\left(\mathbf{q}+\frac{\mathbf{k}}{2},\frac{\omega}{2}+\Omega\right)\right|^2\right\}. \qquad (2.37b)
\end{aligned}
$$

In the above and from now on, $\int_{\mathbf{q}} \equiv \int^\Lambda d^{d_s}\mathbf{q}/(2\pi)^{d_s}$ and $\int_\Omega \equiv \int_{-\infty}^{\infty} d\Omega/2\pi$ are used for notational brevity. Since we are interested in the hydrodynamic limit, we focus on the leading order in $\mathbf{k},\omega$. Using the bare propagators $G_{0\alpha}(\mathbf{k},\omega) = (D_\alpha \mathbf{k}^2 - i\omega)^{-1}$, the $\omega \to 0$ limit can be taken right away, modifying Eq.(2.37a) to

$$
\begin{aligned}
G_\|(\mathbf{k}) &= G_{0\|}(\mathbf{k}) + 2G_{0\|}^2(\mathbf{k})\int_{\mathbf{q}}\left(\mathbf{q}+\tfrac{\mathbf{k}}{2}\right)\cdot\left(\mathbf{q}-\tfrac{\mathbf{k}}{2}\right)\ \mathbf{k}\cdot\left(\mathbf{q}+\tfrac{\mathbf{k}}{2}\right) \\
&\quad \times\int_\Omega\left\{\frac{\lambda_\|^2 T_\|}{\left(D_\|\left[\mathbf{q}-\frac{\mathbf{k}}{2}\right]^2+i\Omega\right)\left(D_\|^2\left[\mathbf{q}+\frac{\mathbf{k}}{2}\right]^4+\Omega^2\right)}\right. \\
&\qquad \left.+\frac{n\lambda_\times\lambda_\perp T_\perp}{\left(D_\perp\left[\mathbf{q}-\frac{\mathbf{k}}{2}\right]^2+i\Omega\right)\left(D_\perp^2\left[\mathbf{q}+\frac{\mathbf{k}}{2}\right]^4+\Omega^2\right)}\right\}. \qquad (2.38)
\end{aligned}
$$

Above and from now on, I use $G(\mathbf{k}) \equiv G(\mathbf{k},0)$. After performing the frequency integrals,

$$
\begin{aligned}
G_\|(\mathbf{k}) &= G_{0\|}(\mathbf{k})\left\{1+\frac{1}{D_\| k^2}\left(\frac{\lambda_\|^2 T_\|}{D_\|^2}+\frac{n\lambda_\times\lambda_\perp T_\perp}{D_\perp^2}\right)\right. \\
&\qquad \left.\times\int_{\mathbf{q}}\frac{\left(1-\frac{x^2}{4}\right)\left(x\cos\theta+\frac{x^2}{2}\right)}{\left(1+x\cos\theta+\frac{x^2}{4}\right)2\left(1+\frac{x^2}{4}\right)}\right\}, \qquad (2.39)
\end{aligned}
$$

where $x = k/q$ and $\mathbf{k}\cdot\mathbf{q} = kq\cos\theta$. We can now expand the integrand in a power series in x, keeping only the leading order since $x \propto k \to 0$. The angular part of the q integration can be readily done using the identities

$$
\int_{\mathbf{q}} f(q) = \frac{S_{d_s}}{(2\pi)^{d_s}}\int_0^\Lambda dq\ q^{d_s-1}f(q), \qquad \int_{\mathbf{q}}\cos\theta f(q) = 0,
$$

$$
\int_{\mathbf{q}}\cos^2\theta f(q) = \frac{S_{d_s}}{d_s(2\pi)^{d_s}}\int_0^\Lambda dq\ q^{d_s-1}f(q),
$$

where S_{d_s} is the surface area of a d_s-dimensional unit sphere. The result is,

$$\int_{\mathbf{q}} \ldots = \frac{k^2}{2} \frac{S_{d_s}}{(2\pi)^{d_s}} \int_0^{\Lambda} dq\; q^{d_s-3} \left(\frac{1}{2} - \frac{1}{d_s}\right). \tag{2.40}$$

This integral is infrared divergent for $d_s < 2$. The RG procedure is used to overcome this problem. Integrating over the larger momenta in an outer shell $\Lambda(1-\delta\ell) < q < \Lambda$, where $\delta\ell$ is infinitesimal, we obtain

$$G^{<}_{0\parallel}(\mathbf{k}) = G_{0\parallel}(\mathbf{k}) \left\{ 1 - \frac{\delta\ell K_{d_s}}{d_s/(2-d_s)} \left(\frac{\lambda_\parallel^2 T_\parallel}{4D_\parallel^3} + \frac{n\lambda_\times \lambda_\perp T_\perp}{4D_\parallel D_\perp^2} \right) \right\}, \tag{2.41}$$

where $K_{d_s} = S_{d_s}\Lambda^{d_s-2}/(2\pi)^{d_s}$.

An effective tension defined through $G^{<}_{\parallel}(\mathbf{k}) = 1/(D^{<}_{\parallel}k^2)$, is now obtained as

$$D^{<}_{\parallel} = D_\parallel \left\{ 1 + \frac{\delta\ell K_{d_s}}{d_s/(2-d_s)} \left(\frac{\lambda_\parallel^2 T_\parallel}{4D_\parallel^3} + \frac{n\lambda_\times \lambda_\perp T_\perp}{4D_\parallel D_\perp^2} \right) \right\}. \tag{2.42}$$

Under a rescaling $k \to (1-\delta\ell)k$, $\omega \to (1-\zeta\delta\ell)\omega$, $r_\alpha \to (1-\nu_\alpha\delta\ell)r_\alpha$, the effective tension $\tilde{D}_\parallel$ scales as

$$\tilde{D}_\parallel = D_\parallel + \frac{dD_\parallel}{d\ell}\delta\ell = D^{<}_{\parallel}[1 + \delta\ell(\zeta - 2)].$$

Combining the two, we arrive at the differential recursion relation for $D_\parallel$,

$$\frac{dD_\parallel}{d\ell} = D_\parallel \left\{ \zeta - 2 + \frac{K_{d_s}}{d_s/(2-d_s)} \left(\frac{\lambda_\parallel^2 T_\parallel}{4D_\parallel^3} + \frac{n\lambda_\times \lambda_\perp T_\perp}{4D_\parallel D_\perp^2} \right) \right\}. \tag{2.43}$$

For $d_s = 1$, this reduces to the form given in Eqs.(2.26).

Very similar steps are followed for the transverse propagator. Starting from Eq.(2.37b), we have

$$\begin{aligned} G_\perp(\mathbf{k}) \;=\; & G_{0\perp}(\mathbf{k}) + 2G_{0\perp}^2(\mathbf{k}) \int_{\mathbf{q}} \left(\mathbf{q}+\tfrac{\mathbf{k}}{2}\right)\cdot\left(\mathbf{q}-\tfrac{\mathbf{k}}{2}\right)\; \mathbf{k}\cdot\left(\mathbf{q}+\tfrac{\mathbf{k}}{2}\right) \\ & \times \int_\Omega \left\{ \frac{\lambda_\times \lambda_\perp T_\perp}{\left(D_\parallel \left[\mathbf{q}-\frac{\mathbf{k}}{2}\right]^2 + i\Omega\right)\left(D_\perp^2 \left[\mathbf{q}+\frac{\mathbf{k}}{2}\right]^4 + \Omega^2\right)} \right. \\ & \left. + \frac{\lambda_\perp^2 T_\parallel}{\left(D_\perp \left[\mathbf{q}-\frac{\mathbf{k}}{2}\right]^2 + i\Omega\right)\left(D_\parallel^2 \left[\mathbf{q}+\frac{\mathbf{k}}{2}\right]^4 + \Omega^2\right)} \right\}. \end{aligned} \tag{2.44}$$

The frequency integrals are very similar, and upon performing them, we arrive at

$$G_\perp(\mathbf{k}) = G_{0\perp}(\mathbf{k})\left\{1+\frac{1}{D_\perp k^2}\right.$$
$$\times\int_{\mathbf{q}}\left[\frac{\lambda_\times\lambda_\perp T_\perp\left(1-\frac{x^2}{4}\right)\left(x\cos\theta+\frac{x^2}{2}\right)}{D_\perp\left(1+x\cos\theta+\frac{x^2}{4}\right)\left((D_\perp+D_\parallel)\left(1+\frac{x^2}{4}\right)+(D_\perp-D_\parallel)x\cos\theta\right)}\right.$$
$$\left.\left.+\frac{\lambda_\perp^2 T_\parallel\left(1-\frac{x^2}{4}\right)\left(x\cos\theta+\frac{x^2}{2}\right)}{D_\parallel\left(1+x\cos\theta+\frac{x^2}{4}\right)\left((D_\parallel+D_\perp)\left(1+\frac{x^2}{4}\right)+(D_\parallel-D_\perp)x\cos\theta\right)}\right]\right\}. \tag{2.45}$$

Following similar steps as with $D_\parallel$, the final result, after some rearrangement, becomes

$$\frac{dD_\perp}{d\ell} = D_\perp\left\{\zeta-2+K_{d_s}\left[\frac{\lambda_\perp[(\lambda_\times T_\perp/D_\perp)+(\lambda_\perp T_\parallel/D_\parallel)]}{2D_\perp(D_\perp+D_\parallel)}\left(\frac{2-d_s}{d_s}\right)\right.\right.$$
$$\left.\left.+\frac{(D_\perp-D_\parallel)}{(D_\perp+D_\parallel)}\frac{\lambda_\perp[(\lambda_\times T_\perp/D_\perp)-(\lambda_\perp T_\parallel/D_\parallel)]}{D_\perp(D_\perp+D_\parallel)}\left(\frac{1}{d_s}\right)\right]\right\}. \tag{2.46}$$

2D Spectral Density Function Renormalization

Steps very similar to Appendix 2C are followed in order to determine the renormalization of the spectral density function. We can take the $(\mathbf{k},\omega)\to 0$ right away to arrive at

$$2T_\parallel^< = 2T_\parallel+2\left(-\frac{\lambda_\parallel}{2}\right)^2\int_{\mathbf{q}>}\int_\Omega \mathbf{q}\cdot\mathbf{q}\,\mathbf{q}\cdot\mathbf{q}\left(\frac{(2T_\parallel)^2}{(D_\parallel^2q^4+\Omega^2)^2}\right)$$
$$+2n\left(-\frac{\lambda_\times}{2}\right)^2\int_{\mathbf{q}>}\int_\Omega \mathbf{q}\cdot\mathbf{q}\,\mathbf{q}\cdot\mathbf{q}\left(\frac{(2T_\perp)^2}{(D_\perp^2q^4+\Omega^2)^2}\right), \tag{2.47}$$

$$2T_\perp^< = 2T_\perp+2(-\lambda_\perp)^2\int_{\mathbf{q}>}\int_\Omega(\mathbf{q}\cdot\mathbf{q})^2\left(\frac{(2T_\parallel)(2T_\perp)}{(D_\parallel^2q^4+\Omega^2)(D_\perp^2q^4+\Omega^2)}\right), \tag{2.48}$$

where $\int_{\mathbf{q}>}\equiv\int_{\Lambda(1-\delta\ell)<q<\Lambda}d^{d_s}\mathbf{q}/(2\pi)^{d_s}$. Upon performing the rescaling and arranging the terms as usual, we obtain

$$\frac{dT_\parallel}{d\ell} = T_\parallel\left\{\zeta-2\nu_\parallel-d_s+K_{d_s}\frac{\lambda_\parallel^2T_\parallel}{4D_\parallel^3}\right\}+nK_1\frac{\lambda_\times^2T_\perp^2}{4D_\perp^3}, \tag{2.49}$$

$$\frac{dT_\perp}{d\ell} = T_\perp\left\{\zeta-2\nu_\perp-d_s+K_{d_s}\frac{\lambda_\perp^2T_\parallel}{D_\parallel D_\perp(D_\parallel+D_\perp)}\right\}. \tag{2.50}$$

2E Vertex Renormalization

First, I calculate the effective three-point vertex functions $\Gamma_{\|}$, $\Gamma_{\times}$, and $\Gamma_{\perp}$, in the $\omega \to 0$ limit. Let $\hat{k}_i \equiv (\mathbf{k}_i, \omega_i)$. All the diagrams up to one-loop order are shown in Fig. 2-6. After averaging over shell momenta, the first correction term for $\Gamma_{\|}$ is

$$\Gamma^{<}_{\|a}\left(\hat{k}_1;\frac{\hat{k}_1}{2}+\hat{k}_2,\frac{\hat{k}_1}{2}-\hat{k}_2\right)=\Gamma_{0\|}\left(\hat{k}_1;\frac{\hat{k}_1}{2}+\hat{k}_2,\frac{\hat{k}_1}{2}-\hat{k}_2\right)\frac{\lambda_{\|}^2}{\left(\frac{\mathbf{k}_1}{2}+\mathbf{k}_2\right)\cdot\left(\frac{\mathbf{k}_1}{2}-\mathbf{k}_2\right)}$$
$$\times\int_{\mathbf{q}>}\int_{\Omega}\left(\mathbf{q}+\tfrac{\mathbf{k}_1}{2}\right)\cdot\left(\mathbf{q}-\tfrac{\mathbf{k}_1}{2}\right)\left(\tfrac{\mathbf{k}_1}{2}+\mathbf{k}_2\right)\cdot(\mathbf{q}-\mathbf{k}_2)\left(\tfrac{\mathbf{k}_1}{2}-\mathbf{k}_2\right)\cdot(\mathbf{q}-\mathbf{k}_2)$$
$$\times 2T_{\|}G_{0\|}\left(\frac{\mathbf{k}_1}{2}+\mathbf{q},\Omega\right)G_{0\|}\left(\frac{\mathbf{k}_1}{2}-\mathbf{q},-\Omega\right)\left|G_{0\|}(\mathbf{q}-\mathbf{k}_2,\Omega)\right|^2, \quad (2.51)$$

where $\Gamma_{0\|}(\hat{k}_a+\hat{k}_b;\hat{k}_a,\hat{k}_b)\equiv-(\lambda_{\|}/2)\mathbf{k}_a\cdot\mathbf{k}_b G_{0\|}(\hat{k}_a)G_{0\|}(\hat{k}_b)$ is the bare vertex function. It is enough to consider only the leading term in the propagators, which simplifies the evaluation. Upon performing the frequency integral, this equation simplifies to

$$\Gamma^{<}_{\|a}=\Gamma_{0\|}\frac{\lambda_{\|}^2 T_{\|}}{2D_{\|}^3}\int_{\mathbf{q}>}q^{-2}\frac{\frac{x^2}{4}\cos^2\theta_1-y^2\cos^2\theta_2}{\frac{x^2}{4}-y^2}, \quad (2.52)$$

where $x=k_1/q$, $y=k_2/q$, $\mathbf{k}_1\cdot\mathbf{q}=k_1 q\cos\theta_1$, $\mathbf{k}_2\cdot\mathbf{q}=k_2 q\cos\theta_2$. The spherical part of the integral is now easily computed to give

$$\Gamma^{<}_{\|a}=\delta\ell\Gamma_{0\|}\left(\frac{K_{d_s}}{d_s}\right)\frac{\lambda_{\|}^2 T_{\|}}{2D_{\|}^3}. \quad (2.53)$$

Other correction terms are computed similarly. For example,

$$\Gamma^{<}_{\|b}\left(\hat{k}_1;\frac{\hat{k}_1}{2}+\hat{k}_2,\frac{\hat{k}_1}{2}-\hat{k}_2\right)=\Gamma_{0\|}\left(\hat{k}_1;\frac{\hat{k}_1}{2}+\hat{k}_2,\frac{\hat{k}_1}{2}-\hat{k}_2\right)\frac{\lambda_{\|}^2}{\left(\frac{\mathbf{k}_1}{2}+\mathbf{k}_2\right)\cdot\left(\frac{\mathbf{k}_1}{2}-\mathbf{k}_2\right)}$$
$$\times\int_{\mathbf{q}>}\int_{\Omega}\left(\mathbf{q}+\frac{\mathbf{k}_1}{2}\right)\cdot\left(\frac{\mathbf{k}_1}{2}-\mathbf{q}\right)\left(\frac{\mathbf{k}_1}{2}+\mathbf{k}_2\right)\cdot\left(\mathbf{q}+\frac{\mathbf{k}_1}{2}\right)\left(\frac{\mathbf{k}_1}{2}-\mathbf{k}_2\right)\cdot(\mathbf{q}-\mathbf{k}_2)$$
$$\times 2T_{\|}G_{0\|}\left(\frac{\mathbf{k}_1}{2}-\mathbf{q},-\Omega\right)G_{0\|}\left(\mathbf{k}_2-\mathbf{q},-\Omega\right)\left|G_{0\|}\left(\mathbf{q}+\frac{\mathbf{k}_1}{2},\Omega\right)\right|^2 \quad (2.54)$$

which gives

$$\Gamma^{<}_{\|b}=-\delta\ell\Gamma_{0\|}\left(\frac{K_{d_s}}{d_s}\right)\frac{\lambda_{\|}^2 T_{\|}}{4D_{\|}^3}. \quad (2.55)$$

In the limit $k_1, k_2 \to 0$, $\Gamma^{<}_{\|b}=\Gamma^{<}_{\|c}$. Therefore, the sum of the contributions from the three diagrams adds up to zero. The remaining three diagrams are almost identical to the first three and they contribute

$$\begin{aligned}\Gamma^{<}_{\|d} &= \delta\ell\Gamma_{0\|}n\left(\frac{K_{d_s}}{d_s}\right)\frac{2(\lambda_{\times}/\lambda_{\|})\lambda_{\perp}^2 T_{\perp}}{D_{\perp}^3},\\ \Gamma^{<}_{\|e} &= \Gamma^{<}_{\|f}=-\delta\ell\Gamma_{0\|}n\left(\frac{K_{d_s}}{d_s}\right)\frac{(\lambda_{\times}/\lambda_{\|})\lambda_{\perp}^2 T_{\perp}}{D_{\perp}^3},\end{aligned} \quad (2.56)$$

also adding up to zero. Thus, to this order, $\Gamma_{\|}$ does not have any corrections due to renormalization, giving the recursion relation

$$\frac{d\lambda_{\|}}{d\ell} = \lambda_{\|}(\zeta + \nu_{\|} - 2). \tag{2.57}$$

For the calculation of the corrections to $\Gamma_\times$ and $\Gamma_\perp$, it is useful to observe the simple rules that will give us the correct result by inspection of diagrams, rather than doing the very similar and lengthy calculation over again. First, it is clear that leading order terms are sufficient for the propagators. This makes it easy to evaluate frequency integrals. Also, the momentum shell integral always gives the contribution $\delta\ell K_{d_s}/d_s$. An important rule determines the overall sign of each contribution. Diagrams of type $\Gamma_{\|a}$, where the noise contraction is adjacent to both outgoing propagators, have a positive overall sign whereas diagrams where the noise contraction joins the incoming propagator to an outgoing one are negative. These set of rules simplify the task of calculating vertex corrections to evaluating simple frequency integrals, and yield the final results

$$\begin{aligned}
\Gamma_\times^< &= \Gamma_{0\times}\left\{1 + \delta\ell\frac{K_{d_s}}{d_s}\left[\frac{\lambda_{\|}\lambda_\times T_\perp}{D_{\|}D_\perp(D_{\|}+D_\perp)} - \frac{\lambda_{\|}\lambda_\perp T_{\|}}{D_{\|}^2(D_{\|}+D_\perp)}\right.\right. \\
&\qquad \left.\left. + \frac{\lambda_\perp^2 T_{\|}}{D_{\|}D_\perp(D_{\|}+D_\perp)} - \frac{\lambda_\perp\lambda_\times T_\perp}{D_\perp^2(D_{\|}+D_\perp)}\right]\right\}, \qquad (2.58) \\
\Gamma_\perp^< &= \Gamma_{0\perp}\left\{1 + \delta\ell\frac{K_{d_s}}{d_s}\left[\frac{\lambda_{\|}\lambda_\perp T_{\|}(3D_{\|}+D_\perp)}{2D_{\|}^2(D_{\|}+D_\perp)^2} - \frac{\lambda_\perp\lambda_\times T_\perp}{2D_\perp^2(D_{\|}+D_\perp)} - \frac{\lambda_{\|}\lambda_\times T_\perp}{D_\perp(D_{\|}+D_\perp)^2}\right.\right. \\
&\qquad \left.\left. + \frac{\lambda_\perp\lambda_\times T_\perp(3D_\perp+D_{\|})}{2D_\perp^2(D_{\|}+D_\perp)^2} - \frac{\lambda_{\|}\lambda_\perp T_{\|}}{2D_{\|}^2(D_{\|}+D_\perp)} - \frac{\lambda_\perp^2 T_{\|}}{4D_{\|}(D_{\|}+D_\perp)^2}\right]\right\}. \qquad (2.59)
\end{aligned}$$

After rescaling and rearranging terms, these give rise to the recursion relations given in Eqs.(2.26), with the substitution of K_{d_s}/d_s for K_1 in the d_s dimensional case.

Chapter 3

Depinning of Driven Directed Lines

3.1 Introduction and Summary

The study of dynamical critical phenomena associated with the pinning-depinning transition in random media has become a subject of considerable interest in recent years. This is due to the importance of pinning in a wide variety of technologically important phenomena such as flux line (FL) motion in Type-II superconductors, dynamics of interfaces (phase boundaries, invasion fronts, cracks, surface growth, to name a few), and charge-density wave (CDW) transport. These systems are characterized by a rough energy landscape due to the randomness in the medium. At zero temperature there are two distinct "phases", distinguished by an order parameter (henceforth called velocity) that measures the dynamic response, such as the average velocity for a FL, or current for a CDW. For small driving forces, the system is trapped by one of the many available metastable stationary states, and is "pinned" to the impurities in the medium. Critical behavior emerges as the stationary states disappear, and the system starts moving with a nonzero velocity, when the driving force is increased above a threshold value. Extensive experimental [49], theoretical[50, 51, 52], and simulation[53] work has been done to understand the properties of this transition in CDW systems. There are also numerous studies on the depinning of driven interfaces[54, 55, 56, 57, 58, 59]. A better theoretical understanding of this dynamical phase transition was recently achieved, and critical exponents were calculated through an ϵ-expansion for both CDW systems[51] and driven interfaces[55, 56]. More recently, I performed similar calculations (with Mehran Kardar) for the depinning of an elastic line in a bulk random medium, like a polymer in a gel network, a FL in a type-II superconductor, or a screw dislocation in a crystal[60]. In this chapter, I present a detailed report of this study on the dynamical critical behavior associated with the depinning of a FL, and in general on the depinning of directed manifolds in random media, through methods similar to those used for CDWs and interfaces.

Specifically, let us consider the geometry of the FL shown in Fig. 3-1. The superconductor is subject to a magnetic field $\vec{B} = B\hat{x}$ along the x-axis, and a bulk supercurrent $\vec{J} = J\hat{z}$ along the z-axis. A FL is oriented along $\vec{B}$ on the average,

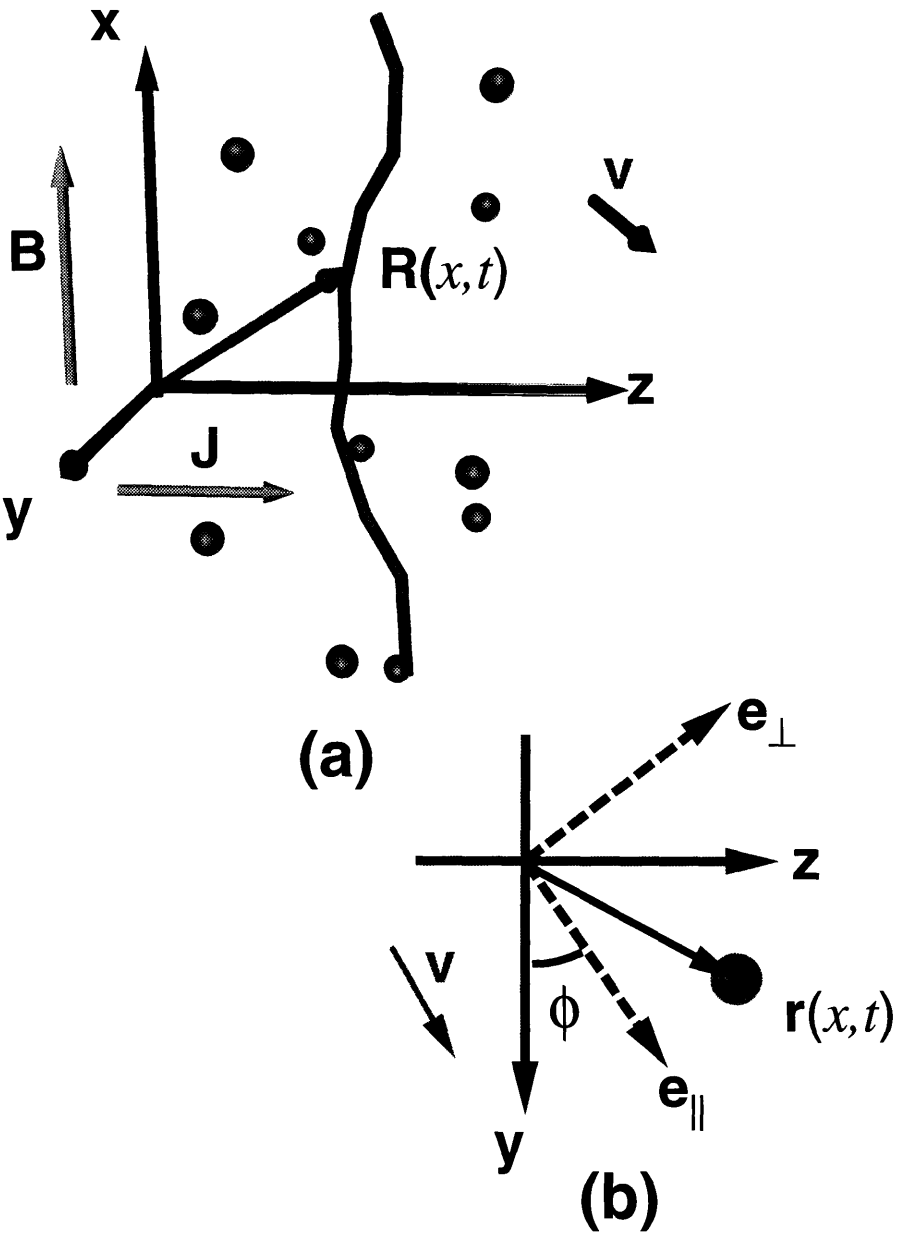

Figure 3-1: Geometry of the FL in a medium with impurities. (a) Three dimensional geometry. (b) A cross section of the medium at fixed x. The average drift velocity $\mathbf{v} = v\mathbf{e}_{\|}$ makes an angle ϕ with the $y-$axis.

but deviates from a straight line due to impurities in the superconductor, which are represented by a potential $V(x,y,z)$. The conformations of the FL are described by $\vec{R}(x,t) = x\hat{x} + \mathbf{r}(x,t)$, where $\mathbf{r}(x,t) = y(x,t)\hat{y} + z(x,t)\hat{z}$ is a *two component* vector, lying in a plane normal to the magnetic field. The bulk current $\vec{J}$ drives the FL along the y-direction through the Lorentz Force $\vec{F}_L = \Phi_0 \vec{J} \times \vec{B}$. ($\Phi_0$ is the flux quantum.) If the bulk current is large enough, the FL drifts with an average velocity $\mathbf{v}$. Due to the chiral nature of the supercurrents around the FL, $\mathbf{v}$ is in general not along the y-direction, but makes an angle ϕ with the y-axis. This is usually called the *Hall angle*, and although typically small[61], it can be significant near the depinning transition.

It is more convenient to work with components of $\mathbf{r}$ that are parallel and perpendicular to $\mathbf{v}$, i.e.

$$\mathbf{r}(x,t) = r_{\|}(x,t)\mathbf{e}_{\|} + r_{\perp}(x,t)\mathbf{e}_{\perp}, \tag{3.1}$$

where the unit vectors $\mathbf{e}_{\|}$ and $\mathbf{e}_{\perp}$ are rotated by ϕ from the y- and z-axes respectively, as shown in Fig. 3-1b. In Sec. 3.2 I show that, under very general assumptions, the equation of motion for small deviations around a straight line, generalized to d-dimensional internal coordinates $\mathbf{x} \in \Re^d$, can be written as

$$\eta \partial_t r_{\|} = K_{11}\nabla^2_{\mathbf{x}} r_{\|} + K_{12}\nabla^2_{\mathbf{x}} r_{\perp} + F + \tilde{f}_{\|}(\mathbf{x}, \mathbf{r}(\mathbf{x},t)), \tag{3.2a}$$

$$\eta \partial_t r_{\perp} = K_{21}\nabla^2_{\mathbf{x}} r_{\|} + K_{22}\nabla^2_{\mathbf{x}} r_{\perp} + \tilde{f}_{\perp}(\mathbf{x}, \mathbf{r}(\mathbf{x},t)), \tag{3.2b}$$

where η is the viscosity the FL and $F = \Phi_0 J$. The moduli $K_{\alpha\gamma}$ relate the elastic force to the local curvature and are in general nondiagonal for a sample with orientation-dependent core energy, or nonzero Hall angle (cf. Sec. 3.2). The random forces $\tilde{f}_{\alpha}$ that arise from the impurity potential V are taken to have zero mean with correlations

$$\langle \tilde{f}_{\alpha}(\mathbf{x},\mathbf{r}) \tilde{f}_{\gamma}(\mathbf{x}',\mathbf{r}') \rangle = \delta^d(\mathbf{x}-\mathbf{x}') \tilde{\Delta}_{\alpha\gamma}(\mathbf{r}-\mathbf{r}'), \tag{3.3}$$

where $\tilde{\Delta}$ is a function that decays rapidly for large values of its argument. (The indices $\alpha, \gamma, \ldots = \{\|, \perp\}$.)

Ignoring fluctuations of the FL transverse to the direction of average velocity, i.e. setting $r_{\perp} = 0$, leads to an interface depinning model studied by Nattermann, Stepanow, Tang, and Leschhorn (NSTL)[55], and by Narayan and Fisher (NF)[56]. Hence, the major difference between Eqs.(3.2) (henceforth called the "vector depinning model") and the previously studied "interface model" is the existence of transverse fluctuations, making the position of the line $\mathbf{r}$ a vector instead of a scalar "height" variable. The effects of such transverse fluctuations for large driving forces and average velocities, when the randomness in the medium can be approximated as uncorrelated in space and time, were shown (in Refs. [47, 18] and Chapter 2) to create a much richer dynamical phase diagram than the corresponding interface growth model, namely the Kardar-Parisi-Zhang (KPZ) equation[31]. Then, the natural questions to ask are: How do these transverse fluctuations scale near the depinning threshold, and how do they influence the critical dynamics of longitudinal fluctuations?

In order to make these questions more quantifiable, consider the exponents that characterize the critical behavior near the depinning transition. Let $\mathbf{F}(\mathbf{v})$ denote the

driving force required to move the FL with a velocity $\mathbf{v} = v\mathbf{e}_{\|}$. For small values of $F = |\mathbf{F}|$, the line is pinned by the disorder in the medium. There is a threshold force F_c, such that the line moves with a nonzero average velocity v iff $F > F_c$.[1] For F slightly above threshold, the average velocity is expected to scale as

$$v = A(F - F_c)^{\beta}, \tag{3.4}$$

where β is the velocity exponent and A is a nonuniversal constant. Superposed on the steady advance of the line are rapid "jumps" as portions of the line depin from strong pinning centers. Such jumps are similar to avalanches in other slowly forced systems and have a power-law distribution in size, cut off at a characteristic correlation length ξ. On approaching the threshold, ξ diverges as

$$\xi \sim (F - F_c)^{-\nu}, \tag{3.5}$$

defining a correlation length exponent ν. At length scales up to ξ, the interface is self-affine, with correlations satisfying the dynamic scaling form

$$\langle [r_{\|}(\mathbf{x},t) - r_{\|}(\mathbf{0},0)]^2 \rangle = |\mathbf{x}|^{2\zeta_{\|}} g_{\|}(t/|\mathbf{x}|^{z_{\|}}), \tag{3.6}$$

$$\langle [r_{\perp}(\mathbf{x},t) - r_{\perp}(\mathbf{0},0)]^2 \rangle = |\mathbf{x}|^{2\zeta_{\perp}} g_{\perp}(t/|\mathbf{x}|^{z_{\perp}}), \tag{3.7}$$

where ζ_α and z_α are roughness and dynamic exponents, respectively. The scaling functions g_α go to a constant as their arguments approach 0; $\zeta_{\|}$ and $\zeta_{\perp}$ are the longitudinal and transverse wandering exponents of an instantaneous line profile; $z_{\|}$ and $z_{\perp}$ characterize scaling of relaxation times of longitudinal and transverse modes with wave vector through $\tau_\alpha(q) \sim q^{-z_\alpha}$. Beyond the length scale ξ, regions move more or less independently of each other and the system is no longer critical. The behavior of the moving line is described by the exponents calculated in Chapter 2 for time dependent noise. Ignoring any potential nonlinearities leads to a regular diffusion equation with white noise, for which the roughness and dynamic exponents are $\zeta_{\|}^{+} = \zeta_{\perp}^{+} = (2-d)/2$, $z^{+} = 2$. In the interface model, transverse fluctuations do not exist, thus, $\zeta_{\perp}$ and $z_{\perp}$ are not defined.

Equations (3.2) can be analyzed using the formalism of Martin, Siggia, and Rose (MSR)[11]. A renormalization group (RG) treatment of the "interface model", studied by NSTL[55] and NF[56], indicates an upper critical dimension of $d_c = 4$, and exponents in $d = 4-\epsilon$ dimensions, given to one-loop order as $\zeta = \epsilon/3$ and $z = 2-2\epsilon/9$. NSTL obtained this result by directly averaging the MSR generating functional Z, and calculating the renormalization of the force-force correlation function $\tilde{\Delta}(r)$. NF, on the other hand, expanded Z around a saddle point solution corresponding to a mean-field approximation[62] to Eqs.(3.2) which involves *temporal* force-force correlations $C(vt)$. They point out some of the deficiencies of conventional low-frequency analysis, and suggest that the roughness exponent is equal to $\epsilon/3$ to all orders in perturbation theory. They also show that for two different classes of disordered systems, random-field and random-bond disorder, the zero temperature interface dynamics is

[1] In an anisotropic medium, F_c may depend on the drift direction $\mathbf{e}_{\|}$. For simplicity, this dependence is suppressed for now and critical exponents are defined for a fixed direction of the velocity.

essentially the same near threshold. Their argument remains valid for vector depinning, and our results will be applicable to both types of randomness. As demonstrated in Section 3.3, the longitudinal exponents of the "vector" model are identical to those of the depinning interface, and given by

$$\zeta_{\|} = \epsilon/3, \tag{3.8}$$
$$z_{\|} = 2 - 2\epsilon/9 + O(\epsilon^2). \tag{3.9}$$

Other exponents are determined by exact exponent identities from $\zeta_{\|}$ and $z_{\|}$ as

$$\nu = \frac{1}{2-\zeta_{\|}} = \frac{3}{6-\epsilon}, \tag{3.10}$$
$$\beta = (z_{\|} - \zeta_{\|})\nu = 1 - \epsilon/9 + O(\epsilon^2). \tag{3.11}$$

Following the formalism of NF, I employ a perturbative expansion of the disorder-averaged MSR partition function around a mean-field solution for scalloped impurity potentials[56]. We show that slightly above threshold, transverse fluctuations do not significantly affect the dynamics of longitudinal fluctuations, apart from shifting the threshold force F_c. Specifically, the exponents and exponent identities given in Eqs. (3.8–3.11) for $d < d_c$ are also correct for the vector depinning model. However, transverse fluctuations turn out to scale differently, with $\zeta_{\perp} \neq \zeta_{\|}$ and $z_{\perp} \neq z_{\|}$. In particular, in an *isotropic* medium with Hall angle $\phi = 0$ (Model A in Section 3.2), the renormalization of transverse temporal force-force correlations $C_{\perp}(vt)$ yields

$$\zeta_{\perp} = \zeta_{\|} - \frac{d}{2} = -2 + \frac{5\epsilon}{6}, \tag{3.12}$$

correct to all orders in ϵ. The transverse dynamic exponent is given by an *exact* exponent identity:

$$z_{\perp} = z_{\|} + \frac{1}{\nu} = 4 - \frac{5\epsilon}{9} + O(\epsilon^2). \tag{3.13}$$

These conclusions can also be generalized to more than one transverse direction: the results do not depend on the number of transverse coordinates. For the FL ($\epsilon = 3$), the critical exponents are then predicted to be

$$\begin{array}{lll} \zeta_{\|} = 1, & z_{\|} \approx 4/3, & \nu = 1, \\ \beta \approx 1/3, & \zeta_{\perp} = 1/2, & z_{\perp} \approx 7/3. \end{array} \tag{3.14}$$

This implies that in a type II superconductor driven slightly above threshold, flux lines are contained mostly in the plane normal to the current, up to the correlation length scale ξ. This may have a noticeable effect on the dynamics of entanglement of flux lines near depinning. These results also rationalize the use of a "planar approximation" in numerical simulations of FL depinning[63].

Another important consideration is the role of anisotropy in the bulk material. It was recently shown that anisotropy leads to new universality classes in interface depinning[64]. We show that this happens as well for FL depinning, in an even richer

fashion. The presence of a nonzero Hall angle affects the critical behavior in a manner similar to anisotropy. These issues are discussed in more detail in Section 3.8.

The rest of the chapter is organized as follows: In Section 3.2, the general form of the equation of motion for a single FL is derived, starting from a reparametrization invariant (RI) description of the FL dynamics. In Section 3.3, the connection of Eqs. (3.2) to the interface depinning problem is first established for the simple case of an isotropic medium with zero Hall angle. Then, the linear response of the system is examined to derive the exponent identities (3.10),(3.11), and (3.13), which are later shown to be consistent with a formal RG treatment of the problem in more general circumstances. In Section 3.4, the MSR formalism is presented and the generating functional is expanded around a self-consistent saddle point solution, given by a mean-field theory. In Section 3.5, response and connected correlation functions of the mean-field theory are calculated; these correspond to the bare propagators and vertex functions in a perturbative expansion. In Section 3.6, critical exponents are determined through an ϵ-expansion near $d = 4$ dimensions, and in Section 3.7 these are compared with numerical results obtained by directly integrating the equations of motion. Finally, in Section 3.8 the physical significance of these results, the roles of nonlinear terms and anisotropy, and applicability of similar methods to related problems are discussed.

3.2 Equations of Motion for a FL

In this section we derive a phenomenological equation that describes the coarse-grained (in space and time) evolution of a single FL in a bulk type-II superconductor. The configuration of the FL at time t is described by $\vec{R}(s,t)$, where s is an arbitrary parameter which we shall later equate to the $x-$component of $\vec{R}$. The equations of motion are obtained by balancing the "conservative" and "dynamical" forces. Conservative forces are derived from the energy functional and depend only on the instantaneous configuration $\vec{R}(s)$ of the FL. They include the elastic force, random forces due to the impurity potential V, and the Lorentz force due to the bulk current. Dynamical forces, on the other hand, depend explicitly on the local velocity of the FL and comprise the dissipative and Magnus forces[65].

For notational simplicity, we set the external magnetic field $\vec{B}$ along the x-axis and the the average velocity $\vec{v}$ along $\mathbf{e}_{||}$, suppressing the possible dependence of parameters on the relative orientation of $\vec{B}$ and $\mathbf{e}_{||}$ due to anisotropy in the underlying material. Such complications will be taken up later in Sec. 3.8. An important consideration is the requirement that the equation of motion be invariant under an arbitrary reparametrization $\vec{R}(s) \to \vec{R}(s')$ of the curve. One such reparametrization invariant quantity is the infinitesimal arc length $dl = ds\sqrt{g}$, where $g \equiv \partial_s\vec{R}\cdot\partial_s\vec{R}$ is the metric. The only physically observable motions of the FL are orthogonal to the local unit tangent vector

$$\hat{t} = \frac{1}{\sqrt{g}}\partial_s\vec{R}.$$

Assuming that the FL motion is overdamped, the conservative force $\vec{F}_T$, which is derived below, is balanced by dynamical forces that are proportional to the local normal velocity $\vec{v}_n = \mathcal{P} \cdot \partial_t \vec{R} = \partial_t \vec{R} - (\partial_t \vec{R} \cdot \hat{t})\hat{t}$. (Here, $\mathcal{P}_{ij} \equiv \delta_{ij} - \hat{t}_i \hat{t}_j$ projects any vector onto the local normal plane.) Dynamical forces are not necessarily parallel to $\vec{v}_n$: In general, there is an angle ϕ (called the Hall angle) between the applied force and the velocity of the FL. Physically, this is due to the Magnus force which is orthogonal to the velocity, and the Hall effect in the normal core of the FL[66]. The equation of motion can then be written as

$$\eta \mathcal{P} \cdot \left\{ \cos\phi \, \partial_t \vec{R} + \sin\phi (\partial_t \vec{R}) \times \hat{t} \right\} = \vec{F}_T. \tag{3.15}$$

To determine the conservative force $\vec{F}_T$, consider the energy cost associated with a particular coarse-grained configuration $\vec{R}(s)$ of the FL in the absence of a bulk current, which is

$$E\left[\vec{R}(s)\right] = \int ds \sqrt{g} \left\{ \frac{\partial_s \vec{R} \cdot \boldsymbol{\sigma} \cdot \partial_s \vec{R}}{g} + V(\vec{R}(s)) \right\}. \tag{3.16}$$

In the above equation, the symmetric tensor $\boldsymbol{\sigma}$ gives the core energy per unit length of the FL, and can be nondiagonal for an anisotropic sample. (Anharmonic contributions to the core energy can be ignored in a coarse-grained description and we will systematically keep only the leading order elastic terms.) The restoring force $\vec{F}_B$ is given by the energy cost of an infinitesimal virtual displacement $\delta\vec{R}(s)$. After some rearrangement, we arrive at

$$\begin{aligned} \delta E &= -\int ds \sqrt{g} \, \delta\vec{R} \cdot \mathcal{P} \cdot \left\{ 2\boldsymbol{\sigma} \cdot \vec{\kappa} - \left(\hat{t} \cdot \boldsymbol{\sigma} \cdot \hat{t} \right) \vec{\kappa} + V(\vec{R})\vec{\kappa} - \nabla_{\vec{R}} V(\vec{R}) \right\} \\ &\equiv -\int ds \sqrt{g} \, \delta\vec{R} \cdot \vec{F}_B, \end{aligned} \tag{3.17}$$

where $\vec{\kappa} = g^{-1} \mathcal{P} \cdot \partial_s^2 \vec{R}$ is the local curvature vector. To leading order, the random potential $V(\vec{R})$ that multiplies $\vec{\kappa}$ can be approximated by its spatial average, and eliminated without loss of generality by choosing $\langle V \rangle = 0$. $\vec{f} = -\nabla_{\vec{R}} V(\vec{R})$ acts as a random force on each segment of the FL, whose correlations in general satisfy

$$\langle f_\alpha(\vec{R}) f_\gamma(\vec{R}') \rangle = \Delta_{\alpha\gamma}(\vec{R} - \vec{R}'). \tag{3.18}$$

For now, we do not restrict the form of Δ, apart from the reasonable expectation that it decays quickly beyond a characteristic impurity size a. When a bulk current $\vec{J}$ is present, the FL is also subject to a Lorentz force $\vec{F}_L = \Phi_0 \vec{J} \times \hat{t}$, where Φ_0 is the flux quantum. Thus, the total conservative force acting on a section of the FL is given as

$$\vec{F}_T = \mathcal{P} \cdot \left\{ \frac{2\boldsymbol{\sigma} \cdot \mathcal{P} \cdot \partial_s^2 \vec{R} - (\hat{t} \cdot \boldsymbol{\sigma} \cdot \hat{t}) \partial_s^2 \vec{R}}{g} + \Phi_0 \vec{J} \times \hat{t} + \vec{f} \right\}. \tag{3.19}$$

For an isotropic sample in the extreme type-II limit, the Bardeen-Stephen model gives[66]

$$\begin{aligned}\sigma_{ij} &\approx \delta_{ij}\left(\frac{\Phi_0}{4\pi\lambda_s}\right)^2 \ln\left(\frac{\xi_s}{\lambda_s}\right), \\ \eta &\approx \frac{\Phi_0^2}{2\pi\xi_s^2 c^2 \rho_n}, \\ \tan\phi &\approx \frac{\rho_n}{\rho_n^H},\end{aligned}$$

where λ_s is the London penetration depth, ξ_s is the coherence length, and ρ_n, ρ_n^H are normal and Hall resistivities of the non-superconducting core region, respectively. More general expressions for these phenomenological parameters can be derived from a mesoscopic model based on a time-dependent Ginzburg-Landau theory[67].

Equation (3.15) is highly nonlinear and generalizes those of Ref.[68] to the three-dimensional and anisotropic case. We now pick $\{\hat{x}, \mathbf{e}_\parallel, \mathbf{e}_\perp\}$ as our coordinate axes, and x as the arbitrary parameter s, representing the FL as $\vec{R}(x,t) = x\hat{x} + r_\parallel(x,t)\mathbf{e}_\parallel + r_\perp(x,t)\mathbf{e}_\perp$. In this representation, $g = 1 + (\partial_x r_\parallel)^2 + (\partial_x r_\perp)^2$, $\vec{J} = J_\parallel \mathbf{e}_\parallel + J_\perp \mathbf{e}_\perp$, $\vec{f} = f_x\hat{x} + f_\parallel \mathbf{e}_\parallel + f_\perp \mathbf{e}_\perp$, and

$$\boldsymbol{\sigma} = \begin{pmatrix} \sigma_x & \sigma_{x\parallel} & \sigma_{x\perp} \\ \sigma_{x\parallel} & \sigma_\parallel & \sigma_\times \\ \sigma_{x\perp} & \sigma_\times & \sigma_\perp \end{pmatrix}.$$

After some rearrangement, and elimination of higher-order terms coming from the elastic energy of the FL, we obtain the following evolution equations for the components $r_\parallel$ and $r_\perp$:

$$\begin{aligned}\frac{\eta}{\cos\phi}\partial_t r_\parallel &= [(2\sigma_\parallel - \sigma_x) - 2\sigma_\times \tan\phi]\partial_x^2 r_\parallel + [2\sigma_\times - (2\sigma_\perp - \sigma_x)\tan\phi]\partial_x^2 r_\perp \\ &+ \frac{\Phi_0}{\sqrt{g}}\left\{J_\perp\left[1 + (\partial_x r_\parallel)^2\right] - J_\parallel\left[\partial_x r_\parallel \partial_x r_\perp - \tan\phi\sqrt{g}\right]\right\} \\ &+ f_\parallel\left[1 + \frac{\tan\phi}{\sqrt{g}}\partial_x r_\parallel \partial_x r_\perp\right] - f_\perp\frac{\tan\phi}{\sqrt{g}}\left[1 + (\partial_x r_\parallel)^2\right] \\ &- f_x\left[\partial_x r_\parallel - \frac{\tan\phi}{\sqrt{g}}\partial_x r_\perp\right], \qquad (3.20a)\end{aligned}$$

$$\begin{aligned}\frac{\eta}{\cos\phi}\partial_t r_\perp &= [2\sigma_\times + (2\sigma_\parallel - \sigma_x)\tan\phi]\partial_x^2 r_\parallel + [(2\sigma_\perp - \sigma_x) + \sigma_\times \tan\phi]\partial_x^2 r_\perp \\ &+ \frac{\Phi_0}{\sqrt{g}}\left\{J_\perp\left[\partial_x r_\parallel \partial_x r_\perp + \tan\phi\sqrt{g}\right] - J_\parallel\left[1 + (\partial_x r_\perp)^2\right]\right\} \\ &+ f_\parallel\frac{\tan\phi}{\sqrt{g}}\left[1 + (\partial_x r_\perp)^2\right] + f_\perp\left[1 - \frac{\tan\phi}{\sqrt{g}}\partial_x r_\parallel \partial_x r_\perp\right] \\ &- f_x\left[\partial_x r_\perp + \frac{\tan\phi}{\sqrt{g}}\partial_x r_\parallel\right]. \qquad (3.20b)\end{aligned}$$

These equations are clearly too complicated for an exhaustive analysis. However, it is possible to perform a gradient expansion of the RHS of Eqs.(3.20) when the fluctuations around the straight line are small, i.e. $(\partial_x r_\parallel)^2, (\partial_x r_\perp)^2 \ll 1$. In that case, Eqs.(3.20) simplify to

$$\begin{aligned}
\frac{\eta}{\cos\phi}\partial_t r_\parallel &= [(2\sigma_\parallel - \sigma_x) - 2\sigma_\times \tan\phi]\partial_x^2 r_\parallel + [2\sigma_\times - (2\sigma_\perp - \sigma_x)\tan\phi]\partial_x^2 r_\perp \\
&\quad + \Phi_0\left(J_\perp + J_\parallel \tan\phi\right) + f_\parallel - f_\perp \tan\phi, \qquad (3.21a) \\
\frac{\eta}{\cos\phi}\partial_t r_\perp &= [2\sigma_\times + (2\sigma_\parallel - \sigma_x)\tan\phi]\partial_x^2 r_\parallel + [(2\sigma_\perp - \sigma_x) + \sigma_\times \tan\phi]\partial_x^2 r_\perp \\
&\quad + \Phi_0\left(-J_\parallel + J_\perp \tan\phi\right) + f_\perp - f_\parallel \tan\phi, \qquad (3.21b)
\end{aligned}$$

neglecting all terms of $O\left((\partial_x r_\parallel)^2, (\partial_x r_\perp)^2\right)$ or higher.

So far, we have not enforced the condition that $\mathbf{e}_\parallel$ points along the average velocity of the FL. This is satisfied by the self-consistency relation

$$\langle \partial_t r_\perp \rangle = 0. \qquad (3.22)$$

In the small fluctuation limit where Eqs.(3.21) are valid, this condition is satisfied simply by setting $J_\parallel = J_\perp \tan\phi$. In order to study the scaling properties of this system in the framework of a field theory, we generalize the FL to a manifold with d-dimensional internal coordinates $\mathbf{x} \in \Re^d$. Further rearrangements, and addition of an infinitesimal external force $\boldsymbol{\varepsilon}(\mathbf{x}, t)$ in order to study response functions, lead to

$$\begin{aligned}
\eta\partial_t r_\parallel &= K_{11}\nabla_{\mathbf{x}}^2 r_\parallel + K_{12}\nabla_{\mathbf{x}}^2 r_\perp + F + \tilde{f}_\parallel(\mathbf{x}, \mathbf{r}(\mathbf{x}, t)) + \varepsilon_1(\mathbf{x}, t), \qquad (3.23a) \\
\eta\partial_t r_\perp &= K_{21}\nabla_{\mathbf{x}}^2 r_\parallel + K_{22}\nabla_{\mathbf{x}}^2 r_\perp + \tilde{f}_\perp(\mathbf{x}, \mathbf{r}(\mathbf{x}, t)) + \varepsilon_2(\mathbf{x}, t), \qquad (3.23b)
\end{aligned}$$

where $F = \Phi_0\sqrt{J_\parallel^2 + J_\perp^2} = \Phi_0 J$, and

$$\begin{aligned}
\begin{pmatrix} K_{11} & K_{12} \\ K_{21} & K_{22} \end{pmatrix} &= \begin{pmatrix} \cos\phi & -\sin\phi \\ \sin\phi & \cos\phi \end{pmatrix}\begin{pmatrix} 2\sigma_\parallel - \sigma_x & 2\sigma_\times \\ 2\sigma_\times & 2\sigma_\perp - \sigma_x \end{pmatrix}, \\
\begin{pmatrix} \tilde{f}_\parallel \\ \tilde{f}_\perp \end{pmatrix} &= \begin{pmatrix} \cos\phi & -\sin\phi \\ \sin\phi & \cos\phi \end{pmatrix}\begin{pmatrix} f_\parallel \\ f_\perp \end{pmatrix}.
\end{aligned}$$

The correlations of the random forces satisfy

$$\langle \tilde{f}_\alpha(\mathbf{x}, \mathbf{r})\tilde{f}_\gamma(\mathbf{x}, \mathbf{r}')\rangle = \delta^d(\mathbf{x} - \mathbf{x}')\tilde{\Delta}_{\alpha\gamma}(\mathbf{r} - \mathbf{r}'). \qquad (3.23c)$$

(Note that while both $\mathbf{r}$ and $\mathbf{x}$ are represented by bold characters, $\mathbf{r}$ remains two dimensional, while $\mathbf{x}$ has been promoted to a d-dimensional vector.)

In the special case of an isotropic medium with $\phi = 0$, the equations further reduce to

$$\begin{aligned}
\eta\partial_t r_\parallel &= K\nabla_{\mathbf{x}}^2 r_\parallel + F + f_\parallel(\mathbf{x}, \mathbf{r}(\mathbf{x}, t)) + \varepsilon_1(\mathbf{x}, t), \qquad (3.24a) \\
\eta\partial_t r_\perp &= K\nabla_{\mathbf{x}}^2 r_\perp + f_\perp(\mathbf{x}, \mathbf{r}(\mathbf{x}, t)) + \varepsilon_2(\mathbf{x}, t), \qquad (3.24b)
\end{aligned}$$

where the correlations of the random forces satisfy

$$\langle f_\alpha(\mathbf{x},\mathbf{r}) f_\gamma(\mathbf{x},\mathbf{r}')\rangle = \delta_{\alpha\gamma}\delta^d(\mathbf{x}-\mathbf{x}')\Delta(|\mathbf{r}-\mathbf{r}'|). \tag{3.24c}$$

We shall henceforth refer to Eqs.(3.24) as Model A. Anisotropy and/or a nonzero Hall angle changes the scaling properties of the critical region, and we shall refer to this more general case, described by Eqs.(3.23), as Model B.

3.3 The Vector Depinning Model

In this section, we study some properties of the system described by Eqs.(3.23) and (3.24), in detail. Due to statistical translational symmetry in time t and internal coordinates $\mathbf{x}$, we use the real $(\mathbf{x},t)$ and Fourier $(\mathbf{q},\omega)$ domains interchangeably when dealing with statistical averages.

The vector depinning model differs from the CDW or interface problems due to the presence of transverse fluctuations $r_\perp(\mathbf{x},t)$. It is sometimes useful to recast the equations such that $r_\perp$ appears as a function of $r_\parallel$ rather than t. The asymmetry in $r_\parallel$ and $r_\perp$ occurs because $r_\parallel$ almost always moves in the forward direction[2], and therefore is a monotonous function of t. Thus, for any particular realization of the random force $f(\mathbf{x},\mathbf{r})$, there is a unique point $r_\perp(\mathbf{x},r_\parallel)$ that is visited by the line for given coordinates $(\mathbf{x},r_\parallel)$. The evolution of $r_\perp(\mathbf{x},r_\parallel)$ can be obtained schematically, by dividing Eq.(3.23b) by (3.23a), as

$$\frac{\partial r_\perp}{\partial r_\parallel} = \frac{K_{21}\nabla_{\mathbf{x}}^2 r_\parallel + K_{22}\nabla_{\mathbf{x}}^2 r_\perp + \tilde{f}_\perp}{K_{11}\nabla_{\mathbf{x}}^2 r_\parallel + K_{12}\nabla_{\mathbf{x}}^2 r_\perp + \tilde{f}_\parallel + F}. \tag{3.25}$$

We shall see that in most cases, the scaling properties of $r_\perp$ in relation to $r_\parallel$ can be obtained heuristically by inspecting Eq.(3.25).

3.3.1 Model A

First of all, we establish the connection between Eq.(3.24) and the interface depinning model for the special case of an isotropic system with $\phi = 0$ (Model A). For a particular realization of randomness $\mathbf{f}(\mathbf{x},\mathbf{r})$, Eq.(3.24a) can be written as

$$\eta\partial_t r_\parallel = K\nabla_{\mathbf{x}}^2 r_\parallel + f'\left(\mathbf{x}, r_\parallel(\mathbf{x},t)\right) + F + \varepsilon_1(\mathbf{x},t), \tag{3.26}$$

where $f'(\mathbf{x},r_\parallel) = f_\parallel\left(\mathbf{x}, r_\parallel, r_\perp(\mathbf{x},r_\parallel)\right)$ and $r_\perp(\mathbf{x},r_\parallel)$ is determined by Eq.(3.25). It is quite plausible that, after averaging over all $\mathbf{f}$, the correlations in f' will also be short-ranged, albeit different from those of $\mathbf{f}$, since the dissipative dynamics will avoid maxima of the random potential, effectively reducing the average forces. In that case, the equation reduces exactly to the model studied by NSTL and NF. Thus, the scaling

[2]This is not strictly true, but backward motion happens very rarely and can be ignored at larger length scales, since the probability of backward motion decreases exponentially at increasing length scales.

of longitudinal fluctuations of the FL near threshold will not change upon taking into account transverse components, and the exponent relations (3.8–3.11) hold for Model A as well. We expect this argument to hold even for Model B [Eqs.(3.23)] as long as $\nabla_{\mathbf{x}}^2 r_\perp \ll \nabla_{\mathbf{x}}^2 r_\parallel$, or when $\zeta_\perp < \zeta_\parallel$.

For the interface model, it is possible to show that $v(F)$ is a single valued function using the "no passing rule" of Middleton[52]. The rule states that no interface (or CDW) can overtake another, if initially every point on the first interface is behind the second one. This rule does not apply to the vector model: It is in principle possible to have coexistence of moving and stationery FLs, allowing for the possibility of a discontinuous (multi-valued) $\mathbf{v}(\mathbf{F})$. However, since a moving line samples an arbitrarily large region in the medium, it is plausible that the velocity self-averages at long times, resulting in a single valued $\mathbf{v}(\mathbf{F})$ (i.e., no hysteresis). However, finite-size systems do suffer from such hysteresis which adversely affects numerical simulations of the model. These issues are further discussed in Sec. 3.7.

Several exponent identities can be deduced from the form of the linear response,

$$\chi_{\alpha\gamma}(\mathbf{q},\omega) = \left\langle \frac{\partial r_\alpha(\mathbf{q},\omega)}{\partial \varepsilon_\gamma(\mathbf{q},\omega)} \right\rangle, \tag{3.27}$$

in the $(\mathbf{q},\omega) \to (\mathbf{0},0)$ limit. Due to the statistical symmetry of Eqs.(3.24) under the transformation $r_\perp \to -r_\perp$, the linear response is diagonal. Let us first set $\omega = 0$ and examine the static response: An additional static force $\boldsymbol{\varepsilon}(\mathbf{q})$ with zero spatial average (no $\mathbf{q} = 0$ component) can be exactly compensated by the coordinate change

$$\mathbf{r}'_\alpha(\mathbf{q},t) = \mathbf{r}_\alpha(\mathbf{q},t) + (Kq^2)^{-1}\varepsilon_\alpha(\mathbf{q}).$$

The distribution of $\mathbf{f}$ does not change in the primed coordinates. Thus, the static linear response has the form

$$\chi_{\alpha\gamma}(\mathbf{q},\omega=0) = \delta_{\alpha\gamma}\frac{1}{Kq^2}. \tag{3.28}$$

Since $\varepsilon_\parallel$ scales like the applied force, the form of the linear response at the correlation length ξ gives the exponent identity

$$\zeta_\parallel + 1/\nu = 2. \tag{3.29}$$

Considering the transverse linear response seems to imply $\zeta_\perp = \zeta_\parallel$. However, as will be shown below, the static part of the transverse linear response becomes irrelevant at the critical RG fixed point, since $z_\perp > z_\parallel$.

Now set $\mathbf{q} = \mathbf{0}$ and consider the response to a spatially uniform, but time-dependent, external force $\boldsymbol{\varepsilon}(t)$. The leading term in the dynamic response is intricately connected to $\mathbf{v}(\mathbf{F})$: When a slowly varying uniform external force $\boldsymbol{\varepsilon}(t)$ is applied, the FL responds as if the instantaneous external force $\mathbf{F} + \boldsymbol{\varepsilon}$ is a constant, i.e. it moves with the average velocity

$$\langle \partial_t r_\alpha \rangle = v_\alpha(\mathbf{F}+\boldsymbol{\varepsilon}) \approx v_\alpha(\mathbf{F}) + \frac{\partial v_\alpha}{\partial F_\gamma}\varepsilon_\gamma. \tag{3.30}$$

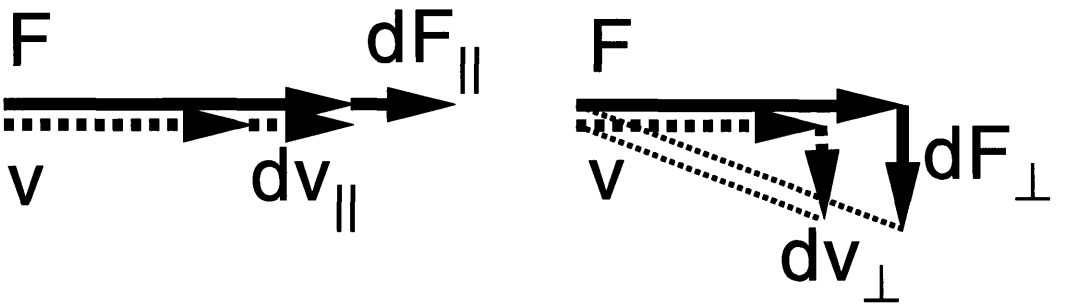

Figure 3-2: A graphical demonstration of Eqs.(3.32- 3.33). When a longitudinal force is applied, the direction is not changed and all changes are in the magnitude of $F(v)$. For a transverse force, $\mathbf{v}$ changes direction to remain parallel to $\mathbf{F}$.

Since in an isotropic medium, $\mathbf{F}$ and $\mathbf{v}$ are always parallel,

$$\mathbf{F}(\mathbf{v}) = F(v)\hat{v}. \tag{3.31}$$

For small deviations around $\mathbf{v} = v\mathbf{e}_{||}$, we thus obtain (see Fig. 3-2)

$$\frac{\partial F_{||}}{\partial v_{||}} = \frac{dF}{dv}, \tag{3.32}$$

$$\frac{\partial F_{\perp}}{\partial v_{\perp}} = \frac{F}{v}. \tag{3.33}$$

Therefore, near the depinning transition,

$$\chi_{||}(\mathbf{q}=0,\omega) \simeq \frac{1}{-i\omega(dF/dv)+O(\omega^2)}, \tag{3.34}$$

$$\chi_{\perp}(\mathbf{q}=0,\omega) \simeq \frac{1}{-i\omega(F_c/v)+O(\omega^2)}. \tag{3.35}$$

Comparing these with the static response, we see that near threshold, the relaxation of fluctuations with wavelength ξ gives

$$\tau_{||}(q=\xi^{-1}) \sim \left(q^2\frac{dv}{dF}\right)^{-1} \sim \xi^{2+(\beta-1)/\nu} \sim \xi^{z_{||}}, \tag{3.36}$$

$$\tau_{\perp}(q=\xi^{-1}) \sim \left(q^2\frac{v}{F_c}\right)^{-1} \sim \xi^{2+\beta/\nu} \sim \xi^{z_{\perp}}, \tag{3.37}$$

which in turn yield

$$\beta = 1+(z_{||}-2)\nu, \tag{3.38}$$

$$z_{\perp} = z_{||}+1/\nu. \tag{3.39}$$

Thus, $z_{\perp} > z_{||}$ as noted earlier. Dynamic relaxation times scale very differently for longitudinal and transverse components as $\mathbf{v} \to 0$, since $(dv/dF) \sim (F-F_c)^{\beta-1}$ whereas $v/F \sim (F-F_c)^{\beta}$.

3.3.2 Model B

A similar linear response analysis can be made for the more general case of Model B. The leading contributions to the static and dynamic part of the inverse linear response are given by

$$\chi^{-1}_{\alpha\gamma}(\mathbf{q}, \omega = 0) = K_{\alpha\gamma} q^2, \tag{3.40}$$

$$\chi^{-1}_{\alpha\gamma}(\mathbf{q} = \mathbf{0}, \omega) = -i\omega(\partial v_\alpha / \partial F_\gamma)^{-1}. \tag{3.41}$$

The relation between the external force and the drift velocity can in general be written as

$$\mathbf{F}(\mathbf{v}) = F(v, \theta)\left[\cos\phi(v, \theta)\hat{v} + \sin\phi(v, \theta)\hat{x} \times \hat{v}\right]. \tag{3.42}$$

Both F and ϕ in general depend on the orientation of $\hat{v}$, parametrized by an angle θ in the yz-plane. Then, for small deviations around $\mathbf{v} = v\mathbf{e}_{\|}$,

$$\begin{pmatrix} dF_{\|} \\ \\ dF_{\perp} \end{pmatrix} = \begin{pmatrix} A_{11} & -\frac{1}{v}A_{12} \\ \\ A_{21} & \frac{1}{v}A_{22} \end{pmatrix} \begin{pmatrix} dv_{\|} \\ \\ dv_{\perp} \end{pmatrix}, \tag{3.43}$$

where

$$\begin{aligned} A_{11} &= \partial_v(F\cos\phi), \\ A_{21} &= \partial_v(F\sin\phi), \\ A_{12} &= F\sin\phi - \partial_\theta(F\cos\phi), \\ A_{22} &= F\cos\phi + \partial_\theta(F\sin\phi). \end{aligned}$$

The scaling of diagonal elements in the linear response are the same as in Model A. Therefore, exponent identities (3.38-3.39) hold in the more general case of Model B as well.

3.4 MSR Formalism

We use the formalism of MSR[11] to compute response and correlation functions for the dynamical system described by Eqs. (3.23). After some rearranging, we obtain

$$\begin{aligned} \eta\frac{\partial r_\alpha(\mathbf{x}, t)}{\partial t} &= \int d^d x'\, J_{\alpha\gamma}(\mathbf{x} - \mathbf{x}') r_\gamma(\mathbf{x}', t) \\ &\quad - r_\alpha(\mathbf{x}, t) + \tilde{f}_\alpha\left(\mathbf{x}, \mathbf{r}(\mathbf{x}, t)\right) + F_\alpha + \varepsilon_\alpha(\mathbf{x}, t), \end{aligned} \tag{3.44}$$

where the tensor $\mathbf{J}$ is given by its Fourier transform as $J_{\alpha\gamma}(\mathbf{q}) = \delta_{\alpha\gamma} - K_{\alpha\gamma}q^2$. Introducing an auxiliary field $\hat{\mathbf{r}}(\mathbf{x}, t)$, the generating functional Z is given by

$$Z = \int [d\mathbf{r}][d\hat{\mathbf{r}}]\mathcal{J}[\mathbf{r}]\exp(S), \tag{3.45}$$

where

$$S = i\int d^d x\, dt\, \hat{r}_\alpha(\mathbf{x}, t)\left\{\eta\partial_t r_\gamma - K_{\alpha\gamma}\nabla^2_{\mathbf{x}} r_\gamma - F_\alpha - \tilde{f}_\alpha\left(\mathbf{x}, \mathbf{r}(\mathbf{x}, t)\right) - \varepsilon_\alpha(\mathbf{x}, t)\right\}. \tag{3.46}$$

Clearly, this coarse-grained continuum picture of the system breaks down at length scales shorter than the core radius of the FL. Therefore, there is a natural cutoff Λ in $\mathbf{q}$-space for the functional integrals in Eq. (3.45). Z can be used to generate response and correlation functions of $\mathbf{r}$, since integrating over $\hat{\mathbf{r}}$ gives delta functions that impose the solution to the equation of motion (3.44). The Jacobian $\mathcal{J}[\mathbf{r}]$ fixes the renormalization of Z such that the delta functions integrate to unity, and will be suppressed henceforth. Since $Z = 1$ independent of the realization of randomness, response and correlation functions can also be generated using the disorder-averaged generating function $\overline{Z} = \int [d\mathbf{r}][d\hat{\mathbf{r}}]\langle \exp(S)\rangle$. For example, the two-point correlation function is given by

$$\langle r_\alpha(\mathbf{x},t) r_\gamma(\mathbf{x}',t')\rangle = \int [d\mathbf{r}][d\hat{\mathbf{r}}] r_\alpha(\mathbf{x},t) r_\gamma(\mathbf{x}',t')\langle \exp(S)\rangle,$$

and the linear response is

$$\left\langle \frac{\delta r_\alpha(\mathbf{x},t)}{\delta \varepsilon_\gamma(\mathbf{x}',t')} \right\rangle = -i \int [d\mathbf{r}][d\hat{\mathbf{r}}] r_\alpha(\mathbf{x},t)\hat{r}_\gamma(\mathbf{x}',t')\langle \exp(S)\rangle.$$

In order proceed, we discretize in $\mathbf{x}$-space: $\mathbf{r}(\mathbf{x},t) \to \mathbf{r}_i(t)$. Introducing two conjugate fields $\mathbf{R}_i(t), \hat{\mathbf{R}}_i(t)$, $\overline{Z}$ can be rewritten as

$$\overline{Z} = \int [d\mathbf{R}][d\hat{\mathbf{R}}] \exp(\tilde{S}), \tag{3.47}$$

$$\tilde{S} = \sum_j \ln \overline{Z}_j \left(\mathbf{R}_j, \hat{\mathbf{R}}_j\right) - i \int dt \sum_{i,j} \hat{\mathbf{R}}_i(t) \cdot \mathbf{J}_{ij}^{-1} \cdot \mathbf{R}_j(t), \tag{3.48}$$

where $\overline{Z}_j \left(\mathbf{R}_j, \hat{\mathbf{R}}_j\right)$ is given by

$$\begin{aligned} \overline{Z}_j = \int [d\mathbf{r}_j][d\hat{\mathbf{r}}_j] \Big\langle \exp \int dt \Big[& i\hat{\mathbf{R}}_j(t) \cdot \mathbf{r}_j(t) \\ & + i\hat{\mathbf{r}}_j(t) \cdot \left\{ \eta \partial_t \mathbf{r}_j(t) - \mathbf{R}_j(t) + \mathbf{r}_j(t) - \tilde{\mathbf{f}}_j\left(\mathbf{r}_j(t)\right) - \mathbf{F} - \boldsymbol{\varepsilon}_j(t) \right\} \Big] \Big\rangle . \end{aligned} \tag{3.49}$$

Note that this factorization of the disorder-dependent part of the action to local functionals $\overline{Z}_j$ is possible only if the random forces $\tilde{\mathbf{f}}_j$ are independent at each site j, as assumed in Eq. (3.3). $\overline{Z}_j$ can be evaluated by an expansion around the saddle-point approximation. The integrand of the exponential is a maximum when, for each j,

$$\begin{aligned} -\sum_i \mathbf{J}_{ij}^{-1} \cdot \hat{\mathbf{R}}_i^0 - \langle \hat{\mathbf{r}}_j \rangle_{\mathrm{MF}} = \mathbf{0}, \\ -\sum_i \mathbf{J}_{ij}^{-1} \cdot \mathbf{R}_i^0 + \langle \mathbf{r}_j \rangle_{\mathrm{MF}} = \mathbf{0}, \end{aligned}$$

which has a solution $\hat{\mathbf{R}}_j^0 = \mathbf{0}$, $\mathbf{R}_j^0 = \mathbf{v}t$ for all j. Here, $\mathbf{v}$ is determined self-consistently as a function of $\mathbf{F}$ by requiring $\langle \mathbf{r}_j \rangle_{\mathrm{MF}} = \mathbf{v}t$, where averages ($\langle \ldots \rangle_{\mathrm{MF}}$) are generated from $\overline{Z}_j$ evaluated at the saddle point, which is identical for each j:

$$Z_{\mathrm{MF}} = \int [d\mathbf{r}_j][d\hat{\mathbf{r}}_j] \left\langle \exp i \int dt\ \hat{\mathbf{r}}_j(t) \cdot \left\{ \eta \partial_t \mathbf{r}_j(t) - \mathbf{v}t + \mathbf{r}_j(t) - \tilde{\mathbf{f}}_j\left(\mathbf{r}_j(t)\right) - \mathbf{F} - \boldsymbol{\varepsilon}_j(t) \right\} \right\rangle . \tag{3.50}$$

$Z_{\rm MF}$ can be identified as the MRS generating function for a mean-field (MF) approximation to Eq. (3.44), obtained by setting $J_{\alpha\gamma}(\mathbf{x}-\mathbf{x}') = \delta_{\alpha\gamma}N^{-1}$, where $N = \int d^dx$. (The first term in the RHS of (3.44) is then self-consistently equal to $\langle\mathbf{r}\rangle_{\rm MF} = \mathbf{v}t$.) Redefining the field variables as $\mathbf{R} \to \mathbf{R} + \mathbf{v}t$, $i\hat{\mathbf{R}} \to \hat{\mathbf{R}}$ (for notational simplicity), the expansion for $\ln \overline{Z}_j\left(\mathbf{R}_j, \hat{\mathbf{R}}_j\right)$ is given by

$$\ln \overline{Z}_j\left(\mathbf{R}_j, \hat{\mathbf{R}}_j\right) = \sum_{\{m_\alpha, n_\alpha\}=0}^{\infty} \left(\prod_\alpha \frac{1}{m_\alpha! n_\alpha!}\right) \tag{3.51}$$
$$\times \int \prod_\alpha \left\{ \prod_{s_\alpha=1}^{m_\alpha} dt_{\alpha s_\alpha} \hat{R}_{j\alpha}(t_{\alpha s_\alpha}) \prod_{s'_\alpha=1}^{n_\alpha} dt'_{\alpha s'_\alpha} R_{j\alpha}(t'_{\alpha s'_\alpha}) \right\} \mathcal{V}_{\{m_\alpha,n_\alpha\}}\left(\{t_{\alpha s_\alpha}\}; \{t'_{\alpha s'_\alpha}\}\right).$$

The vertex functions $\mathcal{V}$ are obtained by evaluating derivatives of $\ln \overline{Z}_j$ with respect to the fields *at the saddle point*, and are given precisely by connected correlation and response functions of the MF system described by Eq. (3.50):

$$\mathcal{V}_{\{m_\alpha,n_\alpha\}}\left(\{t_{\alpha s_\alpha}\}; \{t'_{\alpha s'_\alpha}\}\right) = \left[\prod_\alpha \prod_{s'_\alpha=1}^{n_\alpha} \frac{\partial}{\partial \varepsilon_{j\alpha}(t'_{\alpha s'_\alpha})}\right] \left\langle \prod_\alpha \prod_{s_\alpha=1}^{m_\alpha} \overline{r}_{j\alpha}(t_{\alpha s_\alpha}) \right\rangle_{\rm MF,c}. \tag{3.52}$$

Thus, once the mean-field system is solved, correlation functions of $\mathbf{R}, \hat{\mathbf{R}}$ can be studied through a momentum space RG treatment to obtain the scaling exponents of the fields in the long-time, large wavelength (hydrodynamic) limit. $\mathbf{R}$ and $\hat{\mathbf{R}}$ are like coarse-grained forms of the original fields $\mathbf{r}$ and $\hat{\mathbf{r}}$ since all correlation functions of $\mathbf{r}, \hat{\mathbf{r}}$ are equal to corresponding correlation functions of $\mathbf{R}, \hat{\mathbf{R}}$ in the hydrodynamic limit[51]. Therefore, it is sufficient to find the scaling behavior of $\mathbf{R}, \hat{\mathbf{R}}$ to deduce the desired critical exponents.

3.5 Mean Field Theory

In this section, we calculate response and correlation functions of the local system described by $Z_{\rm MF}$, which gives the vertex functions in the diagrammatic expansion of $\tilde{S}$. We will only need to calculate the leading terms as higher order vertices will turn out to be irrelevant in the critical region. Due to the averaging, $Z_{\rm MF}$ is identical at all sites j, and it is sufficient to examine a single point. Setting $\overline{\mathbf{r}}(t) \equiv \mathbf{r}_j(t) - \mathbf{v}t$, and $\varepsilon(t) \equiv \varepsilon_j(t)$, the equation of motion becomes

$$\eta\left(\frac{d\overline{r}_\alpha}{dt} + v_\alpha\right) = -\overline{r}_\alpha + F_\alpha + \tilde{f}_\alpha\left(\mathbf{v}t + \overline{\mathbf{r}}(t)\right) + \varepsilon_\alpha(t). \tag{3.53}$$

$\mathbf{F}$ is determined as a function of $\mathbf{v}$ self-consistently by requiring that $\langle\overline{\mathbf{r}}\rangle_{\rm MF} = \mathbf{0}$. The scaling behavior of $\mathbf{F}_{\rm MF}(\mathbf{v})$ near threshold can be determined from the following argument: For $v \ll \eta^{-1}F$, the particle follows a local minimum P of the effective potential

$$V_{\rm eff}(\overline{\mathbf{r}}, t) = V\left(\mathbf{x}, \mathbf{v}t + \overline{\mathbf{r}}(t)\right) + \frac{|\overline{\mathbf{r}}(t)|^2}{2} - \mathbf{F}\cdot\overline{\mathbf{r}}(t).$$

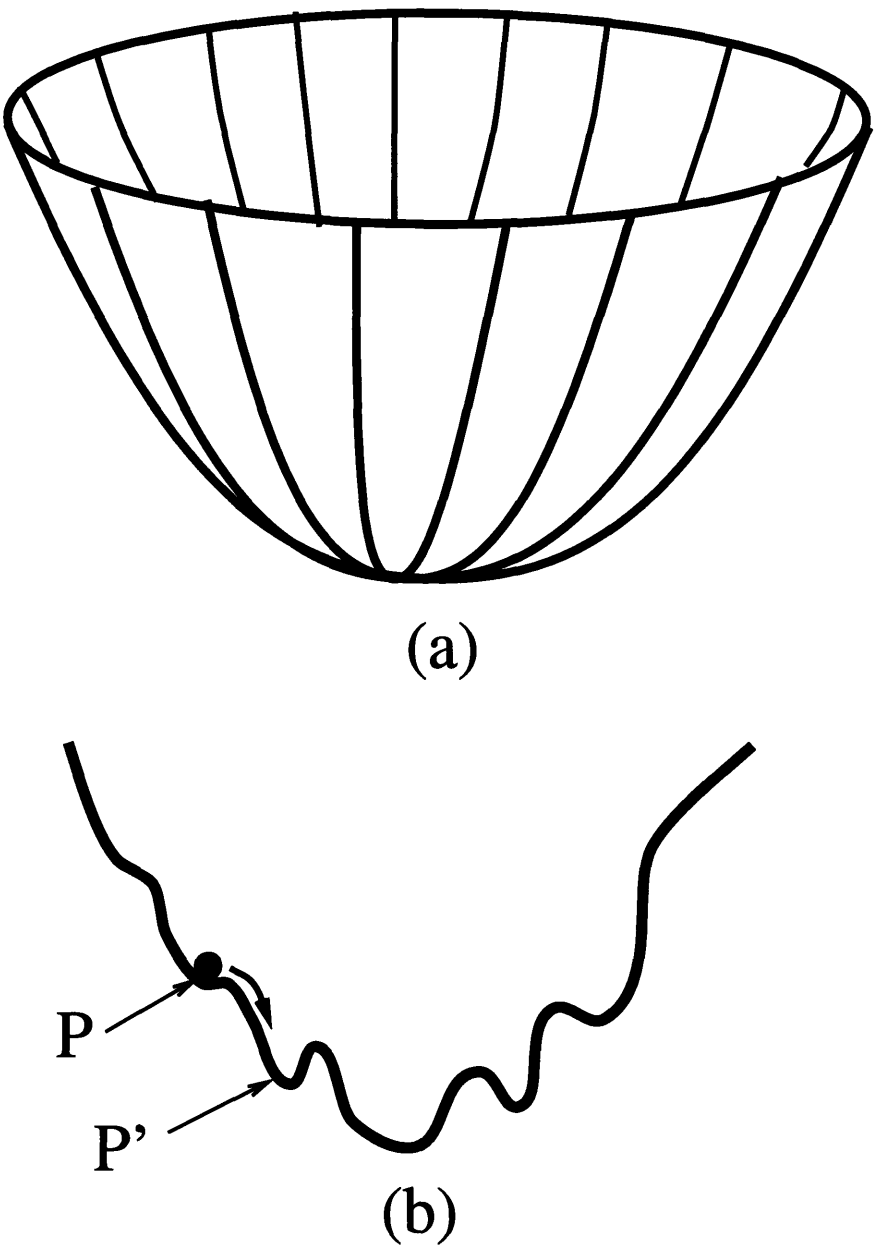

Figure 3-3: (a) The effective potential V_{eff}. The random part (not shown) superimposed on the paraboloid slides with velocity $-\mathbf{v}$. (b) A cross section of V_{eff}. The particle stays in a local minimum P for a time of $O(v^{-1})$, after which the minimum disappears and the particle finds another local minimum P' within a finite time. Time averages are dominated by the slow portion of the motion as $v \to 0$.

A representative snapshot of $V_{\mathbf{eff}}$, which consists of a paraboloid centered at $\overline{\mathbf{r}} = \mathbf{F}$ with a superimposed random potential, is shown in Fig. 3.5. The position of the local minimum P shifts with a velocity of $O(v)$ as time progresses. Eventually, P disappears at a saddle point as it is pushed up the sides of the hyperparaboloid. At this moment, the particle quickly moves to a new local minimum P', after which it starts following the slow motion of P', as shown in Fig. 3.5. For scalloped random potentials with discontinuous derivatives at the saddle points, the particle starts moving with a velocity of $O(1)$ (i.e., independent of v as $v \to 0$) *as soon as* P disappears, and reaches the vicinity of P' in $O(1)$ time, giving the result $\beta_{\mathrm{MF}} = 1$.[3] We have also numerically integrated Eq. (3.53) (for Model A) to verify that $\beta_{\mathrm{MF}} = 1$.

Now we proceed to compute vertex functions $\mathcal{V}_{\{m_\alpha,n_\alpha\}}\left(\{t_{\alpha s_\alpha}\};\{t'_{\alpha s'_\alpha}\}\right)$ in the perturbative expansion of $\tilde{S}$, which correspond to response and connected correlation functions of the MF theory, in increasing order in the field variables $\mathbf{R}, \hat{\mathbf{R}}$. From now on, we set $m = m_{\|} + m_{\perp}$, and $n = n_{\|} + n_{\perp}$.

3.5.1 Average position (m=1, n=0)

By construction $\langle \overline{\mathbf{r}} \rangle_{\mathrm{MF}} = 0$, but we prefer to expand around the true $\mathbf{F}(\mathbf{v})$ instead of the mean-field value of the force $\mathbf{F}_{\mathrm{MF}}(\mathbf{v})$. Since the effect of an additional uniform static force $\mathbf{F} - \mathbf{F}_{\mathrm{MF}}(\mathbf{v})$ can be fully counteracted by a shift in $\overline{\mathbf{r}}$, this does not affect connected correlation or response functions. Thus, the only effect of this shift is to produce an additional term $\sum_i [\mathbf{F} - \mathbf{F}_{\mathrm{MF}}(\mathbf{v})] \cdot \hat{\mathbf{R}}_i$ in $\tilde{S}$, which only has a $q = 0$ component and does not directly enter the renormalization of higher order terms.

3.5.2 Linear Response (m=1, n=1)

The linear response is given by the rank 2 tensor,

$$\tilde{\chi}_{\alpha\gamma}(t - t') = \left\langle \frac{\delta \overline{r}_\alpha(t)}{\delta \varepsilon_\gamma(t')} \right\rangle_{\mathrm{MF}}.$$

We are only interested in the low-frequency form of the Fourier transformed linear response $\tilde{\chi}(\omega)$, i.e. when $\boldsymbol{\varepsilon}$ is slowly varying in time. In this case, we can write $\boldsymbol{\varepsilon}(t) \approx \boldsymbol{\varepsilon}_0 + \boldsymbol{\varepsilon}_1 t$, neglecting terms proportional to $\ddot{\boldsymbol{\varepsilon}}$. To find the response $\overline{\mathbf{r}}_{\boldsymbol{\varepsilon}}(t)$, let us define

$$\overline{\mathbf{r}}'_{\boldsymbol{\varepsilon}}(t) = \overline{\mathbf{r}}_{\boldsymbol{\varepsilon}}(t) - \boldsymbol{\varepsilon}_0 - \boldsymbol{\varepsilon}_1 t - \mathbf{F}_{\mathrm{MF}}(\mathbf{v}) + \mathbf{F}_{\mathrm{MF}}(\mathbf{v} + \boldsymbol{\varepsilon}_1).$$

Taking a time derivative and using Eq.(3.53), we obtain

$$\eta(\dot{\overline{\mathbf{r}}}'_{\boldsymbol{\varepsilon}} + \mathbf{v} + \boldsymbol{\varepsilon}_1) = -\overline{\mathbf{r}}'_{\boldsymbol{\varepsilon}} + \mathbf{F}_{\mathrm{MF}}(\mathbf{v} + \boldsymbol{\varepsilon}_1) + \tilde{\mathbf{f}}((\mathbf{v} + \boldsymbol{\varepsilon}_1)t + \overline{\mathbf{r}}'_{\boldsymbol{\varepsilon}} - \mathbf{F}_{\boldsymbol{\varepsilon}}), \tag{3.54}$$

where $\mathbf{F}_{\boldsymbol{\varepsilon}} = \mathbf{F}_{\mathrm{MF}}(\mathbf{v} + \boldsymbol{\varepsilon}_1) - \mathbf{F}_{\mathrm{MF}}(\mathbf{v}) - \boldsymbol{\varepsilon}_0$. But now, $\langle \overline{\mathbf{r}}'_{\boldsymbol{\varepsilon}} \rangle = \mathbf{0}$ by definition of $\mathbf{F}_{\mathrm{MF}}$. (The random force $\tilde{\mathbf{f}}$ is evaluated at points shifted by a constant amount $\mathbf{F}_{\boldsymbol{\varepsilon}}$, but this has no significance upon averaging over randomness.) This gives

$$\langle \overline{\mathbf{r}}_{\boldsymbol{\varepsilon}}(t) \rangle = \boldsymbol{\varepsilon}(t) + \mathbf{F}_{\mathrm{MF}}(\mathbf{v}) - \mathbf{F}_{\mathrm{MF}}\left(\mathbf{v} + \dot{\boldsymbol{\varepsilon}}(t)\right) + O(\ddot{\boldsymbol{\varepsilon}}). \tag{3.55}$$

[3] In contrast, for smooth potentials, there is a v-dependent acceleration time just after P disappears, which contributes to the critical dynamics and gives $\beta_{\mathrm{MF}} = 3/2$.[50, 52].

Expanding $\mathbf{F}_{\rm MF}(\mathbf{v}+\dot{\epsilon})$ for small $\dot{\epsilon}$, we obtain

$$\tilde{\chi}_{\alpha\gamma}(\omega) = \delta_{\alpha\gamma} + i\omega \left[\frac{\partial F_{{\rm MF}\alpha}(\mathbf{v})}{\partial v_\gamma}\right]_{\mathbf{v}=v\mathbf{e}_\parallel} + O(\omega^2). \tag{3.56}$$

Since $\beta_{\rm MF} = 1$, the linear response tensor will have the form

$$\tilde{\boldsymbol{\chi}}(\omega) = \mathbf{1} + i\omega \begin{pmatrix} A_{11} & -\frac{1}{v}A_{12} \\ A_{21} & \frac{1}{v}A_{22} \end{pmatrix}, \tag{3.57}$$

where $A_{\alpha\gamma}$ approach constants as $v \to 0$ [cf. Eq.(3.43)]. For Model A, $\tilde{\boldsymbol{\chi}}(\omega)$ is diagonal due to symmetry, and $A_{12} = A_{21} = 0$.

3.5.3 Nonlinear response (m=1, n>1)

Assuming that $\mathbf{F}_{\rm MF}(\mathbf{v})$ has a Taylor expansion around $\mathbf{v} = v\mathbf{e}_\parallel$ for $v > 0$, we can expand the RHS of Eq. (3.55) to obtain the nonlinear response of the model. The leading term in the low-frequency limit is proportional to ω^n, and it is straightforward to show that the contribution of these terms to $\tilde{S}$ is

$$-\frac{1}{n_\parallel! n_\perp!} \int d^dx\, dt\, \hat{R}_\alpha(\mathbf{x},t)(\partial_t R_\parallel)^{n_\parallel}(\partial_t R_\perp)^{n_\perp} \left[\frac{\partial^n F_\alpha(\mathbf{v})}{\partial^{n_\parallel} v_\parallel \partial^{n_\perp} v_\perp}\right]_{\mathbf{v}=v\mathbf{e}_\parallel}. \tag{3.58}$$

These terms are irrelevant at the RG fixed point, as we shall show later.

3.5.4 Two-point Correlation Functions (m=2, n≥0)

At low velocities, the particle spends most of the time near a local minimum, jumping abruptly to the next one when this minimum disappears. Therefore, the time scale associated with the correlation functions is given by the temporal separation between two consecutive jumps, which scales as $1/v$. In the $v \to 0$ limit, the correlation functions depend on t only through the rescaled time variable $u \equiv vt$, since the positions of successive minima near threshold are determined by energetic considerations, and do not depend on v. (The correlation functions may also depend on the drift direction $\hat{v}$. We shall suppress this dependence for notational brevity.) Let us define

$$\langle \overline{r}_\alpha(t)\overline{r}_\gamma(t')\rangle_{{\rm MF},c} \equiv C_{\alpha\gamma}\left(v(t-t')\right). \tag{3.59}$$

Since successive positions of the local minima are uncorrelated, we expect that $C_{\alpha\gamma}(u)$ decay quickly as a function of $u \equiv vt$ for $|u| > 1$. By definition,

$$\begin{aligned} C_\parallel(u) &\equiv C_{11}(u) = C_{11}(-u), \\ C_\perp(u) &\equiv C_{22}(u) = C_{22}(-u), \\ \frac{1}{2}C_\times(u) &\equiv C_{12}(u) = C_{21}(-u). \end{aligned}$$

As a result of the abrupt jumps from one minimum to another, $C_{\alpha\gamma}(vt)$ have a discontinuous derivative at the origin, rounded at a scale of $O(v)$. In Model A, $C_\times(u) = 0$ due to symmetry.

The only other important terms in the effective action $\tilde{S}$ involve the series $m = 2, n = n_\parallel > 0, n_\perp = 0$. All vertex functions associated with this series are given by the response of connected correlation functions to *longitudinal* forces. These response functions are intimately related to the two-point correlation functions $C_{\alpha\gamma}(u)$ by the following argument: Static forces only change linear response, and do not affect connected correlation functions. For a slowly varying external force $\varepsilon(t)\mathbf{e}_\parallel$, however, the system will respond as if the instantaneous velocity is $(v + \dot{\varepsilon})\mathbf{e}_\parallel$. Neglecting terms proportional to $\ddot{\varepsilon}$,

$$\begin{aligned}\left[\langle \overline{r}_\alpha(t)\overline{r}_\gamma(t')\rangle_{\mathrm{MF},c}\right]_\varepsilon &= C_{\alpha\gamma}\left((v+\dot{\varepsilon})(t-t')\right) + O(\ddot{\varepsilon}) \\ &\approx C_{\alpha\gamma}\left(v(t-t') + \varepsilon(t) - \varepsilon(t')\right).\end{aligned}$$

Now, Taylor expanding $C_{\alpha\gamma}$ around $v(t-t')$ and taking successive functional derivatives with respect to ε, we finally obtain the contribution of this series to $\tilde{S}$ as

$$\begin{aligned}\mathcal{U} = \sum_{n=1}^{\infty} \frac{1}{2!n!} \int d^dx\, dt\, dt'\, \hat{R}_\alpha(\mathbf{x},t)\hat{R}_\gamma(\mathbf{x},t') \\ \times U_{\alpha\gamma,n}\left(v(t-t')\right)\left[R_\parallel(\mathbf{x},t) - R_\parallel(\mathbf{x},t')\right]^n,\end{aligned} \tag{3.60}$$

where $U_{\alpha\gamma,n}(u)$ is the nth derivative of $C_{\alpha\gamma}(u)$.

The vertices with $m = 2, n_\perp > 0$ and $m > 3$ are all irrelevant, as shown in the next section.

3.6 Scaling and RG

The terms in $\tilde{S}$ that are up to second order in the fields are

$$\begin{aligned}\tilde{S}_0 = &- \int dt\, d^dx \left[\mathbf{F} - \mathbf{F}_{\mathrm{MF}}(\mathbf{v})\right]\cdot\hat{\mathbf{R}}(\mathbf{x},t) \\ &- \frac{1}{2}\int_{\mathbf{q},\omega} \begin{bmatrix}\hat{\mathbf{R}}(-\mathbf{q},-\omega) \\ \mathbf{R}(-\mathbf{q},-\omega)\end{bmatrix}^{\mathrm{T}} \cdot \begin{bmatrix} -\mathbf{C}(\omega) & \mathbf{J}^{-1}(\mathbf{q}) - \tilde{\boldsymbol{\chi}}(\omega) \\ \mathbf{J}^{-1}(-\mathbf{q}) - \tilde{\boldsymbol{\chi}}(-\omega) & \mathbf{0}\end{bmatrix} \cdot \begin{bmatrix}\hat{\mathbf{R}}(\mathbf{q},\omega) \\ \mathbf{R}(\mathbf{q},\omega)\end{bmatrix},\end{aligned} \tag{3.61}$$

where $J^{-1}_{\alpha\gamma}(\mathbf{q}) = \left(\delta_{\alpha\gamma} - K_{\alpha\gamma}q^2\right)^{-1} \approx \delta_{\alpha\gamma} + K_{\alpha\gamma}q^2$ for small q. For notational brevity, I use $\int_{\mathbf{q},\omega}$ to denote $\int \frac{d^dq}{(2\pi)^d}\frac{d\omega}{2\pi}$. Using Eq.(3.57), the quadratic form in the action can be written as

$$-\frac{1}{2}\int_{\mathbf{q},\omega} \begin{bmatrix}\hat{R}_\parallel(-\mathbf{q},-\omega) \\ \hat{R}_\perp(-\mathbf{q},-\omega) \\ R_\parallel(-\mathbf{q},-\omega) \\ \frac{1}{v}R_\perp(-\mathbf{q},-\omega)\end{bmatrix}^{\mathrm{T}} \cdot \mathcal{Q}(\mathbf{q},\omega) \cdot \begin{bmatrix}\hat{R}_\parallel(\mathbf{q},\omega) \\ \hat{R}_\perp(\mathbf{q},\omega) \\ R_\parallel(\mathbf{q},\omega) \\ \frac{1}{v}R_\perp(\mathbf{q},\omega)\end{bmatrix}, \tag{3.62}$$

where

$$\mathcal{Q}(\mathbf{q},\omega) = \begin{bmatrix} -C_{\|}(\omega) & -\frac{1}{2}C_{\times}(\omega) & K_{11}q^2 - i\omega A_{11} & vK_{12}q^2 + i\omega A_{12} \\ -\frac{1}{2}C_{\times}(-\omega) & -C_{\perp}(\omega) & K_{21}q^2 - i\omega A_{21} & vK_{22}q^2 - i\omega A_{22} \\ K_{11}q^2 + i\omega A_{11} & K_{21}q^2 + i\omega A_{21} & 0 & 0 \\ vK_{12}q^2 - i\omega A_{12} & vK_{22}q^2 + i\omega A_{22} & 0 & 0 \end{bmatrix}.$$

Neglecting all higher order terms in the action, we arrive at a Gaussian theory, in which different Fourier modes are decoupled, and which can be solved by inverting the matrix in Eq.(3.62). (See Appendix 3A.) The quadratic action (3.61) remains invariant under the scale transformation

$$\begin{aligned} &\mathbf{x} \to b\mathbf{x}, && t \to b^2 t, \\ &R_{\|} \to b^{2-d/2} R_{\|}, && R_{\perp} \to b^{2-d} R_{\perp}, \\ &\hat{R}_{\|} \to b^{-2-d/2} \hat{R}_{\|}, && \hat{R}_{\perp} \to b^{-2-d/2} \hat{R}_{\perp}, \\ &v \to b^{-d/2} v, && F - F_{\mathrm{MF}} \to b^{-d/2}(F - F_{\mathrm{MF}}), \end{aligned} \tag{3.63}$$

except for terms proportional to K_{12} and K_{22} which vanish at the depinning transition as $v \to 0^+$. For $d > 4$, all higher order terms in $\tilde{S}$ decay away upon rescaling, and we recover an asymptotically quadratic theory with critical exponents $\beta = 1$, $z_{\|} = 2$, $\nu = 2/d$, $\zeta_{\|} = (4-d)/2$, $\zeta_{\perp} = 2 - d$. The remaining exponent, $z_{\perp}$, can be found by comparing the static and dynamic parts of the transverse linear response. This gives $z_{\perp} = 2 + d/2 = z_{\|} + 1/\nu$, as shown previously by the exponent identity (3.13). The exponents related to longitudinal fluctuations, not surprisingly, are identical to corresponding exponents in the interface problem[56]. However, we have also calculated new exponents characterizing transverse fluctuations. We see that even the simple Gaussian theory exhibits anisotropic exponents.

At $d = d_c = 4$ dimensions, the scaling dimension of $R_{\|}$ changes sign and we cannot neglect its higher powers anymore. Simple dimensional analysis indicates that the only higher order terms in $\tilde{S}$ which become marginal at $d = d_c$ involve vertex functions $U_{\alpha\gamma,n}$, given in Eq.(3.60). This series can be summed up over n, together with the $n = 0$ term $C_{\alpha\gamma}$ included in the Gaussian theory, to yield

$$\frac{1}{2}\int d^d x\, dt\, dt' \hat{R}_{\alpha}(\mathbf{x},t)\hat{R}_{\gamma}(\mathbf{x},t')C_{\alpha\gamma}\left(v(t-t') + R_{\|}(\mathbf{x},t) - R_{\|}(\mathbf{x},t')\right). \tag{3.64}$$

All higher order terms in $\tilde{S}$ are formally irrelevant since they involve additional powers of $\hat{R}_{\|}$, $\hat{R}_{\perp}$, or $R_{\perp}$, whose scaling exponents are less than zero.

For $d < d_c$, the vertex functions $U_{\alpha\gamma,n}$ become more and more relevant for increasing n under the rescaling (3.63), and the fixed point moves away from the Gaussian

theory. In $d = 4 - \epsilon$ dimensions, we look for new fixed points with different scaling properties:

$$\begin{aligned} &\mathbf{x} \to b\mathbf{x}, && t \to b^{z_\parallel} t, \\ &R_\parallel \to b^{\zeta_\parallel} R_\parallel, && R_\perp \to b^{\zeta_\perp} R_\perp, \\ &\hat{R}_\parallel \to b^{\theta_\parallel - d} \hat{R}_\parallel, && \hat{R}_\perp \to b^{\theta_\perp - d} \hat{R}_\perp, \\ &F - F_{\rm MF} \to b^{-1/\nu}(F - F_{\rm MF}), && \mathbf{v} \to b^{-\beta/\nu}\mathbf{v}. \end{aligned} \tag{3.65}$$

To calculate the new exponents to first order in ϵ, we employ a one-loop momentum shell RG scheme, treating all non-Gaussian terms in the action (i.e. $\mathcal{U}$ in Eq.(3.60)), as a perturbation. Perturbative calculations proceed by expanding $\langle e^{\mathcal{U}} \rangle_0$, where $\langle \cdots \rangle_0$ denotes averaging with respect to the Gaussian action $\tilde{S}_0$, in powers of $\mathcal{U}$. A renormalization transformation is then constructed as follows: **(1)** Perform the averages only over short wavelength fluctuations $\hat{\mathbf{R}}^>, \mathbf{R}^>$ with wavenumbers $\Lambda/b < |\mathbf{q}| < \Lambda$, where $b = e^{\delta\ell}$. The resulting coarse grained action is perturbatively given by

$$\tilde{S}^< = \tilde{S}_0^< + \langle \mathcal{U} \rangle_0^> + \frac{1}{2}\langle \mathcal{U}^2 \rangle_{0,c}^> + O(\mathcal{U}^3). \tag{3.66}$$

(2) Apply the rescaling transformations given in (3.65), bringing back the short-distance cutoff Λ to its original value. **(3)** The exponents are then determined from the fixed points associated with the RG flows of the the action. Since Models A and B are characterized by distinct fixed points, we shall discuss them separately.

3.6.1 Model A

In the low frequency, small wave vector limit, the effective action for Model A is

$$\begin{aligned} \tilde{S}^{(A)} \;=\; & -\int dt\, d^dx\, [F - F_{\rm MF}(v)] \hat{R}_\parallel(\mathbf{x},t) \\ & - \int_{\mathbf{q},\omega} \Big\{ \hat{R}_\parallel(-\mathbf{q},-\omega) R_\parallel(\mathbf{q},\omega)(Kq^2 - i\omega A_{11}) \\ & \qquad + \hat{R}_\perp(-\mathbf{q},-\omega) R_\perp(\mathbf{q},\omega)(Kq^2 - i\omega A_{22}/v) \Big\} \\ & + \frac{1}{2}\int d^dx\, dt\, dt'\, \hat{R}_\parallel(\mathbf{x},t)\hat{R}_\parallel(\mathbf{x},t') C_\parallel \Big(v(t-t') + R_\parallel(\mathbf{x},t) - R_\parallel(\mathbf{x},t') \Big) \\ & + \frac{1}{2}\int d^dx\, dt\, dt'\, \hat{R}_\perp(\mathbf{x},t)\hat{R}_\perp(\mathbf{x},t') C_\perp \Big(v(t-t') + R_\parallel(\mathbf{x},t) - R_\parallel(\mathbf{x},t') \Big) . \end{aligned} \tag{3.67}$$

The Gaussian part has the correlation functions,

$$\langle \hat{R}_\parallel(-\mathbf{q},-\omega) R_\parallel(\mathbf{q},\omega) \rangle_0 \;=\; \frac{1}{Kq^2 - i\omega A_{11}}, \tag{3.68a}$$

$$\langle \hat{R}_\perp(-\mathbf{q},-\omega) R_\perp(\mathbf{q},\omega) \rangle_0 \;=\; \frac{1}{Kq^2 - i\omega A_{22}/v}, \tag{3.68b}$$

$$\langle R_{\|}(-\mathbf{q},-\omega)R_{\|}(\mathbf{q},\omega)\rangle_0 = \frac{C_{\|}(\omega)}{K^2q^4+(\omega A_{11})^2}, \tag{3.68c}$$

$$\langle R_{\perp}(-\mathbf{q},-\omega)R_{\perp}(\mathbf{q},\omega)\rangle_0 = \frac{C_{\perp}(\omega)}{K^2q^4+(\omega A_{22}/v)^2}. \tag{3.68d}$$

The vertex functions $U_{\alpha\gamma,n} = 0$ for $\alpha \neq \gamma$, and these terms are not generated by the RG transformation. The renormalization of remaining vertex functions $U_{\|,n}$, and $U_{\perp,n}$ for $n > 0$ can be recast into a functional renormalization of $C_{\|}(vt)$ and $C_{\perp}(vt)$, provided that vt and $R_{\|}$ scale in the same way, i.e. $\zeta_{\|} = z_{\|} - \beta/\nu$. This relation can be independently obtained from Eqs. (3.29) and (3.38), derived in Sec. 3.3 from more general (and nonperturbative) arguments. The renormalized vertex functions are then obtained from successive derivatives of $C(vt)$ as

$$U_{\alpha,n}(u) = C_{\alpha}^{(n)}(u). \tag{3.69}$$

This ensures that the form of Eq.(3.67) is retained under renormalization, albeit with renormalized parameters. Eqs. (3.68c) and (3.68d) suggest that $C_{\alpha}(vt)$ may be interpreted as *temporal* correlation functions of an effective force generated by the quenched disorder.

The renormalization of some terms in Eq.(3.67) do not get any contribution from the momentum shell averaging step, giving rise to additional exponent relations that are correct to all orders in the ϵ expansion. The first relation is due to the fact that F never appears explicitly in any of the contractions or higher order vertex functions. Thus, the renormalization of the term proportional to $F - F_{\rm MF}$ can be written as

$$\frac{\partial(F-F_{\rm MF})}{\partial\ell} = (z_{\|}+\theta_{\|})(F-F_{\rm MF}) + \text{constant}, \tag{3.70}$$

where "constant" refers to an expression that does not involve F. This RG flow equation can be rewritten as

$$\frac{\partial(F-F_c)}{\partial\ell} = (z_{\|}+\theta_{\|})(F-F_c), \tag{3.71}$$

with a suitable choice of F_c. Hence, higher order corrections may shift the threshold force, but do not influence the scaling of $F - F_c$. This implies that

$$z_{\|} + \theta_{\|} - 1/\nu = 0. \tag{3.72}$$

Furthermore, there are no contractions that contribute to the renormalization of K or A_{22}. Thus,

$$\theta_{\|} + z_{\|} + \zeta_{\|} - 2 = 0, \tag{3.73}$$

$$\theta_{\perp} + \zeta_{\perp} + \beta/\nu = 0, \tag{3.74}$$

respectively. As a result, all critical exponents are determined in terms of $\zeta_{\|}$, $\zeta_{\perp}$ and $z_{\|}$. These exponents can be computed by constructing RG flow equations for the remaining parameters.

Renormalization of C_α

After performing the momentum shell integration and rescaling, details of which are given in Appendix 3B, we arrive at the recursion relations for the renormalized functions $C_\alpha(u)$:

$$\frac{\partial C_{\|}(u)}{\partial \ell} = [\epsilon + 2\theta_{\|} + 2(z_{\|} - 2)]C_{\|}(u) + \zeta_{\|} u C'_{\|}(u) - K_d \left\{ [C'_{\|}(u)]^2 + [C_{\|}(u) - C_{\|}(0)]C''_{\|}(u) \right\}, \tag{3.75}$$

$$\frac{\partial C_{\perp}(u)}{\partial \ell} = [\epsilon + 2\theta_{\perp} + 2(z_{\|} - 2)]C_{\perp}(u) + \zeta_{\|} u\, C'_{\perp}(u) - K_d \left\{ [C_{\|}(u) - C_{\|}(0)]C''_{\perp}(u) \right\}. \tag{3.76}$$

The constant $K_d \equiv S_d \Lambda^{d-4}/[(2\pi)^d K^2]$, where S_d is the area of the unit sphere in d-dimensions. Primes denote derivatives with respect to u. Terms proportional to $uC'_\alpha(u)$ arise from the rescaling of u. We look for fixed-point solutions $C^*_\alpha(u)$ that decay to 0 when $|u|$ is large, since they are related to correlation functions of the system, which are expected to vanish for large time differences.

Not surprisingly, the functional recursion relation for $C_{\|}(u)$ is identical to the one obtained in Ref. [56]. In fact, all higher loop corrections are identical as well. This is in excellent harmony with the argument presented in Sec. 3.3, and allows us to use the results of NF. Setting $\partial C^*_{\|}/\partial \ell = 0$, and integrating Eq. (3.75) from $u = -\infty$ to ∞, we get

$$[\epsilon + 2\theta_{\|} + 2(z_{\|} - 2) - \zeta_{\|}] \int_{-\infty}^{\infty} C^*_{\|}(u)\, du = 0. \tag{3.77}$$

Provided that the RG flows go to a fixed-point solution with $\int C^* \neq 0$, this implies that $\zeta_{\|} = \epsilon - 2[2 - (z_{\|} + \theta_{\|})]$. The mean-field correlation function satisfies this integral condition for both random-field and random-bond disorder, since C is essentially insensitive to the value of the random potential between consecutive local minima P, where the line moves quickly. There are other fixed points with $\int C^* = 0$, but they are irrelevant for our discussion. Thus, from Eqs. (3.29) and (3.72), we obtain

$$\zeta_{\|} = \epsilon/3, \tag{3.78}$$

$$\nu = \frac{3}{6 - \epsilon}. \tag{3.79}$$

NF prove that these results are correct to *all orders* in ϵ, by showing that the contributions to the renormalization of $C_{\|}(u)$ from higher-order terms is a complete derivative with respect to u. Upon integration over u, such higher order terms do not alter Eq.(3.77), leaving the exponents unchanged.

Using $\zeta_{\|} = \epsilon/3$, an implicit solution for $C^*_{\|}(u)$ is obtained as

$$C^*_{\|}(u) - C^*_{\|}(0) - C^*_{\|}(0) \ln\left(\frac{C^*_{\|}(u)}{C^*_{\|}(0)}\right) = \frac{C^*(0)}{2}\left(\frac{u}{u_0}\right)^2,$$

where $u_0 \equiv \sqrt{3K_d C^*(0)/\epsilon}$. $C^*_{\|}(0)$ is arbitrary, and can be changed by a rescaling of the fields $R_{\|}$. Expanding the logarithm for small u, we see that there is a kink at the origin, as

$$\frac{C^*_{\|}(u)}{C^*_{\|}(0)} = \left[1 - \frac{|u|}{u_0} + \frac{1}{3}\left(\frac{u}{u_0}\right)^2\right] + O(|u/u_0|^3). \tag{3.80}$$

For $|u| \gg u_0$, the fixed point solution behaves like a Gaussian, and

$$C^*_{\|}(u) \approx C^*_{\|}(0) \exp\left[-\frac{u^2}{2u_0^2}\right].$$

We next examine the fixed-point solution $C^*_{\perp}(u)$, which is the new element of our computation. Setting $\partial C^*_{\perp}/\partial \ell = 0$ and looking at the limit $u \to 0^+$, we get (assuming that $C^*_{\perp}(0^+) \neq 0$)

$$[\epsilon + 2\theta_{\perp} + 2(z_{\|} - 2)]C^*_{\perp}(0^+) = 0. \tag{3.81}$$

Combined with Eqs.(3.29), (3.38), and (3.74), this result implies

$$\zeta_{\perp} = \zeta_{\|} - \frac{d}{2} = -2 + \frac{5\epsilon}{6}. \tag{3.82}$$

In Appendix 3C, we show that this result is in fact correct to all orders in ϵ since there are no contributions to $C^*_{\perp}(0^+)$ from momentum-shell integration. The fixed point solution (for $u > 0$) satisfies the equation

$$\frac{d}{du} \ln |C^{*\prime}_{\perp}(u)| = \frac{u}{u_0^2}\left[\frac{C^*_{\|}(u)}{C^*_{\|}(0)} - 1\right]^{-1}. \tag{3.83}$$

Upon integrating twice, Eq. (3.83) leads to

$$C^*_{\perp}(u) = -\frac{C^{*\prime}_{\perp}(0^+)}{u_0} \int_u^{\infty} du' \exp\left\{-\frac{1}{u_0^2}\int_{0+}^{u'} du'' \frac{u''}{1 - \left[C^*_{\|}(u'')/C^*_{\|}(0)\right]}\right\}, \tag{3.84}$$

where $C^{*\prime}_{\perp}(0^+)$ is arbitrary in the same sense as $C^*_{\|}(0)$. For $|u| \gg u_0$, Eq.(3.83) gives

$$C^*_{\perp}(u) \approx C\frac{u_0^2}{u} \exp\left[-\frac{u^2}{2u_0^2}\right], \tag{3.85}$$

where C is a constant related to $C^{*\prime}_{\perp}(0^+)$. The numerical solution for the fixed point functions $C^*_{\alpha}(u)$ are shown in Fig. 3-4. The qualitative features of $C^*_{\|}$ and $C^*_{\perp}$ are similar: both have a discontinuous derivative at the origin, and decay as a Gaussian for large values of $|u|$. However, note that their scaling dimensions differ by $\zeta_{\|}$.

The exponent $\zeta_{\|} = \epsilon/3$ can also be obtained by naive dimensional arguments: In dimensions $d > 4$, the random force can be expanded as $f_{\|}(\mathbf{x}, r_{\|}, r_{\perp}) = f_{\|}(\mathbf{x}, 0, 0) + O(r_{\|}, r_{\perp})$. Since both $r_{\|}$ and $r_{\perp}$ have negative scaling dimensions ($\zeta_{\|}, \zeta_{\perp} < 0$), the correction terms can be ignored. The random force scales as $b^{-d/2}$ under a scaling $\mathbf{x} \to b\mathbf{x}$, leading to the Gaussian roughness of $\zeta_{\|} = 2 - d/2$. A similar scaling

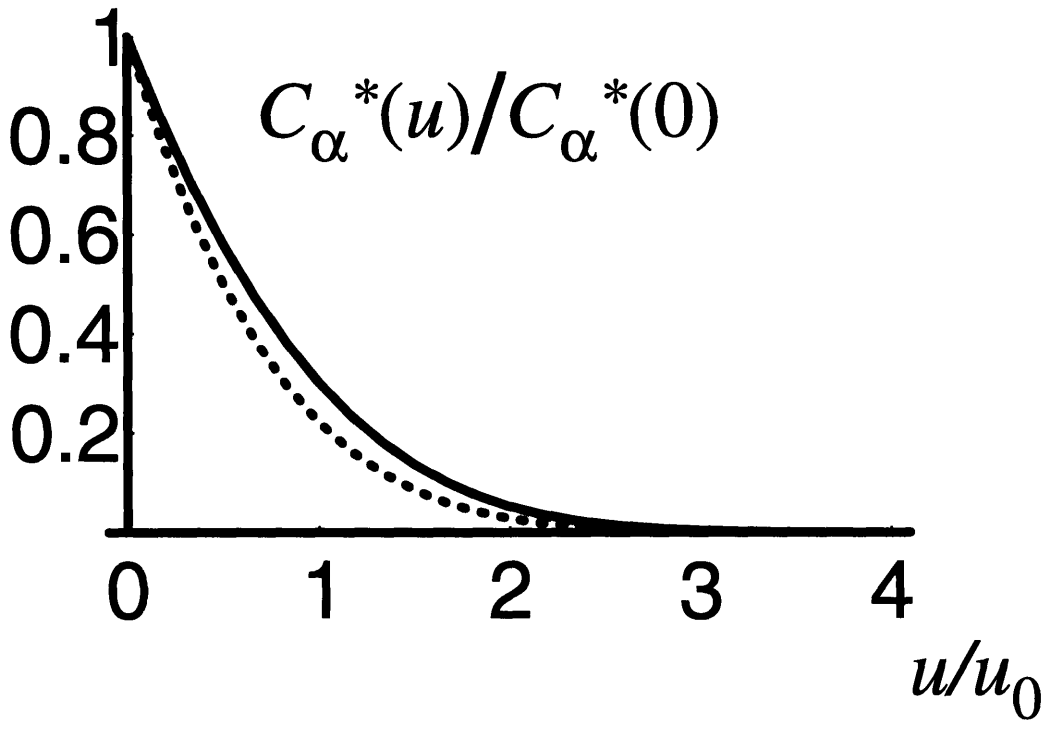

Figure 3-4: Fixed point functions $C_{\|}^*(u)$ (solid line) and $C_{\perp}^*(u)$ (dotted line), normalized to yield 1 at the origin. Their values for $u < 0$ (not shown) are found from $C_\alpha^*(u) = C_\alpha^*(-u)$.

argument applied to Eq.(3.25) leads to $\zeta_\perp = \zeta_{\|} - d/2 = 2 - d$. For $d < 4$, the scaling dimension of $r_{\|}$ is positive, and higher powers of $r_{\|}$ in an expansion of $f_{\|}(\mathbf{x}, r_{\|}, r_\perp)$ are more relevant. It is then reasonable to assume that in this case the statistical properties of $f_{\|}$ at large $r_{\|}$ are crucial. If uncorrelated at large separation, $f_{\|}(\mathbf{x}, r_{\|}, 0)$ scales as $b^{-(d+\zeta_{\|})/2}$. When equated to $b^{\zeta_{\|}-2}$ for the scaling of $\nabla_{\mathbf{x}}^2 r_{\|}$, this leads to $\zeta_{\|} = \epsilon/3$ in agreement with the RG treatment. Essentially, the statement regarding the non-renormalization of $\int du\, C_{\|}(u)$ justifies the above "naive" scaling. However, a similar reasoning from Eq.(3.25) would have concluded $\zeta_\perp - \zeta_{\|} = -(d + \zeta_{\|})/2$, in disagreement with Eq.(3.82). In this case, $\int du\, C_\perp(u)$ *is* renormalized, but $C_\perp(0)$ is not; suggesting that despite the presence of relevant higher order powers in the expansion of $f_\perp(\mathbf{x}, r_{\|}, r_\perp)$ around $\mathbf{r} = \mathbf{0}$, the scaling properties are still controlled by $f_\perp(\mathbf{x}, 0, 0)$. We have no physical motivation for this rather curious conclusion.

Propagator Renormalization

The only one remaining exponent is $z_{\|}$, which can be obtained by examining the renormalization of A_{11}. One-loop contributions arise from the $n = 2$ term in $\langle \mathcal{U} \rangle_0^>$,

which is

$$\frac{1}{4}\int d^dx \int_{-\infty}^{\infty} dt \int_{-\infty}^{\infty} dt' \hat{R}_{\|}(\mathbf{x},t)\hat{R}_{\|}(\mathbf{x},t')[R_{\|}(\mathbf{x},t) - R_{\|}(\mathbf{x},t')]^2 C''_{\|}\left(v(t-t')\right).$$

Replacing $[R_{\|}(\mathbf{x},t')]^2$ with $[R_{\|}(\mathbf{x},t)]^2$ does not change the integral. Thus, upon further manipulation, this term in the action can be written as

$$\int d^dx \int_{-\infty}^{\infty} dt \int_{-\infty}^{t} dt' \hat{R}_{\|}(\mathbf{x},t)\hat{R}_{\|}(\mathbf{x},t')R_{\|}(\mathbf{x},t)[R_{\|}(\mathbf{x},t) - R_{\|}(\mathbf{x},t')]C''_{\|}\left(v(t-t')\right).$$

Since a contraction forces t and t' to be within $O(1)$ of each other, and we are only interested in the first time derivative, we can substitute $R_{\|}(\mathbf{x},t) - R_{\|}(\mathbf{x},t') \approx (t-t')\partial_t R_{\|}(\mathbf{x},t)$. Now, contracting $\hat{R}_{\|}(\mathbf{x},t')$ with $R_{\|}(\mathbf{x},t)$ and integrating over the momentum shell, we obtain a contribution to A_{11} equal to

$$-\delta\ell \frac{S_d\Lambda^d}{(2\pi)^d A_{11}} \int_0^{\infty} d\tilde{t}\,\tilde{t}\, e^{-K\Lambda^2\tilde{t}/A_{11}} C''_{\|}(v\tilde{t}). \tag{3.86}$$

The minus sign comes from the opposite overall signs of $m = 1$ and $m = 2$ terms in Eq. (3.67). For $v \to 0$, we can set the argument of $C''_{\|}$ to zero. However, this causes a problem: $C''_{\|}$ has a term proportional to $\delta(vt)$ in the low-frequency analysis, this term diverges as $1/v$ for $vt \to 0$. This apparent divergence cannot be avoided within the low-frequency analysis we have used so far. The propagator is sensitive to high-frequency behavior of the vertex functions. Careful analysis of the high frequency structure of $C''_{\|}$ shows that the terms that contribute to the diverging part of $C''_{\|}(0)$ *do not* enter the renormalization of the propagator. (See Appendix 3D.) This is essentially due to the causal nature of the response: Perturbations right after a jump do not influence the motion before the jump. The correct way to avoid these divergent terms within the low-frequency analysis is to use $C''_{\|}(0^+)$ instead of $C''_{\|}(0)$. Near the fixed point, this can be calculated to $O(\epsilon)$ from Eq. (3.80) as $C^{*''}_{\|}(0^+) = 2\epsilon/(9K_d)$, resulting in

$$A^{<}_{11} = A_{11} - \delta\ell A_{11} K_d C^{*''}_{\|}(0^+) = A_{11}[1 - \delta\ell(2\epsilon/9)].$$

Finally, after performing the rescaling, we obtain the recursion relation

$$\frac{\partial A_{11}}{\partial \ell} = A_{11}[\theta_{\|} + \zeta_{\|} - 2\epsilon/9], \tag{3.87}$$

which yields

$$z_{\|} = 2 - 2\epsilon/9 + O(\epsilon^2). \tag{3.88}$$

3.6.2 Model B

The presence of off-diagonal terms in the action changes the critical scaling properties of Model B. The nonzero contractions that appear in the momentum shell integration

in this case are (cf. Appendix 3A)

$$\langle \hat{R}_{\|}(-\mathbf{q},-\omega)R_{\|}(\mathbf{q},\omega)\rangle_0 = \frac{1}{K_{\|}q^2 - i\omega\rho_{\|}}, \tag{3.89a}$$

$$\langle \hat{R}_{\perp}(-\mathbf{q},-\omega)R_{\|}(\mathbf{q},\omega)\rangle_0 = \frac{\kappa}{K_{\|}q^2 - i\omega\rho_{\|}}, \tag{3.89b}$$

$$\langle R_{\|}(-\mathbf{q},-\omega)R_{\|}(\mathbf{q},\omega)\rangle_0 = \frac{\tilde{C}(\omega)}{K_{\|}^2 q^4 + \omega^2\rho_{\|}^2}, \tag{3.89c}$$

where

$$\begin{aligned} \kappa &\equiv A_{12}/A_{22}, \\ K_{\|} &\equiv K_{11} + \kappa K_{21}, \\ \rho_{\|} &\equiv A_{11} + \kappa A_{21}, \\ \tilde{C}(\omega) &\equiv C_{\|}(\omega) + \kappa \mathrm{Re}[C_{\times}(\omega)] + \kappa^2 C_{\perp}(\omega). \end{aligned}$$

In addition to the nonrenormalization relations (3.72-3.74), the nonrenormalization of K_{21} or A_{12} dictates that

$$\theta_{\|} = \theta_{\perp}. \tag{3.90}$$

This immediately implies the exponent identity

$$\zeta_{\perp} = \zeta_{\|} - 1/\nu. \tag{3.91}$$

The naive scaling argument based on Eq.(3.25) gives an equivalent result when the scaling dimension of $\partial r_{\perp}/\partial r_{\|}$ $(\zeta_{\perp} - \zeta_{\|})$ is equated to the scaling dimension of $f_{\perp}(\mathbf{x}, r_{\|}, 0)$ $[-(d + \zeta_{\|})/2]$. The naive argument works this time, since $\int du\, C_{\perp}(u)$ remains finite at the fixed point (see below).

Under this rescaling, κ and $K_{\|}$ remain unrenormalized, and the renormalizations of $\rho_{\|}$ and $\tilde{C}$ determine the remaining exponents $\zeta_{\|}$ and $z_{\|}$. The recursion relations of vertex functions C_{α} are more complicated, but there is a relatively simple fixed point solution with

$$\tilde{C}^*(u) = 4C_{\|}^*(u) = 2\kappa C_{\times}^*(u) = 4\kappa^2 C_{\perp}^*(u). \tag{3.92}$$

Furthermore, $\tilde{C}(u)$ satisfies a recursion relation identical to that of $C_{\|}(u)$ given in Eq.(3.75). This result once more shows that longitudinal fluctuations, whose correlations are given by Eq.(3.89c), are not altered by the introduction of transverse fluctuations even in the more general case of Model B.

The renormalization of $\rho_{\|}$ also gives results very similar to that of Model A, with the substitutions $C_{\|}'' \to \tilde{C}''$ and $A_{11} \to \rho_{\|}$. Thus, the RG analysis gives the same exponents $\zeta_{\|} = \epsilon/3$ and $z_{\|} = 2 - 2\epsilon/9 + O(\epsilon^2)$. Further details appear in Appendix 3E.

If the Hall Angle ϕ is sufficiently small, the FL can not distinguish between zero and nonzero angles. Therefore, the effective roughness and dynamic exponents at small length and time scales should be given by the Model A fixed point. Note that $\kappa = \tan\phi$ in an isotropic system with nonzero Hall angle (cf. Eq.(3.43)), and κ is in general strongly related to the macroscopic Hall angle. Thus, $\kappa \ll 1$ when the

system is almost Model A-like, and its nonrenormalization determines the cross-over behavior to the Model B fixed point: Under renormalization with Model A exponents, the system remains near the Model A fixed point until the ratio $C_\perp/C_\parallel$ increases to $O(\kappa^{-2})$, as the Model B fixed point is approached. Isotropic effective exponents appear in this crossover regime. The length scale $\xi_\times$ at which the behavior crosses over to the Model B is roughly given by

$$\phi \approx \xi_\times^{\zeta_\perp - \zeta_\parallel},$$

(with Model A exponents for ζ_α), i.e. the anisotropy is noticeable when the angular spread in the direction of a typical avalanche is of the order of ϕ. Thus, for the FL,

$$\xi_\times \sim \phi^{-2},$$

which diverges as $\phi \to 0$. When $\xi < \xi_\times$, the anisotropic fixed point is never approached. Thus, the true critical region can be very small and difficult to observe for small Hall angle.

3.7 Numerical Work

In this section, we present and discuss the results obtained by numerically integrating Eqs. (3.2), providing a test of the analytical results presented so far. There are several difficulties associated with numerically studying critical behavior in a finite system slightly above threshold. In order to obtain meaningful statistical averages one must wait for the system to reach a stationary state. However, for any reasonably broad distribution of pinning forces, the system always gets pinned after a time $\sim e^{(F-F_c)^\nu L}$, where L is the linear extension. Therefore, in order to probe the critical region, it is necessary to go to very large system sizes.

The necessity of integrating big systems, and the large computational cost of implementing quenched disorder, forced us to restrict numerical simulations to $d = 1$, in any case the most physically relevant dimensionality. We were further motivated by the expectation that some exponents were calculated to all orders in ϵ, and thus could be checked even at $\epsilon = 3$.

Integrations were carried out as follows: Coordinates x and t were discretized, but the position $\mathbf{r}$ was left continuous. For each x, the value of the random potential at point $\mathbf{r}$ was determined from a superposition of attractive impurity potentials

$$U_i(\mathbf{r}') = \frac{1}{2} s_i (r'^2 - r_0^2)\Theta(r_0 - r'),$$

where Θ is the step function and r' is the distance from the center of the impurity. The impurity centers were randomly placed with a density w; their strengths s_i were randomly drawn from a uniform distribution $[0, s_{\max})$. The range r_0, of the impurity potential was kept constant. This construction creates a random scalloped potential landscape, eliminating any additional crossover effects that could arise from a smooth potential.

Unless noted otherwise, all presented results were obtained using a grid size $\Delta x = 1$, and a time step $\Delta t = 0.02$, in order to optimize computational constraints. (Smaller values of Δx or Δt did not lead to significant improvements.) Free boundary conditions were preferred over periodic ones since scaling was observed over a larger range of length scales in the former case. Other simulation parameters were $K = 1$, $w = 1$, $r_0 = 1$, $s_{\max} = 2$. We expected a threshold force close to 1 for these parameters. A summary of our findings is presented below.

The velocity exponent β can be extracted from a plot of velocity versus external force. Such a plot is given in Fig. 3.7 for a system of size $L = 2048$. Each data point was obtained by a time average over 10^5 time units and took about 30 hours of CPU time on a Silicon Graphics R4000 workstation. The best power law fit gives an exponent $\beta \approx 0.31$, but a weaker logarithmic dependence, which corresponds to $\beta = 0$, seems to provide a better fit to the data. The conclusion is that higher order terms in v give very large corrections to the scaling of v, since either β is very small or exactly zero. $\beta = 0$ would imply that $z_{\|} = 1$, a possibility discussed by NF for interfaces in $1 + 1$ dimensions[56]. The threshold force F_c, is between 0.93 and 0.94.

The roughness exponents $\zeta_{\|}, \zeta_{\perp}$ are extracted from equal-time correlation functions

$$\left\langle [r_\alpha(\mathbf{x}, t) - r_\alpha(\mathbf{x}', t)]^2 \right\rangle \sim |\mathbf{x} - \mathbf{x}'|^{2\zeta_\alpha}.$$

Results for a system of size 2048, at a driving force of 0.95 $[(F - F_c)/F_c \approx 10^{-2}]$, are shown in Fig. 3.7. The averages were taken over a time interval of 10^5, after waiting for all correlations to reach steady-state. The results are in overall agreement with the predicted values of the exponents, even at $\epsilon = 3$. The slightly smaller value of $\zeta_{\|}$ is expected, since determination of the roughness exponent from equal-time correlations becomes unreliable as the exponent approaches unity, and is inappropriate if it exceeds 1[69]. The deviations of transverse correlations from the scaling form are likely to be due to crossover effects: The analysis of transverse fluctuations in the critical region is correct only when $v/F \ll 1$, because then the static part of the transverse propagator can be neglected. However, in our simulations $v/F \approx 0.4$, suggesting that the critical region is much smaller for transverse fluctuations compared to longitudinal ones.

In order to determine the dynamical exponent $z_{\|}$ independently, we also examined fluctuations in the overall velocity as a function of time. The resulting measurement were related to the previously defined exponents by the following argument[70]: Slightly above threshold, the motion of the line can be thought as a superposition of avalanches of various sizes l, with an average lifetime $l^{z_{\|}}$ and moment $l^{d+\zeta_{\|}}$. Such avalanches occur if a portion of the line finds a region of size $l^{d+\zeta_{\|}}$ with weak impurities. Thus, ignoring all power-law prefactors, the probability of such an avalanche for $l \gg \xi$ is

$$P(l) \sim \exp\left\{-(l/\xi)^{d+\zeta_{\|}}\right\}.$$

Velocities at two separate times are correlated if there is an avalanche that is active at both times. Therefore, it is reasonable to assume that at large times, the contribution of an avalanche of size l to $\langle v(t)v(0)\rangle_c$ is proportional to $e^{-t/l^{z_{\|}}}$. The total contribution of all avalanches is given by an integral over all sizes l with the probability measure

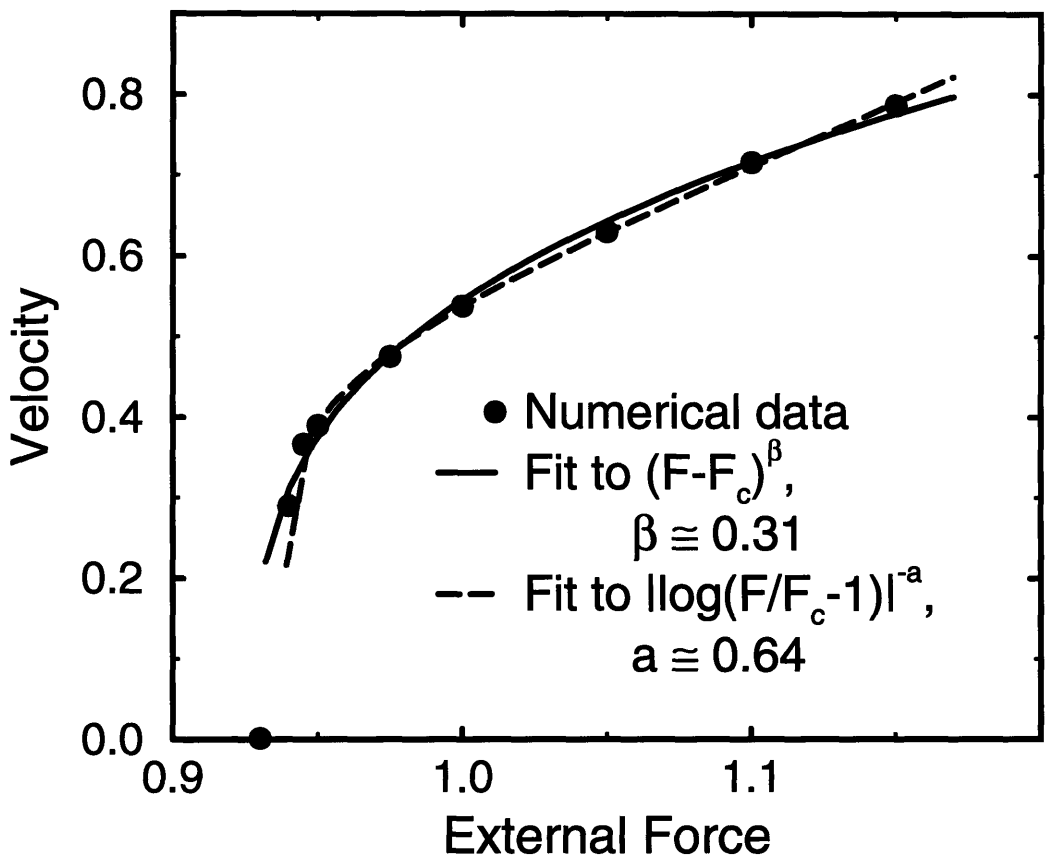

Figure 3-5: A plot of average velocity versus external force for a system of size 2048. Statistical errors are smaller than symbol sizes. Both fits have three adjustable parameters: The threshold force, the exponent, and an overall multiplicative constant.

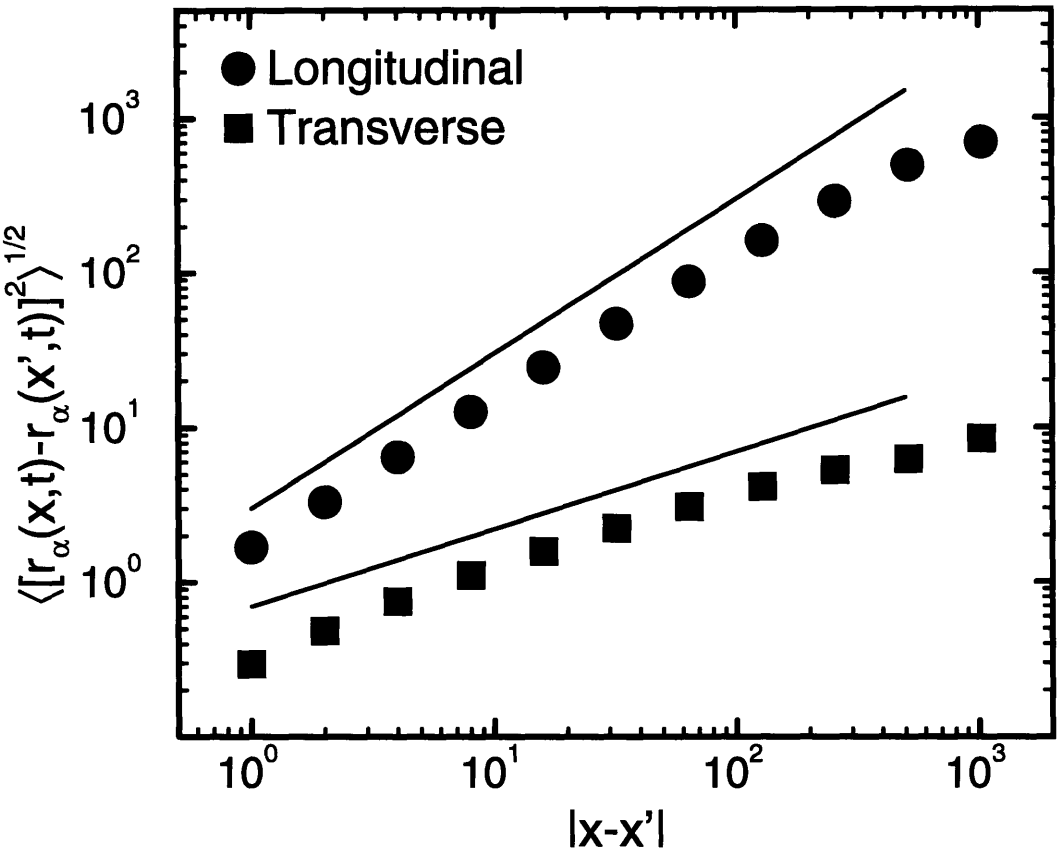

Figure 3-6: A plot of equal time correlation functions versus separation, for a system of size 2048 at $F = 0.95$. The observed roughness exponents are close to the theoretical predictions of $\zeta_{\|} = 1$, $\zeta_{\perp} = 0.5$, which are shown as solid lines for comparison.

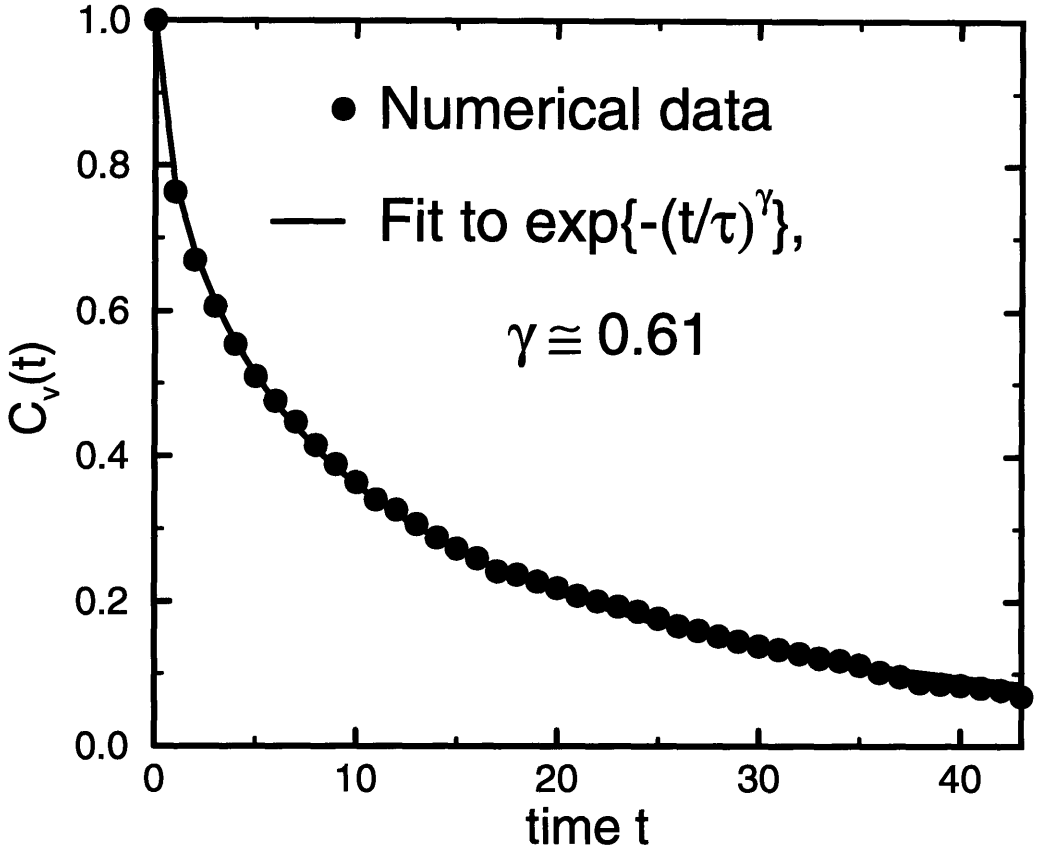

Figure 3-7: Velocity correlation versus time, for the same system in Fig. 3.7. A stretched exponential is a good fit to the data.

$P(l)\,dl$. This integral can be evaluated by a the saddle point approximation, resulting in a stretched exponential

$$C_v(t) = \frac{\langle v(t)v(0)\rangle_c}{\langle v^2\rangle_c} \sim e^{-(t/\tau)^\gamma},$$

where $\gamma = (d + \zeta_\parallel)/(z_\parallel + d + \zeta_\parallel)$. The numerical results and the fit are shown in Fig. 3.7. (It should be noted that a comparable fit can also be achieved by a sum of two exponentials.) Assuming that $\zeta_\parallel = 1$, we arrive at $z \approx 1.28$, which is consistent with the value of $\beta \approx 0.31$ found from the velocity-force relation. It is not clear whether these estimates are reliable since corrections to the scaling form can be large and nonnegligible. However, it can be safely concluded that $z_\parallel$ is between 1 and 4/3, the $O(\epsilon)$ RG prediction.

Computed longitudinal exponents are also in good agreement with results from 1+1 dimensional interface depinning models. Numerical integration of Eq.(3.24a) for an elastic interface[71] (no transverse component) has yielded critical exponents $\zeta = 0.97 \pm 0.05$ and $\nu = 1.05 \pm 0.1$. Similarly, the force vs. velocity data has been adequately described by both a velocity exponent $\beta = 0.24 \pm 0.1$ and a logarithmic dependence $v \sim 1/\ln(F - F_c)$, which corresponds to $\beta = 0$. These results provide strong support for our prediction that longitudinal exponents are unchanged when transverse fluctuations are introduced. However, it should also be noted that experiments and various discrete models of interface growth have resulted in scaling behaviors that differ from system to system. A number of different experiments on fluid invasion in porous media[72] give roughness exponents of around 0.8, while imbibition experiments[73, 74] have resulted in $\zeta \approx 0.6$. Some of these results can be explained by the effect of anisotropy, which will be discussed in the next Section. On the other hand, a discrete model studied by Leschhorn[75] gives a roughness exponent of 1.25 at threshold. Since the expansion leading to Eqs.(3.2) breaks down when ζ approaches one, it is not clear how to reconcile the results of Leschhhorn's numerical work[75] with the coarse-grained description of the RG calculation, especially since any model with $\zeta > 1$ cannot have a coarse grained description based on gradient expansions.

3.8 Discussion and Conclusions

In order to put the results we have found so far in better perspective, it is useful to discuss the effect of nonlinear terms that were ignored earlier, aspects of universality, and possible generalizations to other systems. These issues are discussed below.

3.8.1 Nonlinear Terms

The leading order nonlinearities in Eq.(3.20) can be examined by a gradient expansion, being careful to treat terms of $O((\partial_x r)^2, (\partial_x r)^2 \partial_t r)$ accurately. After some rearrangement, we arrive at

$$\frac{\eta\partial_t r_\parallel}{\sqrt{1+{s_\parallel}^2}} = K_{11}\partial_x^2 r_\parallel + K_{12}\partial_x^2 r_\perp + \frac{\lambda_{1\parallel}}{2}{s_\parallel}^2 + \frac{\lambda_{1\perp}}{2}{s_\perp}^2 + \lambda_{1\times}s_\parallel s_\perp + F + \tilde{f}_\parallel(x,\mathbf{r},s_\parallel,s_\perp), \tag{3.93a}$$

$$\frac{\eta\partial_t r_\perp}{\sqrt{1+{s_\perp}^2}} = K_{21}\partial_x^2 r_\parallel + K_{22}\partial_x^2 r_\perp + \frac{\lambda_{2\parallel}}{2}{s_\parallel}^2 + \frac{\lambda_{2\perp}}{2}{s_\perp}^2 + \lambda_{2\times}s_\parallel s_\perp + \tilde{f}_\perp(x,\mathbf{r},s_\parallel,s_\perp), \tag{3.93b}$$

where $s_\parallel \equiv \partial_x r_\parallel, s_\perp \equiv \partial_x r_\perp$, and the random forces are

$$\tilde{f}_\parallel = \frac{(f_\parallel - s_\parallel f_x)}{\sqrt{1+{s_\parallel}^2}}\cos\phi + \frac{s_\parallel s_\perp f_\parallel - [1+{s_\parallel}^2/2 - {s_\perp}^2/2]f_\perp + s_\perp f_x}{\sqrt{1+{s_\parallel}^2}}\sin\phi, \tag{3.93c}$$

$$\tilde{f}_\perp = \frac{(f_\perp - s_\perp f_x)}{\sqrt{1+{s_\perp}^2}}\cos\phi + \frac{[1-{s_\parallel}^2/2 + {s_\perp}^2/2]f_\parallel - s_\parallel s_\perp f_\perp - s_\parallel f_x}{\sqrt{1+{s_\perp}^2}}\sin\phi. \tag{3.93d}$$

The remaining parameters are given by

$$\begin{aligned} F &= \Phi_0 J, \\ \lambda_{1\parallel} &= F(\cos^2\phi - 1), \\ \lambda_{1\perp} &= -F\cos^2\phi, \\ \lambda_{1\times} &= -F\sin^2\phi, \\ \lambda_{2\parallel} &= F\sin\phi\cos\phi, \\ \lambda_{2\perp} &= -F\sin\phi\cos\phi, \\ \lambda_{2\times} &= F\cos^2\phi. \end{aligned}$$

These equations of motion, and their generalizations to $\mathbf{x} \in \Re^d$, have thus been complicated by two factors: There are orientation-dependent terms, and the mean square of the random forces $\tilde{\Delta}_\alpha \equiv \langle {\tilde{f}_\alpha}^2 \rangle$ also depend on the local orientation of the FL. By naive dimensional counting, it can be immediately seen that $\lambda_{1\parallel}, \lambda_{2\parallel}$, and $\lambda_{2\times}$ are relevant with respect to the fixed points we have discussed for $d < 4$. In the case of Model A (isotropic disorder with $\phi = 0$), Eq.(3.93) further simplifies to

$$\frac{\eta\partial_t r_\parallel}{\sqrt{1+{s_\parallel}^2}} = K\partial_x^2 r_\parallel - \frac{F}{2}{s_\perp}^2 + F + \frac{f_\parallel - f_x s_\parallel}{\sqrt{1+{s_\parallel}^2}}, \tag{3.94a}$$

$$\frac{\eta\partial_t r_\perp}{\sqrt{1+{s_\perp}^2}} = K\partial_x^2 r_\perp + F s_\parallel s_\perp + \frac{f_\perp - f_x s_\perp}{\sqrt{1+{s_\perp}^2}}. \tag{3.94b}$$

Note that the three relevant nonlinearities vanish, and that $\tilde{\Delta}_\alpha$ does not depend on orientation up to and including $O(s^2)$. Dimensional counting suggests that the remaining nonlinear terms are irrelevant and Model A exponents are valid for $d > 1$. Many more nonlinear terms become marginal at $d = 1$, and the gradient expansion breaks down. It is unlikely for the critical exponents to change their value discontinuously at $d = 1$, although logarithmic corrections to scaling exponents are quite possible.

The fixed point investigated here is unstable and only approached at the depinning force. Away from the threshold, critical scaling laws are observed at scales smaller than the correlation length scale ξ. Beyond this critical regime, the behavior of Eq. (3.93) is similar to regular diffusion with white noise (a multicomponent Edwards-Wilkinson (EW) equation[76]), or the generalized KPZ equation[15, 18, 47]). A nonzero $\lambda_{1\|}$ of $O(v)$ is generated kinetically in this regime even if the system is initially isotropic with $\phi = 0$, due to the terms on the left-hand side of Eq.(3.93a). For $d \leq 2$, this nonlinearity is relevant, while for $d > 2$, a critical value λ_c separates a weak-coupling region described by the EW equation from a strong-coupling region described by the (generalized) KPZ equation[15, 18, 47].

When $\phi \neq 0$, even in a fully isotropic medium, the relevant nonlinearities are nonzero, and the system is driven away from the "linear" fixed points. We discuss this and other possibilities next.

3.8.2 Anisotropy and Universality

We noted earlier that anisotropy plays an important role in determining scaling properties near depinning, even in the absence of nonlinear terms. To fully understand the effects of anisotropy, *including nonlinear terms*, let us start by considering the simplest prototype of a FL oriented along the $c-$axis of a High T_c superconducting single crystal, such as YBCO. For simplicity, assume that the system is completely isotropic in the $y-z$ plane, with $\phi = 0$. Then, the motion of the FL is governed by Eqs.(3.94), and the only important source of anisotropy is due to $\langle {f_\|}^2 \rangle = \langle {f_\perp}^2 \rangle \neq \langle f_x^2 \rangle$. This causes the mean square magnitude of $\tilde{f}_\|$ to depend on the local orientation as,

$$\tilde{\Delta}_\| \approx \langle {f_\|}^2 \rangle + \left(\langle f_x^2 \rangle - \langle {f_\|}^2 \rangle \right) {s_\|}^2,$$

For interfaces, the depinning force is known to scale with the strength of the disorder[54, 55], i.e. $\tilde{F}_c \sim \Delta^{2/(4-d)}$. Thus, $\tilde{\Delta}_\|$ creates an orientation dependent depinning force[64],

$$F_c(s_\|) \sim \tilde{\Delta}_\|^{2/(4-d)} \sim F_c \left(1 + \frac{2}{4-d} \frac{\langle f_x^2 \rangle - \langle {f_\|}^2 \rangle}{\langle {f_\|}^2 \rangle} {s_\|}^2 \right). \tag{3.95}$$

This leads to a nonzero $\lambda_{1\|}$ when the nonlinear corrections in Eq.(3.94) are taken into account. For interfaces, the depinning transition with a nonzero $\lambda_{1\|}$ is thought to be equivalent to directed percolation depinning[64]. Assuming that transverse fluctuations still do not affect longitudinal ones, for $d = 1$ the critical exponents $\zeta_\|$ and ν are related to the correlation length exponents $\nu_\|^{(DP)}$ and $\nu_\perp^{(DP)}$ of directed percolation through $\nu = \nu_\|^{(DP)} \approx 1.73$ and $\zeta_\| = \nu_\perp^{(DP)}/\nu_\|^{(DP)} \approx 0.63$, while the dynamical exponent is $z_\| = 1$. This in turn gives $\beta = (z_\| - \zeta_\|)\nu = \nu_\perp^{(DP)} - \nu_\|^{(DP)} \approx 0.64$.

Using the connection to interface depinning further, we next consider tilting the FL away from the symmetry axis c. In this case, $\langle f_x f_\| \rangle$ and $\langle f_x f_\perp \rangle$ are nonzero, and F_c depends linearly on $s_\|$, leading to terms proportional to $\partial_x r_\|$ in the equation of motion. These further suppress the roughness exponent to $\zeta_\| = 1/2$[64]. The analysis

Condition		$\zeta_\parallel$	ν	z	β	$\zeta_\perp$	$z_\perp$
Anisotropic medium, generic direction	$\kappa_{\alpha\beta} \neq 0$	0.5	2	1	1	?	?
Anisotropic, FL along symmetry axis	$\kappa_{\alpha\beta} = 0$ $\lambda_{1\parallel} \neq 0$	0.63	1.73	1	0.64	?	?
FL along symmetry axis,linear terms only (Model B)	$\kappa_{\alpha\beta} = 0$ $\phi \neq 0$	1	1	1.3	0.3	0	2.3
Isotropic medium, $\phi = 0$ (Model A)	$\kappa_{\alpha\beta} = 0$ $\lambda_{1\parallel} = 0$	1	1	1.3	0.3	0.5	2.3

Table 3.1: Critical exponents corresponding to some of the universality classes associated with vector depinning. Entries in the first two rows are from Ref.[64]: Transverse exponents are not known and these cases may correspond to more than one universality class identified by distinct $\zeta_\perp, z_\perp$.

of transverse fluctuations for these two situations, and many other possible ones, are complicated by the absence of a suitable perturbative treatment. Different types of anisotropy may lead to distinct transverse exponents even while the longitudinal ones remain identical. (Similar to the difference between Models A and B, although the latter is unstable to the inclusion of nonlinear terms.) To systematically search for universality classes, we may start with the most general equation of motion, which has the gradient expansion,

$$\begin{aligned} \partial_t r_\alpha &= \mu_{\alpha\beta} F_\beta + \kappa_{\alpha\beta} \partial_x r_\beta + K_{\alpha\beta} \partial_x^2 r_\beta \\ &\quad + \frac{1}{2} \Lambda_{\alpha,\beta\gamma} \partial_x r_\beta \partial_x r_\gamma + \tilde{f}_\alpha(x, \mathbf{r}, \partial_x \mathbf{r}, \cdots) + \cdots, \end{aligned} \tag{3.96}$$

and with force-force correlations that depend on $\partial_x \mathbf{r}$. Depending on the presence or absence of various terms allowed by symmetries, these equations encompass many distinct universality classes. The cases that were discussed so far are summarized in Table 3.1.

3.8.3 Generalizations

In many systems, the dynamics involves a wide range of relaxation times. It is sometimes possible to average over "fast" degrees of freedom to obtain an effective equation of motion for "slow" variables. For example, the motion of atoms in a metal can be described by an effective theory that involves only positions of the ions, assuming that the electronic wave function always adjusts to the instantaneous ionic coordinates. Similarly, the critical dynamics of a slowly moving solid-liquid-vapor contact line can

be described by assuming that the liquid-vapor interface instantaneously finds the minimum energy surface dictated by the position of the contact line[17]. The elimination of these additional degrees of freedom may cause effective nonlocal interactions between the remaining modes, which in turn acquire a different dispersion law. For example, in contact line dynamics, the elastic energy associated with a mode of wave vector q is proportional to $|q|$ instead of q^2. In general, one may consider a situation where the elastic energy is proportional to $|q|^\sigma$ for some value of σ. The scaling analysis can be easily generalized to such cases; the most important change is the modification of the upper critical dimension to $d_c = 2\sigma$. The exponents can be easily calculated for general σ, as presented in Chapter 4 for the critical dynamics of a contact line[77] ($\sigma = 1$).

The possibility of experimental verification of our results lies in the ability to accurately measure the motion of individual FLs and the noise spectra (for both normal and Hall voltages) generated by FL motion. Very recently, there have been successful experiments that detected the thermal motion of individual FLs at nominally zero magnetic field and bulk current using SQUID probes, and analyzed the noise correlation between the two ends of the FL[78]. A refinement of such techniques may eventually enable a direct comparison of theoretical results with experiments. For example, it is known that the Hall angle changes sign as a function of temperature in certain superconductors[79]. It would be particularly interesting to observe the increase in transverse roughness (thus the Hall Voltage noise) as the Hall angle approaches zero. Ultimately, it is very desirable to understand the properties of many FLs (solid or glass) near depinning, especially since this situation has much more experimental and technological relevance. One should then start from a coarse-grained theory for the displacements $\mathbf{u}(\mathbf{x},t)$ of the FLs with respect to their equilibrium positions in the Abrikosov lattice and hope to establish a similar RG scheme. However, there are certainly additional complications, such as entanglement[80] and plasticity[81] effects, which are difficult to incorporate in such an approach.

Appendix

3A The Gaussian Theory

In this appendix, I compute all nonzero expectation values for the Gaussian theory, described by the effective action $\tilde{S}_0$ in Eq.(3.61). This is accomplished by inverting the quadratic form, as

$$\begin{bmatrix} \langle \hat{\mathbf{R}}(\mathbf{q},\omega)\hat{\mathbf{R}}^T(-\mathbf{q},-\omega)\rangle_c & \langle \hat{\mathbf{R}}(\mathbf{q},\omega)\mathbf{R}^T(-\mathbf{q},-\omega)\rangle_c \\ \langle \mathbf{R}(\mathbf{q},\omega)\hat{\mathbf{R}}^T(-\mathbf{q},-\omega)\rangle_c & \langle \mathbf{R}(\mathbf{q},\omega)\mathbf{R}^T(-\mathbf{q},-\omega)\rangle_c \end{bmatrix} = \begin{bmatrix} -\mathbf{C}(\omega) & \mathbf{G}^{-1}(\mathbf{q},\omega) \\ \mathbf{G}^{\dagger -1}(\mathbf{q},\omega) & \mathbf{0} \end{bmatrix}^{-1}$$

$$= \begin{bmatrix} \mathbf{0} & \mathbf{G}^\dagger(\mathbf{q},\omega) \\ \mathbf{G}(\mathbf{q},\omega) & \mathbf{G}(\mathbf{q},\omega)\mathbf{C}(\omega)\mathbf{G}^\dagger(\mathbf{q},\omega) \end{bmatrix}.$$

For the case of Model A, the individual matrices are diagonal and the correlation functions can be calculated easily, as given in Eqs.(3.68). For the more general case of Model B, let us first consider the $v \to 0$ limit. Since $R_\perp$ occurs in the combination $R_\perp/v$, expectation values $\langle \hat{R}_\alpha R_\perp \rangle$ and $\langle R_\alpha R_\perp \rangle$ contribute at most $O(v)$ at the momentum-shell integration step. Thus, the contractions that are important for the momentum-shell integration are $\langle \hat{R}_\parallel R_\parallel \rangle$ and $\langle R_\parallel R_\parallel \rangle$. Setting $v = 0$ and inverting the matrix yields

$$\begin{aligned} \mathbf{G}(\mathbf{q},\omega) &= \begin{bmatrix} K_{11}q^2 - i\omega A_{11} & +i\omega A_{12} \\ K_{21}q^2 - i\omega A_{21} & -i\omega A_{22} \end{bmatrix}^{-1} \\ &= \frac{1}{K_\parallel q^2 - i\omega\rho_\parallel} \begin{bmatrix} 1 & \kappa \\ \cdots & \cdots \end{bmatrix}, \qquad (3.97) \\ \mathbf{GCG}^\dagger(\mathbf{q},\omega) &= \frac{1}{{K_\parallel}^2 q^4 + \omega^2\rho_\parallel^2} \begin{bmatrix} \tilde{C}(\omega) & \cdots \\ \cdots & \cdots \end{bmatrix}, \qquad (3.98) \end{aligned}$$

which leads to Eqs.(3.89). To determine the full form of the correlation functions in a renormalized Gaussian theory, we need to perform a full matrix inversion. In the small v limit we obtain,

$$\begin{aligned} \langle |R_\parallel(\mathbf{q},\omega)|^2 \rangle &= \frac{1}{|\det G^{-1}|^2} \Big\{ A_{22}^2\omega^2\tilde{C}(\omega) - vq^2\omega(K_{12}A_{22} + K_{22}A_{12})\mathrm{Im}[C_\times(\omega)] \\ &\qquad + v^2q^4 \left[K_{22}^2 C_\parallel(\omega) - K_{22}K_{12}\mathrm{Re}C_\times(\omega) + K_{12}^2 C_\perp(\omega) \right] \Big\}, \end{aligned}$$

where

$$|\det G^{-1}|^2 \approx [{K_\parallel}^2 q^4 + \rho_\parallel^2\omega^2] \left[v^2q^4 \left([K_{11}K_{22} - K_{21}K_{12}]/K_\parallel \right)^2 + A_{22}^2\omega^2 \right].$$

Similarly,

$$\begin{aligned} \langle |R_\perp(\mathbf{q},\omega)|^2 \rangle &= \frac{v^2}{|\det G^{-1}|^2} \Big\{ \left(K_{21}^2 C_\parallel(\omega) - K_{21}K_{11}\mathrm{Re}[C_\times(\omega)] + K_{11}^2 C_\perp(\omega) \right) q^4 \\ &\qquad - \omega q^2 (K_{11}A_{21} - K_{21}A_{11})\mathrm{Im}[C_\times(\omega)] \\ &\qquad + \omega^2 \left(A_{21}^2 C_\parallel(\omega) - A_{21}A_{11}\mathrm{Re}[C_\times(\omega)] + A_{11}^2 C_\perp(\omega) \right) \Big\}. \end{aligned}$$

At the fixed point found for Model B, Eqs.(3.92) are satisfied, and the correlation functions simplify to

$$\begin{aligned} \langle |R_\parallel(\mathbf{q},\omega)|^2 \rangle &= \frac{\tilde{C}(\omega)}{{K_\parallel}^2 q^4 + \rho_\parallel^2\omega^2} \mathcal{F}_\parallel \left(\frac{K_\perp q^2}{(\omega/v)\rho_\perp} \right), \qquad (3.99) \\ \langle |R_\perp(\mathbf{q},\omega)|^2 \rangle &= \frac{\tilde{C}(\omega)}{4\left[{K_\perp}^2 q^4 + \rho_\perp^2(\omega/v)^2 \right]} \mathcal{F}_\perp \left(\frac{K_\parallel q^2}{\omega\rho_\parallel} \right), \qquad (3.100) \end{aligned}$$

where

$$K_\perp = \left|\frac{K_{11}K_{22}-K_{21}K_{12}}{K_{11}-\kappa K_{21}}\right|, \qquad \rho_\perp = \left|\frac{K_{11}+\kappa K_{21}}{K_{11}-\kappa K_{21}}\right| A_{22},$$

$$\mathcal{F}_\parallel(x) = \left[1+x^2\left(\frac{(K_{22}-K_{12}/\kappa)K_\parallel}{2(K_{11}K_{22}-K_{21}K_{12})}\right)^2\right]\Big/[1+x^2] = \begin{cases}1, & x\ll 1\\ \text{const}, & x\gg 1.\end{cases}$$

$$\mathcal{F}_\perp(x) = \left[1+\frac{1}{x^2}\left(\frac{K_{11}+\kappa K_{21}}{K_{11}-\kappa K_{21}}\frac{A_{11}-\kappa A_{21}}{A_{11}+\kappa A_{21}}\right)^2\right]\Big/\left[1+\frac{1}{x^2}\right] = \begin{cases}\text{const}, & x\ll 1,\\ 1, & x\gg 1.\end{cases}$$

The functions $\mathcal{F}_\alpha$ describe crossovers of the overall amplitudes of the correlations, due to the coupling between longitudinal and transverse modes.

3B Vertex Renormalization

In this appendix, we derive recursion relations for the renormalized vertex functions $U_{\alpha,n}(u) \equiv C_\alpha^{(n)}(u)$. Let us start by considering $U_{\alpha,n}(u)$ for a given n. As usual, we split the fields $\mathbf{R} = \mathbf{R}^< + \mathbf{R}^>$ and $\hat{\mathbf{R}} = \hat{\mathbf{R}}^< + \hat{\mathbf{R}}^>$, where fields with the superscript ">" correspond to fluctuations within the momentum shell $\Lambda e^{-\delta\ell} < q < \Lambda$, which are averaged over. In evaluating $\langle e^{\mathcal{U}}\rangle_0^>$, we encounter two types of nonzero contractions,

$$\begin{aligned}\left\langle \hat{R}_\parallel^>(\mathbf{q},t)R_\parallel^>(-\mathbf{q},t')\right\rangle &= \frac{1}{A_{11}}\exp\left[-\frac{Kq^2(t'-t)}{A_{11}}\right]\Theta(t'-t)\\ &\approx \frac{1}{K\Lambda^2}\delta(t-t'),\\ \left\langle R_\parallel^>(\mathbf{q},t)R_\parallel^>(-\mathbf{q},t')\right\rangle &\approx \frac{1}{K^2\Lambda^4}U_{\alpha,0}\left(v(t-t')\right),\end{aligned}$$

within the momentum shell $\Lambda e^{-\delta\ell} < q < \Lambda$, and for time scales $t - t' \sim O(1/v)$. (From now on, we suppress the subscript 0 for notational simplicity.) Contributions to the renormalization of $U_{\alpha,n}$ come from both $\langle\mathcal{U}\rangle^>$ and $\langle\mathcal{U}^2\rangle_c^>$, as

$$\begin{aligned}\langle\mathcal{U}\rangle^> &= \sum_\alpha \frac{1}{2!(n+2)!}\int d^dx\, dt_1 dt_2\, U_{\alpha,n+2}(1-2)\left\langle \hat{R}_\alpha(1)\hat{R}_\alpha(2)[R_\parallel(1)-R_\parallel(2)]^{n+2}\right\rangle^> + \cdots\\ &= \sum_\alpha \frac{1}{2!(n+2)!}\binom{n+2}{2}\int d^dx\, dt_1 dt_2 U_{\alpha,n+2}(1-2)\hat{R}_\alpha^<(1)\hat{R}_\alpha^<(2)[R_\parallel^<(1)-R_\parallel^<(2)]^n\\ &\qquad\times\left\langle[R_\parallel^>(1)-R_\parallel^>(2)]^2\right\rangle + \cdots,\end{aligned}$$

with obvious abbreviations for the arguments of $U, R, \hat{R}$. Evaluating the expectation values, we get

$$\begin{aligned}\left\langle[R_\parallel^>(1)-R_\parallel^>(2)]^2\right\rangle &= \int^> \frac{d^dq}{(2\pi)^d}\left\{\left\langle R_\parallel^>(\mathbf{q},t_1)R_\parallel^>(-\mathbf{q},t_1)\right\rangle + \left\langle R_\parallel^>(\mathbf{q},t_2)R_\parallel^>(-\mathbf{q},t_2)\right\rangle\right.\\ &\qquad\left. -2\left\langle R_\parallel^>(\mathbf{q},t_1)R_\parallel^>(-\mathbf{q},t_2)\right\rangle\right\}\\ &= 2\delta\ell\frac{\Lambda^d S_d}{(2\pi)^d K^2\Lambda^4}[U_{\parallel,0}(0)-U_{\parallel,0}(v(t_1-t_2))],\end{aligned} \tag{3.101}$$

where $\int^{>}$ denotes integration over the momentum shell and S_d is the surface area of a unit sphere in d-dimensions. Thus, the correction to $U^{<}_{\alpha,n}(u)$ from $\langle \mathcal{U} \rangle^{>}$ is equal to

$$\delta \ell K_d U_{\alpha,n+2}(u)[U_{\|,0}(0) - U_{\|,0}(u)],$$

where $K_d \equiv \Lambda^{d-4} S_d/[(2\pi)^d K^2]$. The contributions from $\langle \mathcal{U}^2 \rangle^{>}_c$ are similarly calculated, as

$$\begin{aligned}
\langle \mathcal{U}^2 \rangle^{>}_c &= \sum_{\alpha,\gamma} \sum_{m=1}^{n+1} \frac{1}{2!m!2!(n+2-m)!} \int d^d x\, dt_1\, dt_2 \int d^d x'\, dt'_1\, dt'_2 \\
&\quad \times U_{\alpha,m}(1-2) U_{\gamma,n+2-m}(1'-2') \\
&\quad \times \left\langle \hat{R}_\alpha(1) \hat{R}_\alpha(2) \hat{R}_\gamma(1') \hat{R}_\gamma(2') [R_\|(1) - R_\|(2)]^m [R_\|(1') - R_\|(2')]^{n+2-m} \right\rangle^{>} + \cdots \\
&= \sum_{m=1}^{n+1} \frac{1}{2!(m-1)!2!(n+1-m)!} \int d^d x\, dt_1\, dt_2 \int d^d x'\, dt'_1\, dt'_2 \\
&\quad \times U_{\|,m}(1-2) U_{\|,n+2-m}(1'-2') [R^{<}_\|(1) - R^{<}_\|(2)]^{m-1} [R^{<}_\|(1') - R^{<}_\|(2')]^{n+1-m} \\
&\quad \times \left\langle \hat{R}_\|(1) \hat{R}_\|(2) \hat{R}_\|(1') \hat{R}_\|(2') [R^{>}_\|(1) - R^{>}_\|(2)][R^{>}_\|(1') - R^{>}_\|(2')] \right\rangle^{>} \\
&\quad + 2 \sum_{\alpha} \sum_{m=1}^{n} \frac{1}{2!m!2!(n+2-m)!} \binom{n+2-m}{2} \int d^d x\, dt_1\, dt_2 \int d^d x'\, dt'_1\, dt'_2 \\
&\quad \times U_{\alpha,m}(1-2) U_{\|,n+2-m}(1'-2') \hat{R}^{<}_\alpha(1') \hat{R}^{<}_\alpha(2') [R^{<}_\|(1) - R^{<}_\|(2)]^m \\
&\quad \times [R^{<}_\|(1') - R^{<}_\|(2')]^{n-m} \left\langle \hat{R}^{>}_\|(1) \hat{R}^{>}_\|(2) [R^{>}_\|(1') - R^{>}_\|(2')]^2 \right\rangle + \cdots . \qquad (3.102)
\end{aligned}$$

The evaluations of the expectation values are tedious but straightforward. As an example, let us evaluate the second half of Eq.(3.102) explicitly. First of all,

$$\begin{aligned}
&\left\langle \hat{R}^{>}_\|(1) \hat{R}^{>}_\|(2) [R^{>}_\|(1') - R^{>}_\|(2')]^2 \right\rangle = \\
&\quad = \left\langle \hat{R}^{>}_\|(1) R^{>}_\|(1') \right\rangle \left\langle \hat{R}^{>}_\|(2) R^{>}_\|(1') \right\rangle + \left\langle \hat{R}^{>}_\|(1) R^{>}_\|(2') \right\rangle \left\langle \hat{R}^{>}_\|(2) R^{>}_\|(2') \right\rangle \\
&\qquad - 2 \left\langle \hat{R}^{>}_\|(1) R^{>}_\|(1') \right\rangle \left\langle \hat{R}^{>}_\|(2) R^{>}_\|(2') \right\rangle - 2 \left\langle \hat{R}^{>}_\|(1) R^{>}_\|(2') \right\rangle \left\langle \hat{R}^{>}_\|(2) R^{>}_\|(2') \right\rangle .
\end{aligned}$$

The first two terms do not contribute to $U^{<}_{\alpha,n}(u)$, since they are proportional to $\delta(t_1 - t'_1)\delta(t_2 - t'_1)$ and $\delta(t_1 - t'_2)\delta(t_2 - t'_2)$ respectively. (These delta functions force t_1 to be equal to t_2. Since the expectation value is multiplied by $[R^{<}_\|(1) - R^{<}_\|(2)]^m$, the final contribution is zero.) The last two terms are equal to

$$-2 \int^{>} \frac{d^d q}{(2\pi)^d} \int^{>} \frac{d^d q'}{(2\pi)^d} [\delta(t_1 - t'_1)\delta(t_2 - t'_2) + \delta(t_1 - t'_2)\delta(t_2 - t'_1)] \frac{\exp\{i(\mathbf{q} + \mathbf{q}') \cdot (\mathbf{x} - \mathbf{x}')\}}{(Kq^2)(Kq'^2)}.$$

Integrating over t'_1, t'_2, $\mathbf{x}'$ (which yields $\delta^d(\mathbf{q} + \mathbf{q}')$) and subsequently over $\mathbf{q}'$, the second half of Eq.(3.102) becomes

$$\begin{aligned}
&- \sum_{\alpha} \sum_{m=1}^{n} \frac{1}{2!n!} \binom{n}{m} \int d^d x dt_1 dt_2 \hat{R}^{<}_\alpha(1) \hat{R}^{<}_\alpha(2) [R^{<}_\|(1) - R^{<}_\|(2)]^n \int^{>} \frac{d^d q}{(2\pi)^d} \frac{1}{K^2 q^4} \\
&\qquad \times \left\{ U_{\alpha,m}(1-2) U_{\|,n+2-m}(1-2) + (-1)^{n-m} U_{\alpha,m}(1-2) U_{\|,n+2-m}(2-1) \right\}.
\end{aligned}$$

The first half of Eq.(3.102) can be evaluated similarly. The full contribution to $U^{<}_{\alpha,n}(u)$ from $\langle \mathcal{U}^2 \rangle^{>}_c$ is thus equal to

$$-\delta\ell K_d \left\{ \delta_{\alpha,\|} \sum_{m=1}^{n+1} \binom{n}{m-1} (-1)^{n+2-m} U_{\|,m}(u) U_{\|,n+2-m}(-u) \right.$$
$$\left. + \sum_{m=1}^{n} \binom{n}{m} \frac{1}{2} \left[U_{\alpha,m}(u) U_{\|,n+2-m}(u) + (-1)^{n+2-m} U_{\alpha,m}(u) U_{\|,n+2-m}(-u) \right] \right\}.$$

(In the expansion of $\langle e^{\mathcal{U}} \rangle^{>}_c$, there is a factor of $1/2$ in front of $\langle \mathcal{U}^2 \rangle^{>}_c$.) Adding all contributions, the effective vertex function $U^{<}_{\|,n}(u)$ is found to be

$$U^{<}_{\|,n}(u) = U_{\|,n}(u) + \delta\ell K_d \left\{ U_{\|,n+2}(u) U_{\|,0}(0) - \sum_{m=0}^{n+1} \binom{n+1}{m} U_{\|,m}(u) U_{\|,n+2-m}(u) \right\}, \tag{3.103}$$

provided that

$$U_{\alpha,m}(u) = (-1)^m U_{\alpha,m}(-u). \tag{3.104}$$

Under the scale transformation (3.65), which brings the momentum cutoff to its original value, we see that $u \to (1 + \zeta_{\|}\delta\ell)u$. Thus, the renormalized vertex function is given by

$$\tilde{U}_{\|,n}(u) \equiv U_{\|,n}(u) + \delta\ell \frac{\partial U_{\|,n}(u)}{\partial \ell} = U^{<}_{\|,n}\left((1 + \zeta_{\|}\delta\ell)u\right) \{1 + \delta\ell[d + 2z_{\|} + 2(\theta_{\|} - d) + n\zeta_{\|}]\}. \tag{3.105}$$

Keeping only terms linear in $\delta\ell$, and identifying $U_{\|,n}(u)$ with the nth derivative of $C_{\|}(u)$, we finally obtain the differential recursion relation for $C_{\|}(u)$:

$$\frac{\partial C_{\|}(u)}{\partial \ell} = [\epsilon + 2\theta_{\|} + 2(z_{\|} - 2)] C_{\|}(u) + \zeta_{\|} u C'_{\|}(u) - K_d \left\{ [C'_{\|}(u)]^2 + [C_{\|}(u) - C_{\|}(0)] C''_{\|}(u) \right\}. \tag{3.106}$$

Note that the identification of $U_{\|,n}(u)$ with the nth derivative of $C_{\|}(u)$ is self-consistent, since recursion relations for $U_{\|,n}(u)$ are correctly recovered by taking n derivatives of Eq.(3.106). Also, Eq.(3.104) is automatically satisfied when this identification is made since $C_{\|}(u) = C_{\|}(-u)$.

A similar computation can be performed for $C_{\perp}(u)$, yielding

$$U^{<}_{\perp,n}(u) = U_{\perp,n}(u) + \delta\ell K_d \left\{ U_{\perp,n+2}(u) U_{\|,0}(0) - \sum_{m=0}^{n} \binom{n}{m} U_{\perp,n+2-m}(u) U_{\|,m}(u) \right\}. \tag{3.107}$$

Upon rescaling, the renormalized vertex function is

$$\tilde{U}_{\perp,n}(u) \equiv U_{\perp,n}(u) + \delta\ell \frac{\partial U_{\perp,0}(u)}{\partial \ell} = U^{<}_{\perp,n}\left((1 + \zeta_{\|}\delta\ell)u\right) \{1 + \delta\ell[d + 2z_{\|} + 2(\theta_{\perp} - d) + n\zeta_{\|}]\}. \tag{3.108}$$

Thus, we obtain the recursion relation

$$\frac{\partial C_{\perp}(u)}{\partial \ell} = [\epsilon + 2\theta_{\perp} + 2(z_{\|} - 2)] C_{\perp}(u) + \zeta_{\|} u C'_{\perp}(u) - K_d \left\{ [C_{\|}(u) - C_{\|}(0)] C''_{\perp}(u) \right\}. \tag{3.109}$$

3C Higher-Order Diagrams

In this appendix, we show that the sum of all contributions to the renormalization of $C_\perp(u)$ from the momentum shell integration step vanish in the limit $u \to 0^+$. This was already explicitly demonstrated for the leading order contributions that come from $\langle \mathcal{U} \rangle_c$ and $\langle \mathcal{U}^2 \rangle_c$. Since the only nonzero contractions involve $R_\parallel$ and $\hat{R}_\parallel$, all contributions to the renormalization of $C_\perp(v(t-t'))$ due to $\langle \mathcal{U}^m \rangle_c$ arise from terms of the form

$$\langle \mathcal{U}^m \rangle_c = \sum_{n=2}^{\infty} \int d^d x\, dt\, dt' \frac{U_{\perp,n}(v(t-t'))}{2!n!} \hat{R}_\perp^<(t) \hat{R}_\perp^<(t') \int \left[\prod_{i=1}^{m-1} d^d x_i\, dt_i\, dt_i' \frac{U_{\parallel,n_i}(v(t_i - t_i'))}{2!n_i!} \right]$$
$$\times \left\langle [R_\parallel^>(\mathbf{x},t) - R_\parallel^>(\mathbf{x},t')]^n \prod_{i=1}^{m-1} \hat{R}_\parallel^>(\mathbf{x}_i,t_i) \hat{R}_\parallel^>(\mathbf{x}_i,t_i') [R_\parallel^>(\mathbf{x}_i,t_i) - R_\parallel^>(\mathbf{x}_i,t_i')]^{n_i} \right\rangle_c + \cdots .$$

The expectation value clearly goes to zero as $(t-t')^n$ in the $t \to t'^+$ limit. This gives us the desired result that $C_\perp(0)$ is unrenormalized to all orders in perturbation theory.

3D High-frequency Structure of $U_{\parallel,2}$

In this appendix, we shall demonstrate that there are no v^{-1} divergences in the renormalization of A_{11}, at least to $O(\epsilon)$. In order to do this, we examine the full form of the bare vertex function $U_{\parallel,2}$ obtained from MF theory,

$$U_{\parallel,2}(t_1,t_2;t_1',t_2') = \frac{\partial^2 \left\langle \overline{r}_\parallel(t_1) \overline{r}_\parallel(t_2) \right\rangle_{MF,c}}{\partial \varepsilon_\parallel(t_1') \partial \varepsilon_\parallel(t_2')}.$$

The low-frequency analysis of this vertex function gives a result proportional to $1/v$ when all times are within $O(1)$ of each other. This may potentially give an $O(1/v)$ contribution to the renormalization of A_{11}. Indeed, an external impulse of magnitude ε right before a "jump" (the fast motion between consequent local minima) shifts the jump time by ε/η and creates a response of $O(1/v)$ right after the jump takes place. However, an impulse right after a jump does not affect the jump time and creates a response of only $O(1)$. Thus a singular response is seen if all times are in the vicinity of a jump, say, at time t_J. $U_{\parallel,2}(t_1,t_2;t_1',t_2')$ can be as large as $O(v^{-2})$ if t_1' and t_2' are both slightly less than t_J, and t_1 and t_2 are both slightly greater than t_J. Considering that the probability of being close to a jump is v, this term can potentially contribute as much as $O(v^{-1})$ to the renormalization of A_{11} upon statistical time-averaging. A careful analysis, and explicit evaluation of this vertex in the case of a periodic potential[82], show that this is the only way a singularity may occur in the RG contributions. However, when the times t_1', t_2' of fields $R_\parallel$ are smaller than the times t_1, t_2 of fields $\hat{R}_\parallel$, the contraction $\left\langle \hat{R}_\parallel(t_i) R_\parallel(t_j') \right\rangle_0$ which appears in the RG contribution is identically zero due to the causality of the propagator. Therefore, the singular part of $C_\parallel^{*\prime\prime}(0)$ does not enter the renormalization of A_{11} (or $\rho_\parallel$ in the case of Model B) to one-loop order.

3E Renormalization of Model B

Details of the RG calculation for Model B are presented in this appendix. For the sake of brevity, we shall only consider the renormalization of the parameters in the Gaussian theory, i.e. the propagator, and the two-point correlation functions $U_{\|,0}(u)$, $U_{\perp,0}(u)$, $U_{\times,0}(u)$. The renormalization of higher-order vertex functions are again related to derivatives of C_α through $U_{\alpha,n}(u) \equiv C_\alpha^{(n)}(u)$.

Nonzero contractions involved in the calculation are given in Eqs.(3.89). The parameters A_{12}, A_{22} (thus κ), and $K_{\alpha\gamma}$ (thus $K_\|, K_\perp$, and $\rho_\perp$) do not get contributions from the momentum shell integration, and give rise to exponent identities discussed in the text. On the other hand, A_{11} and A_{21} (thus $\rho_\|$), as well as the functions $C_\alpha(u)$, are renormalized. Let us start by looking at the renormalization of two-point correlation functions $C_\alpha(u)$. By definition, $C_\|(u) = C_\|(-u)$ and $C_\perp(u) = C_\perp(-u)$, but $C_\times(u) \neq C_\times(-u)$ in general. It is convenient to write $C_\times(u)$ in terms of its even and odd parts $C_{\times S}(u)$ and $C_{\times A}(u)$ respectively, and follow their renormalization separately.

The momentum shell integration procedure is similar to the one presented in Appendix 3B, albeit more cumbersome due to many more nonzero contractions. Nevertheless, carrying out the computation yields

$$C_\alpha^<(u) = C_\alpha(u) - \delta\ell K_d \mathcal{I}_\alpha(u), \tag{3.110}$$

for $u > 0$, where

$$\begin{aligned}
\mathcal{I}_\|(u) &= C_\|''(u)[\tilde{C}(u) - \tilde{C}(0^+)] + C_\|'(u)\tilde{C}'(u) \\
&\quad -\kappa^2 \left\{ C_\|'(u)C_\perp'(u) - [C_{\times S}'(u)/2]^2 + [C_{\times A}'(u)/2]^2 \right\} \\
&\quad +\kappa C_{\times A}(u) \left\{ C_\|'(0^+) + \kappa[C_{\times A}'(0^+)/2] \right\}, \qquad (3.111) \\
\mathcal{I}_\perp(u) &= C_\perp''(u)[\tilde{C}(u) - \tilde{C}(0^+)] + C_\perp'(u)\tilde{C}'(u) \\
&\quad -\left\{ C_\|'(u)C_\perp'(u) - [C_{\times S}'(u)/2]^2 + [C_{\times A}'(u)/2]^2 \right\} \\
&\quad +C_{\times A}(u) \left\{ [C_{\times A}'(0^+)/2] - \kappa C_\perp'(0^+) \right\}, \qquad (3.112) \\
\mathcal{I}_{\times S}(u) &= C_{\times S}''(u)[\tilde{C}(u) - \tilde{C}(0^+)] + C_{\times S}'(u)\tilde{C}'(u) \\
&\quad +2\kappa \left\{ C_\|'(u)C_\perp'(u) - [C_{\times S}'(u)/2]^2 + [C_{\times A}'(u)/2]^2 \right\} \\
&\quad -C_{\times A}(u) \left\{ C_\|'(0^+) + \kappa C_{\times A}'(0^+) - \kappa^2 C_\perp'(0^+) \right\}, \qquad (3.113) \\
\mathcal{I}_{\times A}(u) &= C_{\times A}''(u)[\tilde{C}(u) - \tilde{C}(0^+)] + C_{\times A}'(u)\tilde{C}'(u) \\
&\quad +4\kappa \left\{ C_\|'(u)C_\perp'(0^+) - C_\|'(0^+)C_\perp'(u) \right\} \\
&\quad -C_{\times S}'(u) \left\{ C_\|'(0^+) + \kappa C_{\times A}'(u) - \kappa^2 C_\perp'(0^+) \right\}. \qquad (3.114)
\end{aligned}$$

Thus, the renormalization of $\tilde{C}(u)$ is given by

$$\tilde{C}^<(u) = \tilde{C}(u) - \delta\ell K_d \left\{ \tilde{C}''(u)[\tilde{C}(u) - \tilde{C}(0^+)] + [\tilde{C}'(u)]^2 \right\}, \tag{3.115}$$

which leads to the functional recursion relation

$$\frac{\partial \tilde{C}(u)}{\partial \ell} = [\epsilon + 2\theta_{\|} + 2(z_{\|} - 2)]\tilde{C}(u) + \zeta_{\|} u \tilde{C}'(u) - K_d \left\{ [\tilde{C}'(u)]^2 + [\tilde{C}(u) - \tilde{C}(0)]\tilde{C}''(u) \right\}. \tag{3.116}$$

This is identical to Eq.(3.106), with the substitution $C_{\|}(u) \to \tilde{C}(u)$. It is straightforward to verify that there exists a fixed point where individual matrix elements $C_{\alpha}(u)$ satisfy Eq.(3.92). ($C_{\times A}(u) = 0$ at this fixed point.)

Let us next examine the renormalization of $\rho_{\|}$. Leading order contributions come from $\langle \mathcal{U} \rangle_0^>$, and a calculation along the lines presented in Sec.3.6 gives

$$\begin{aligned} A_{11}^< &= A_{11} - \delta\ell \frac{S_d \Lambda^d}{(2\pi)^d \rho_{\|}} \int_0^{\infty} d\tilde{t}\, \tilde{t}\, e^{-K_{\|}\Lambda^2 \tilde{t}/\rho_{\|}} \left[C_{\|}''(v\tilde{t}) + \frac{\kappa}{2} C_{\times}''(v\tilde{t}) \right], \\ A_{21}^< &= A_{21} - \delta\ell \frac{S_d \Lambda^d}{(2\pi)^d \rho_{\|}} \int_0^{\infty} d\tilde{t}\, \tilde{t}\, e^{-K_{\|}\Lambda^2 \tilde{t}/\rho_{\|}} \left[\frac{1}{2} C_{\times}''(-v\tilde{t}) + \kappa C_{\perp}''(v\tilde{t}) \right], \end{aligned}$$

which can be combined to yield

$$\rho_{\|}^< = \rho_{\|} - \delta\ell \frac{S_d \Lambda^d}{(2\pi)^d \rho_{\|}} \int_0^{\infty} d\tilde{t}\, \tilde{t}\, e^{-K_{\|}\Lambda^2 \tilde{t}/\rho_{\|}} \tilde{C}''(v\tilde{t}). \tag{3.117}$$

The fixed-point function $\tilde{C}^*(u)$ is identical to that of $C_{\|}^*(u)$ in Model A, and its behavior near $u = 0$ is also given by Eq.(3.80). Thus, we obtain

$$\rho_{\|}^< = \rho_{\|} - \delta\ell \rho_{\|} K_d \tilde{C}''(0^+) = \rho_{\|}[1 - \delta\ell(2\epsilon/9)]$$

which leads to the recursion relation

$$\frac{\partial \rho_{\|}}{\partial \ell} = \rho_{\|}[\theta_{\|} + \zeta_{\|} - 2\epsilon/9]. \tag{3.118}$$

Chapter 4

Critical Dynamics of Contact Line Depinning

4.1 Introduction

Wetting phenomena and contact lines (CLs) appear in many manufacturing processes that involve the spreading of a liquid on a solid surface[83]. Some degree of control over the spreading of the liquid and the corresponding creep of the CL is needed to optimize the desired characteristics of such processes. In particular, it is important to know the effect of surface roughness and contaminants on the fluctuations of the CL from microscopic to mesoscopic scales. This chapter studies such effects at length scales from 10^{-1} down to 10^{-7} centimeters. The upper length scale is set by the droplet size or the capillary length (due to gravitation), while the lower length scale is determined by the characteristic size of the microscopic defects.

Surface impurities lead to *CL hysteresis*, i.e. a finite force is needed to start the fluid spreading. The dynamics of the CL at very low velocities has significant similarities to dynamical critical phenomena in related systems. Although the underlying issues of collective depinning for Charge-Density Waves (CDWs) and interfaces have been around for some time, only recently a systematic perturbative approach to the problem was developed. This functional renormalization group (RG) approach to the dynamical equations of motion was originally developed in the context of CDWs by Narayan and Fisher[50, 51] (NF), and extended to interfaces by Nattermann, Stepanow, Tang and Leschhorn (NSTL)[55]. Recently, the scaling exponents of a driven elastic interface subject to quenched impurities near a similar depinning threshold have been calculated through a RG treatment close to four interface dimensions[55, 56]. In this Chapter, I use a similar method to calculate various scaling exponents for the slowly advancing contact line. The distinction between the two cases is that the CL is the termination of the liquid-vapor interface.

Consider the wetting front of a partially wetting liquid on a heterogenous surface in the x-y plane with the average orientation of the contact line in the x direction, as shown in Fig. 4-1. The liquid wedge makes an angle Θ with the surface, which is called the *contact angle*. The CL fluctuates around a straight line due to the disorder on the surface, and its configuration at time t is denoted as $h(x,t)$. Let us assume

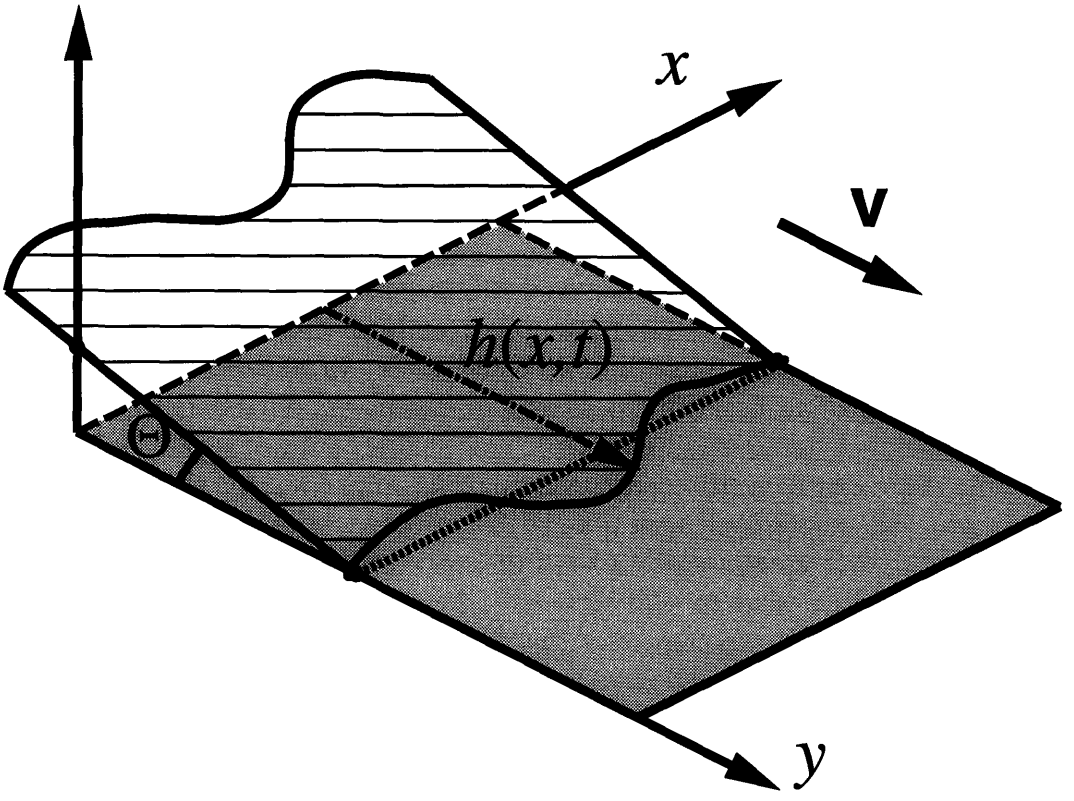

Figure 4-1: Geometry of the system. A partially wetting liquid advances on an inhomogenous surface with velocity v due to a forced contact angle $\Theta > \Theta_a$.

that the partially wetting fluid spreads sufficiently slowly on a heterogenous surface that the liquid-vapor interface evolves adiabatically, i.e., that it responds to changes in the CL shape instantaneously. In this case, fluctuations of the CL around its time-averaged value reflect the competition between impurities on the solid surface and the liquid-vapor surface tension. As derived in Section 4.2, the quasi-static evolution of the CL is described by the equation

$$\mu^{-1}\left(\frac{\partial h(x,t)}{\partial t}\right) = -\frac{\gamma\Theta^2}{\pi}\int_{a<|x-x'|} dx' \frac{h(x,t)-h(x',t)}{(x-x')^2} + f[x,h(x,t)] + F. \qquad (4.1)$$

In the above, F is the force per unit length exerted on the CL, and $f(x,y)$ represent force fluctuations due to the heterogeneities on the surface. The average of f is zero, while its correlations satisfy,

$$\langle f(x,y)f(x',y')\rangle = \Delta(r/a), \qquad (4.2)$$

where $r^2 = (x-x')^2 + (y-y')^2$, a is the characteristic size of defects, and Δ is a function that decays rapidly for large values of its argument.

Surface impurities pin the CL when F is less than the threshold force F_c. For F slightly above threshold, it is reasonable to expect the average velocity of the CL to scale as

$$v = A(F-F_c)^{\beta}, \qquad (4.3)$$

where β is the *velocity exponent*, and A is a nonuniversal constant. Superposed on the steady advance of the CL are rapid "jumps" as portions of the line depin from strong pinning centers. Such jumps are similar to *avalanches* in other slowly forced systems, and have a power-law distribution in size, cut-off at a characteristic correlation length ξ. On approaching the threshold, ξ diverges as

$$\xi \sim (F-F_c)^{-\nu}, \qquad (4.4)$$

defining a *correlation length exponent* ν. At length scales smaller than ξ, the interface is self-affine, i.e. with correlations satisfying the dynamic scaling form

$$\langle (h(x,t)-h(x',t'))^2\rangle = (x-x')^{2\zeta} g\left(\frac{t-t'}{(x-x')^z}\right), \qquad (4.5)$$

where ζ and z are the *roughness* and *dynamic* exponents, respectively. The scaling function g goes to a constant as its argument approaches 0, ζ is the wandering exponent of an instantaneous CL profile, and z relates the average lifetime of an avalanche to its size by $\tau(\xi) \sim \xi^z$.

In many aspects, Eq.(4.1) is similar to the model analyzed by Narayan and Fisher using the formalism of Martin, Siggia, and Rose[11] (MSR), through an expansion around a mean field solution[56]. The main difference is in the energy cost of low-lying fluctuation modes, i.e. the dispersion relation of the Goldstone modes: The energy cost of a disturbance of wave vector q is $E(q) \sim q^2$ for the elastic interface, but $E(q) \sim |q|$ for the CL. The unusual q-dependence of CL dynamics reflects the

fact that perturbations of wave vector q on the CL induce deformations into the liquid-vapor interface up to a distance $|q|^{-1}$.

As discussed in Section 4.3, an investigation similar to that of Chapter 3 yields an upper critical dimension of $d_c = 2\sigma$ for a d-dimensional interface with a dispersion relation $E(q) \sim |q|^\sigma$, and the critical exponents in $d = 2\sigma - \epsilon$ interface dimensions are given by

$$\zeta = \epsilon/3, \qquad z = \sigma - 2\epsilon/9 + O(\epsilon^2). \tag{4.6}$$

The remaining exponents are determined from exponent identities:

$$\nu = 1/(\sigma - \zeta), \qquad \beta = (z - \zeta)\nu. \tag{4.7}$$

The first result comes from an exact statistical symmetry of the system that fixes the form of the static ($\omega = 0$) response function $\langle \partial h(x')/\partial f(x) \rangle$, whereas the second result is due to the scaling of nonlinear response functions, requiring the fluctuations h to scale similarly to the average motion vt of the interface. Thus, the critical exponents for the CL ($d = \sigma = 1$) are

$$\zeta = 1/3, \tag{4.8}$$
$$\nu = 3/2, \tag{4.9}$$
$$z \approx 7/9, \tag{4.10}$$
$$\beta \approx 2/3. \tag{4.11}$$

The result for ζ and ν are correct to all orders in ϵ, whereas the remaining exponents are known only to first order in ϵ.

Numerical integration of Eq.(4.21) for an elastic interface[71] ($\sigma = 2$) has yielded critical exponents $\zeta = 0.97 \pm 0.05$ and $\nu = 1.05 \pm 0.1$, in agreement with the theoretical result $\zeta = \nu = 1$. The velocity exponent $\beta = 0.24 \pm 0.1$ is also consistent with the one-loop theoretical result $1/3$; however, a logarithmic dependence $v \sim 1/\ln(F - F_c)$, which corresponds to $\beta = 0$, also describes the numerical data well. Preliminary numerical integrations[84] for the CL case and the simulation of a cellular automaton for crack growth[85], believed to be in the same universality class, indicate a roughness exponent of $\zeta = 0.35 \pm 0.05$, in good agreement with the theoretical prediction. However, recent experiments by Kumar *et al.* [86] seem to indicate a very large velocity exponent of $\beta = 4 \pm 1$. One possible reason for this discrepancy is addressed in Section 4.4, along with the effects of anisotropy and gravity. Experiments to measure the predicted critical and roughness exponents are suggested as well.

4.2 Equation of Motion for a CL

Consider the geometry shown in Fig. 4-1. In equilibrium on a *homogenous* interface, the macroscopic contact angle Θ is determined by the Young condition,

$$\gamma_{SV} - \gamma_{SL} - \gamma \cos\Theta = 0. \tag{4.12}$$

In the above, γ_{SV}, γ_{SL}, and γ are the interfacial tensions for the solid-vapor, solid-liquid, and liquid-vapor interfaces, respectively. The heterogeneities (i. e. defects) on

the surface can be modeled as fluctuations in the difference of local interfacial energy densities,

$$f(x,y) = \gamma_{SV}(x,y) - \gamma_{SL}(x,y) - \langle \gamma_{SV} - \gamma_{SL} \rangle. \tag{4.13}$$

The average of f is zero, while its correlations satisfy,

$$\langle f(x,y) f(x',y') \rangle = \Delta(r/a), \tag{4.14}$$

where $r^2 = (x-x')^2 + (y-y')^2$, a is the characteristic size of defects, and Δ is a function that decays rapidly for large values of its argument[1]. The CL advances with an average velocity v, but deviates from a straight line due to the disorder on the surface. These fluctuations are denoted by $h(x,t)$, and they satisfy the consistency relation

$$\overline{\langle h(x,t) - vt \rangle} = 0. \tag{4.15}$$

(The overline denotes a *time* average.) The capillary energy associated with small deformations of a CL was calculated by Joanny and de Gennes[17] (in the $\Theta \to 0$ limit) as

$$U_{\rm cap} = \frac{\gamma \Theta^2}{2} \int_0^{\frac{2\pi}{a}} \frac{dq}{2\pi} |q| |h(q)|^2 = \frac{\gamma \Theta^2}{4\pi} \int_{a<|x-x'|} dx\, dx' \, \frac{[h(x) - h(x')]^2}{(x-x')^2}, \tag{4.16}$$

where $h(q)$ is the fourier transform of the contact line profile at a given time, and a is the microscopic cutoff length scale mentioned earlier. The unusual q-dependence of the energy functional, and the resulting nonlocal dynamics, reflects the fact that perturbations of wave vector q on the CL induce deformations into the liquid-vapor interface up to a distance $|q|^{-1}$.

A random contribution to the liquid-surface energy comes from the defects[20],

$$U_{\rm rand} = \int_{-\infty}^{+\infty} dx \int_{-\infty}^{h(x)} dy \; f(x,y). \tag{4.17}$$

If the heterogeneity is strong enough, there is contact angle hysteresis[17, 20]. This arises from many metastable configurations of the CL profile, which are given by local minima of the free energy. The surface tensions γ_{SL}, γ_{SV} in Eq.(4.12) must then be interpreted as spatial averages *over the CL position.* Thus, the macroscopic contact angle will depend on the particular CL profile. If a macroscopic force of F per unit length is exerted on the CL, it will move with a finite velocity v only for $F > F_c$. This occurs when the metastable state with the largest Θ, usually called the *advancing angle* Θ_a[17, 20], becomes unstable. For small capillary numbers, the dynamical contact angle Θ is given by the force balance equation,

$$F - F_c = \gamma(\cos\Theta_a - \cos\Theta). \tag{4.18}$$

[1] If the source of disorder is the roughness of the solid surface, $f(x,y)$ is proportional to the local slope[20], thus we restrict our discussion to surfaces without long-range slope correlations. For a self-affinely rough surface, Δ may have a slow algebraic decay. Such situations will not be explored here.

As the CL slowly advances, energy is dissipated through various mechanisms[20]. If the dissipation in the vicinity of the CL dominates for small v, the drag force at a point x on the CL is simply related to the local velocity $\partial_t h(x,t)$ through a microscopic mobility μ. In this case, the equation of motion for the CL is obtained by equating the drag force to the applied force, $-\delta U/\delta h(x)$, as

$$\mu^{-1}\left(\frac{\partial h(x,t)}{\partial t}\right) = -\frac{\gamma\Theta^2}{\pi}\int\limits_{a<|x-x'|} dx' \frac{h(x,t)-h(x',t)}{(x-x')^2} + f[x,h(x,t)] + F. \qquad (4.19)$$

A recent experiment on depinning from a single defect [87] is in agreement with the deterministic ($f = 0$) form of this dynamics: Upon depinning from the defect, the time evolution of the CL profile is given by

$$h(x,t) \sim \ln\left(\frac{x^2+(ct)^2}{L^2}\right), \qquad (4.20)$$

where the width of the logarithmic profile increases linearly with a characteristic velocity $c = \gamma\Theta^2\mu$ after depinning. L is the macroscopic cutoff size imposed by gravity.

4.3 Scaling and RG

In this section, I present the computation of critical exponents associated with the quasi-static dynamics of a CL, described by Eq.(4.1). In many aspects, Eq.(4.1) is similar to the model analyzed by Narayan and Fisher using the formalism of Martin, Siggia, and Rose[11] (MSR), through an expansion around a mean field solution[56]. The RG treatment is essentially a simpler version of the presentation in Sections 3.4–3.6; with a single-component (scalar) fluctuation. The new ingredient is the additional consideration of nonlocal dynamics, by incorporating different long-range interactions in a systematic way. In general, one can consider an equation of motion generalized to a d-dimensional interface ($\mathbf{x} \in \Re^d$), with a two-point interaction that decays as $|\mathbf{x}|^{-(d+\sigma)}$:

$$\mu^{-1}\partial_t h(\mathbf{x},t) = \mathcal{K}_{d,\sigma}[h(\mathbf{x})] + f[\mathbf{x},h(\mathbf{x},t)] + F. \qquad (4.21)$$

In the above, the generalized interaction kernel $\mathcal{K}_{d,\sigma}[h(\mathbf{x})]$ is given in Fourier space as $\mathcal{K}_{d,\sigma}[h(\mathbf{q})] \sim -|q|^\sigma h[\mathbf{q}]$. For the CL, $d = \sigma = 1$ and Eq.(4.1) is recovered. For $\sigma = 2$, the equation describes an elastic interface studied by NSTL and NF.

There exist a number of scaling relations amongst the exponents which follow from underlying symmetries and non-renormalization conditions.

1. As mentioned earlier, the motion of the line close to the threshold is composed of jumps of segments of size ξ. Such jumps move the interface forward by ξ^ζ over a time period ξ^z. Thus the velocity behaves as,

$$v \sim \frac{\xi^\zeta}{\xi^z} \sim |F-F_c|^{\nu(z-\zeta)} \quad \Longrightarrow \quad \beta = \nu(z-\zeta). \qquad (4.22)$$

2. If the elastic couplings are linear, the response of the line to a *static* perturbation $\varepsilon(x)$ is obtained simply by considering

$$h_\varepsilon(\mathbf{x},t) = h(\mathbf{x},t) - \mathcal{K}_{d,\sigma}^{-1}[\varepsilon(\mathbf{x})], \tag{4.23}$$

where $\mathcal{K}_{d,\sigma}^{-1}$ is the inverse kernel. Since h_ε satisfies Eq.(4.21) subject to a force $F + \varepsilon(\mathbf{x}) + f(\mathbf{x}, h_\varepsilon)$, h satisfies the same equation with a force $F + f(\mathbf{x}, h - \mathcal{K}_{d,\sigma}^{-1}[\varepsilon(\mathbf{x})])$. As long as the statistical properties of the stochastic force are not modified by the above change in its argument, $\partial \langle h \rangle / \partial \varepsilon = 0$, and

$$\left\langle \frac{\partial h_\varepsilon(\mathbf{x})}{\partial \varepsilon(\mathbf{x})} \right\rangle = -\mathcal{K}_{d,\sigma}^{-1}, \quad \text{or} \quad \left\langle \frac{\partial r_\varepsilon(q)}{\partial \varepsilon(q)} \right\rangle = \frac{1}{|q|^\sigma}. \tag{4.24}$$

Since it controls the macroscopic response of the line, the kernel $\mathcal{K}_{d,\sigma}$ cannot change under RG scaling. From Eqs.(4.5) and (4.4), we can read off the scaling of $h(\mathbf{x})$, and the force δF, which using the above non-renormalization must be related by the exponent relation

$$\zeta + \frac{1}{\nu} = \sigma. \tag{4.25}$$

Note that this identity depends on the statistical invariance of noise under the transformation in Eq.(4.23). It is satisfied as long as the correlations $\langle f(\mathbf{x},h) f(\mathbf{x}',h') \rangle$ only depend on $h - h'$. In particular, the identity does not hold if these correlations also depend on the slope $\partial h / \partial x$.

3. A scaling argument related to the Imry–Ma estimate of the lower critical dimension of the random field Ising model, can be used to estimate the roughness exponent[88]. The elastic force on a segment of length ξ scales as $\xi^{\zeta-\sigma}$. If fluctuations in force are uncorrelated in space, they scale as $\xi^{-(\zeta+d)/2}$ over the area of an avalanche. Assuming that these two forces must be of the same order to initiate the avalanche leads to

$$\zeta = \frac{2\sigma - d}{3}. \tag{4.26}$$

This last argument is not as rigorous as the previous two. Nonetheless, all three exponent identities can be established within the RG framework. Thus the only undetermined exponent is the dynamic one, z. An outline of the RG treatment is given next.

Introducing an auxiliary field $\hat{h}(x,t)$, the MSR generating functional is,

$$\begin{aligned} Z &= \int [dh][d\hat{h}] \exp\left\{ i \int d^d\mathbf{x}\, dt\, \hat{h}(\mathbf{x},t) \mathcal{F}[h,f] \right\}, \\ \mathcal{F}[h,f] &= \mu^{-1} \partial_t h(\mathbf{x},t) - \mathcal{K}_{d,\sigma}[h(\mathbf{x})] - f[\mathbf{x}, h(\mathbf{x},t)] - F. \end{aligned} \tag{4.27}$$

Mean field (MF) theory is obtained by replacing the capillary forces on a portion of the CL with Hookean springs attached to the average position $\langle h(\mathbf{x},t) \rangle$ of the CL. Defining $h_{\rm MF} \equiv h - vt$, this gives

$$\mu^{-1} \left(\frac{dh_{\rm MF}}{dt} + v \right) = -k h_{\rm MF}(t) + f[vt + h_{\rm MF}(t)] + F, \tag{4.28}$$

independently for each $\mathbf{x}$, and identical to the mean field model analyzed by NF[50, 51]. $v(F)$ is determined by the self-consistency condition $\overline{\langle h_{\rm MF}\rangle} = 0$.

The MF solution depends on the type of irregularity: For smoothly varying $f(x,y)$, $\beta_{\rm MF} = 3/2$, whereas for "mesa" defects, i.e. cusped $f(x,y)$, $\beta_{\rm MF} = 1$ [50, 51, 89]. Some recent experiments on reasonably clean surfaces by Ström et al.[90] are in agreement with Eq.(4.3) for $\beta = 3/2$ in the low capillary number regime. Stokes *et al.*[91] measure an exponent $\beta \approx 2 - 2.5$ on a hysteretic surface, using a new technique of harmonic generation. Even though it is generally believed that the scaling relation in Eq.(4.3) holds[92], it is clear that the prefactor is nonuniversal, and various experiments to date have obtained widely varying v-F behaviors[93]. To our knowledge, there are no experiments so far that have systematically investigated strongly heterogenous surfaces with conclusive accuracy.

Following the treatment of NF[56], I use the mean field solution for cusped potentials, anticipating jumps with velocity of $O(1)$, in which case $\beta_{\rm MF} = 1$. After rescaling and averaging over impurity configurations, we arrive at a generating functional whose low-frequency form is

$$\begin{aligned}
\overline{Z} &= \int [dH][d\hat{H}] \exp(-S), \\
S &= \int d^d\mathbf{x}\, dt\, \left[F - F_{MF}(v)\right] \hat{H}(\mathbf{x},t) + \int \frac{d\omega}{2\pi} \frac{d^d\mathbf{q}}{(2\pi)^d} \hat{H}(-\mathbf{q},-\omega)(-i\omega + |\mathbf{q}|^\sigma) H(\mathbf{q},\omega) \\
&\quad - \frac{1}{2} \int d^d\mathbf{x}\, dt\, dt'\, \hat{H}(\mathbf{x},t)\hat{H}(\mathbf{x},t') C\left[vt - vt' + H(\mathbf{x},t) - H(\mathbf{x},t')\right]. \qquad (4.29)
\end{aligned}$$

In the above expressions, H and $\hat{H}$ are coarse-grained forms of h and $\hat{h}$, in the sense that response and correlation functions of h, $\hat{h}$ are the same as those of H, $\hat{H}$ at low frequencies. F is adjusted to satisfy the condition $\langle H \rangle = 0$. The function $C(v\tau)$ is initially the mean-field correlation function $\langle h_{MF}(t) h_{MF}(t+\tau)\rangle$.

Ignoring the H-dependent terms in the argument of C, the action becomes Gaussian, and is invariant under a scale transformation $x \to bx$, $t \to b^\sigma t$, $H \to b^{(2\sigma-d)/2} H$, $\hat{H} \to b^{-(d+2\sigma)/2}\hat{H}$, $F \to b^{-d/2}F$, and $v \to b^{-d/2}v$. Other terms in the action, of higher order in H and $\hat{H}$, that result from the expansion of C (and other terms not explicitly shown in Eq.(4.29)) decay away at large length and time scales if $d > d_c = 2\sigma$. For $d > d_c$, the interface is smooth ($\zeta_0 < 0$) at long length scales. The critical exponents for $d > d_c$ are given by $z_0 = \sigma$, $\beta_0 = 1$, $\nu_0 = 2/d$.

At $d = d_c$, the action S has an infinite number of marginal terms that can be rearranged as a Taylor series of the marginal function $C\left[vt - vt' + H(\mathbf{x},t) - H(\mathbf{x},t')\right]$, when $v \to 0$. The RG is carried out by integrating over a momentum shell and all frequencies, followed by a scale transformation $x \to bx$, $t \to b^z t$, $H \to b^\zeta H$, and $\hat{H} \to b^{\theta-d}\hat{H}$, where $b = e^\ell$. The correction terms appearing in the renormalization of $F - F_{MF}$ and $C(u)$ are exactly the same as in Ref.[56], with the exception of the form of the bare propagator, which is $(-i\omega + |q|^\sigma)^{-1}$ instead of $(-i\omega + q^2)^{-1}$. The nonrenormalization of F yields the scaling relation

$$\nu = 1/(z + \theta). \qquad (4.30)$$

The renormalization of C in $d = 2\sigma - \epsilon$ interface dimensions, computed to one-loop order, gives the recursion relation,

$$\frac{\partial C(u)}{\partial l} = [\epsilon + 2\theta + 2(z-\sigma)]C(u) + \zeta u \frac{dC(u)}{du} - K_{d,\sigma}\frac{d}{du}\left\{[C(u) - C(0)]\frac{dC(u)}{du}\right\}. \quad (4.31)$$

($K_{d,\sigma}$ is a constant that depends on the parameters in the problem.) NF showed that all higher order corrections contribute to the renormalization of C as total derivatives with respect to u, thus, integrating Eq.(4.31) at the fixed-point solution $\partial C^*/\partial l = 0$, together with Eqs.(4.25) and (4.30), gives $\zeta = \epsilon/3$ to all orders in ϵ, provided that $\int C^* \neq 0$. For the case of a CL ($d = 1$), this gives

$$\zeta = 1/3, \quad \text{and} \quad \nu = 3/2. \quad (4.32)$$

This value of the roughness exponent coincides with the Imry–Ma estimate (4.26) for the *equilibrium* roughness with random-field disorder. This is a consequence of the fact that $C(u)$ remains short-ranged upon renormalization, implying the absence of anomalous contributions to ζ. Note that the disorder- averaged action S involves temporal correlations C, instead of spatial correlations Δ. Therefore, the scaling of fluctuations, and critical exponents, are independent of the type of disorder (random-field or random-bond), as long as $\Delta(r)$ is short-ranged in space.[2] This is not true for interfaces in equilibrium, where random-field and random-bond disorder give different roughness exponents.

To calculate the dynamical exponent z, we need the fixed-point function C^*, which is obtained only to $O(\epsilon)$ from the above analysis. Furthermore, the calculation requires some knowledge of the high-frequency form of response and correlation functions, i.e., a low-frequency analysis of Eq.(4.29) is insufficient to describe scaling properties of the system. Nevertheless, NF calculate the exponent θ for the elastic interface to $O(\epsilon)$ as $\theta + \zeta = (\epsilon - \zeta)/3 + O(\epsilon^2)$.[3] The computation for general σ gives the same result, leading to

$$z = \sigma - 2\epsilon/9 + O(\epsilon^2), \quad (4.33)$$

$$\beta = 1 - 2\epsilon/9\sigma + O(\epsilon^2). \quad (4.34)$$

Thus, for the CL, $z \approx 7/9$ and $\beta \approx 2/3$.

Finally, NF carried their analysis further to speculate exponents *below* the threshold when the driving force is increased monotonically towards F_c[56]. In particular, they postulated an avalanche distribution

$$\text{Prob(width of avalanche} > \ell) \approx \frac{1}{\ell^\kappa}\hat{\rho}(\ell/\xi_-), \quad (4.35)$$

[2]See Section III of Ref.[56] for a detailed discussion about the effect of random field vs. random bond disorder on threshold critical dynamics.

[3]NSTL obtain the same results as NF to $O(\epsilon)$ by directly averaging the MSR generating function.

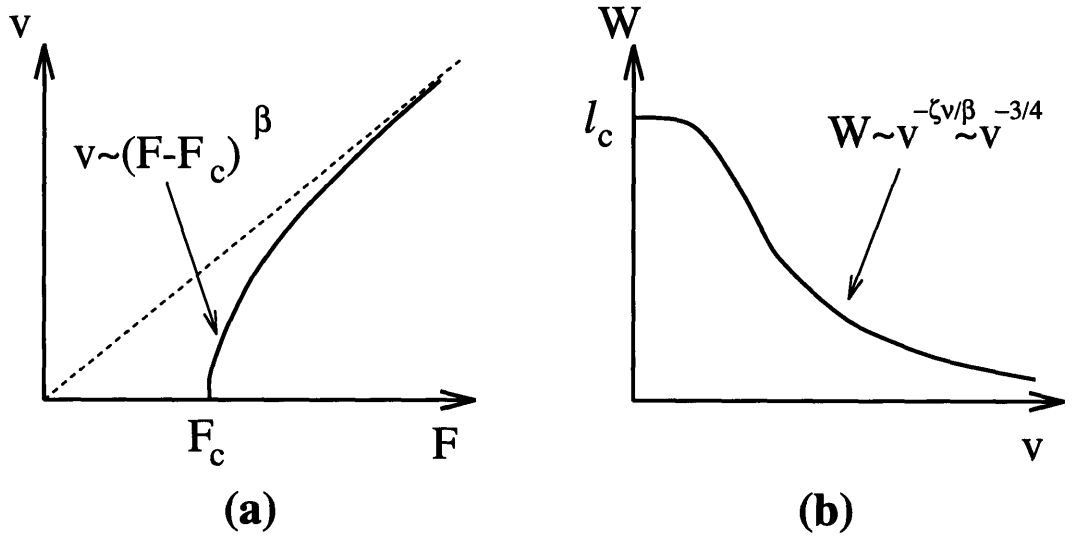

Figure 4-2: Predicted velocity-force behavior for a depinning contact line; $\beta = 7/9$ to first order in $\epsilon = 2 - d$.

with $\xi_- \sim (F_c - F)^{\nu_-}$, and the mean polarizability

$$\chi_\uparrow = \frac{d\langle \int h \rangle}{dF_\uparrow} \sim (F_c - F)^{-\gamma}. \tag{4.36}$$

If $\nu_- = \nu$, and the scaling hypothesis holds for the CL, it then follows that $\kappa = d - 1/\nu_-$, and $\gamma = 1 + \zeta\nu_-$. These exponents are then given exactly by $\gamma = \nu_- = 3/2$, and $\kappa = 1/3$ in $d = 1$.

4.4 Discussion and Conclusions

The calculated scaling exponents describe a CL advancing at low capillary number on a dirty surface, and also apply to surfaces with microscopic roughness, i.e. with short range slope-slope correlations. The roughness exponent of $\zeta = 1/3$, equal to its equilibrium value, can be directly measured by microscopic imaging of a slowly advancing CL. A number of macroscopic experimental tests are also possible: the velocity of the CL is given by by $v \sim (F - F_c)^\beta$ with $\beta < 1$ (See Fig. 4-2). The root mean square width of the CL profile should increase like $W \sim \xi^\zeta \sim v^{-\zeta\nu/\beta}$ as the threshold is approached. These relations can be checked through tensiometric measurements[93], where the capillary force on a solid immersed into a liquid is measured directly.

A dynamical exponent of $z < 1$ suggests that the relaxation of the CL is very different on a dirty surface. Upon depinning from a strong defect, the width of the logarithmic CL profile initially grows faster than linearly in time, in other words, with a characteristic velocity that increases with time: $c(t) \sim t^{(1-z)/z}$. This is, of course, not physical at arbitrarily large length and time scales. We have assumed that the liquid-vapor interface retains its equilibrium shape determined by the CL profile at all times. This picture will break down as characteristic velocities become comparable to

capillary wave velocity $c_{\text{cap}} = \sqrt{\gamma/\rho}$ of the liquid-vapor interface. The scaling regime in between should still be accessible to experiments in which the depinning from a single strong defect is observed on a dirty or rough surface.

In Chapter 3, it was mentioned that anisotropy in the disorder greatly influences the critical behavior of the elastic interface. Fortunately, for the case of the contact line (CL) ($\sigma = 1$), such anisotropies are irrelevant in the RG sense. However, there are other concerns related to the details of the driving force: In most experiments, the velocity of the CL is controlled rather than the external force. The effect of this can be numerically investigated by replacing the external force F in Eq.(4.1) with

$$F' = v - \langle f(x, h(x,t)) \rangle_x, \tag{4.37}$$

and looking at the time average of F' as a function of v, instead of the time average of v as a function of given F. ($\langle \cdots \rangle_x$ denotes an average over the length the interface but not over time. Thus, F' is chosen such that $\langle \partial_t h(x,t) \rangle = v$ at all times.) Even though the critical behavior for both ways of driving may be the same for an infinitely large system, there is a system size dependent region near the depinning threshold where the behavior changes drastically. Preliminary findings on an elastic line suggest that in this region, the velocity exponent β becomes considerably larger than one, in marked contrast with the constant force case, where $\beta \approx 1/3$. This can be qualitatively understood as follows: For a system of finite size, when a constant driving force is applied, the average velocity drops to zero as soon as temporal fluctuations of the instantaneous velocity are comparable with the time-averaged velocity. This is because the time average is then completely dominated by configurations for which the interface is pinned. Thus, the pinning transition becomes truly second order only in the large system limit: In a finite system, an arbitrarily small velocity cannot be sustained. In contrast, for constant velocity driving, each configuration has more or less similar statistical weight, since the interface is constrained to move past any obstacles by suitably increasing the applied external force, and decreasing it when passing through weakly pinning regions. Thus, in the region where a force-driven interface is pinned, the velocity-driven interface will experience fluctuations in the external force comparable to the average force itself. This average force as a function of velocity has an effective velocity exponent much larger than one. This distinction may partially explain the large velocity exponent found in recent CL experiments[91, 86], where the interface was velocity-driven. In addition to this, gravity imposes a finite wavelength cutoff on the roughening of the CL, which may complicate the analysis of experimental results. A proper choice of geometry may help reduce or eliminate this problem.

Chapter 5

Conclusion

Since Chapters 2-4 are written in a nearly self-contained way, there is not much else to be said about the particular points discussed in this thesis. Therefore, I will instead try to answer the question "So what?". The most difficult (and sometimes quite disturbing) inquiry directed to me, quite frequently by friends and acquaintances outside my immediate field of research, is: "So, Deniz, tell me what you're working on." This is a difficult task for most Ph.D. students, who are probably working on some obscure topic not known to all but a few select individuals in their field. Well, if you are working on statistical physics and the theory of critical phenomena, finding the right answer is REALLY tough. I rather like the general answer attempted in Section 1.6 of Binney *et al.*[7], a very nicely written book on the subject of critical phenomena and the renormalization group.

If I talked about how polymers coil, tried to explain superconductivity with the hope of finally getting to the flux lines just to describe their fluctuations, or gave a quick demonstration of the advancing contact line of the droplet on the glass, I would not be able to explain the true nature of my work, although all of these are interesting and stimulating topics. I am by no means an expert on polymers, type-II superconductors, or contact lines. The power and significance of the work presented in this thesis lies in its general applicability to a variety of nonequilibrium systems, including ones that are still poorly understood at the fundamental level. The aim is to obtain useful information about a system from basic knowledge of its symmetry properties, no matter how complex the inner workings are. Understanding the underlying mechanisms of generic scale invariance and critical phenomena at an abstract level is also extremely useful as a starting point for more detailed investigations of specific systems of interest, or as a different approach to already well established fields, such as polymer science. One stark example is the phenomenon of kinetic form birefringence discussed in Chapter 2, which has not been known to the field, but arises naturally from simple symmetry considerations. An experimental verification of this effect should prove to be quite interesting.

Bibliography

[1] Oxford English Dictionary, 2nd Edition.

[2] K. Huang, *Statistical Mechanics*, 2nd Ed., Wiley, New York (1987).

[3] E. Ising, Z. Phys. **31**, 253 (1925).

[4] K. Huang, *ibid.*, Chapter 16.

[5] S.-K. Ma, *Modern Theory of Critical Phenomena*, Frontiers in Physics series, Addison-Wesley, Redwood City (1976).

[6] See K. G. Wilson and J. Kogut, Phys. Rep. C **12**, 75 (1974), for a detailed review and original literature.

[7] J. J. Binney, N. J. Dowrick, A. J. Fisher, and M. E. J. Newman, *The Theory of Critical Phenomena: An Introduction to the Renormalization Group*, Oxford Univ. Press Inc., New York (1993).

[8] B. B. Mandelbrot, *The Fractal Geometry of Nature*, Freeman, San Francisco (1982).

[9] P. Bak, C. Tang, and K. Wiesenfeld, Phys. Rev. Lett. **59**, 381 (1987).

[10] P. C. Hohenberg and B. I. Halperin, Reviews of Modern Physics **49**, 435 (1977).

[11] P.C. Martin, E. Siggia, and H. Rose, Phys. Rev. A **8**, 423 (1973).

[12] M. Kardar, in *Disorder and Fracture*, edited by J.C. Charmet, S. Roux and E. Guyon, Plenum, New York (1990); T. Hwa and M. Kardar, Phys. Rev. A **45**, 7002 (1992).

[13] D. Forster, D.R. Nelson, and M.J. Stephen, Phys. Rev. A **16**, 732 (1977).

[14] J.-P. Bouchaud, E. Bouchaud, G. Lapasset, and J. Planès, Phys. Rev. Lett. **71**, 2240 (1993).

[15] A.-L. Barabasi, Phys. Rev. A **46**, R2977 (1992).

[16] For a recent overview on electrophoresis, see J.W. Jorgenson, in *New Directions in Electrophoretic Methods*, ACS Symposium Series **335**, American Chemical Society, Washington DC (1987).

[17] J.F. Joanny and P.G. de Gennes, J. Chem. Phys. **81**, 552 (1984).

[18] D. Ertaş and M. Kardar, Phys. Rev. E **48**, 1228 (1993).

[19] For an extensive review on polymer dynamics, see M. Doi and S.F. Edwards, *Theory of Polymer Dynamics*, Oxford Univ. Press (1986).

[20] P.G. de Gennes, *Scaling Concepts in Polymer Physics*, Cornell Univ. Press (1979).

[21] R.B. Bird, *Dynamics of Polymeric Liquids*, Vol. 1-2, Wiley, NY (1987).

[22] P.E. Rouse, J. Chem. Phys. **21**, 1272 (1953).

[23] J. Kirkwood and J. Risemann, J. Chem. Phys. **16**, 565 (1948).

[24] B.H. Zimm, J. Chem. Phys. **24**, 269 (1956).

[25] C.J. Farrell, A. Keller, M.J. Miles and D.P. Pope, Polymer **21**, 1292 (1980); M. Adam and M. Delsanti, Macromolecules **10**, 1229 (1977); G. Meyehoff, Z. Physik. Chem. **4**, 335 (1955); R. Mukherjea and P. Rempp, J. Chim. Phys. **56**, 94 (1959); Y. Tsunashima,N. Nemoto and M. Kurata, Macromolecules **16**,584, 1184 (1983).

[26] A. Peterlin, Pure Appl. Chem. **12**, 563 (1966); Adv. Macromol. Chem. **1**, 225 (1968); G.B. Thurston and A.Peterlin, J. Chem. Phys. **46**, 4881 (1967).

[27] P.G. de Gennes, J. Chem. Phys. **60**, 5030 (1974).

[28] See, e. g. R.E. Khayat and R.G. Cox, J. Fluid. Mech. **209**, 435 (1989); and references inside.

[29] E. Medina, T. Hwa, M. Kardar, and Y.-C. Zhang, Phys. Rev. A **39**, 3053 (1989).

[30] Y.-C. Zhang, J. Phys. (France) **51**, 2129 (1990).

[31] M. Kardar, G. Parisi, and Y.-C. Zhang, Phys. Rev. Lett. **56**, 889 (1986).

[32] T. Hwa, Phys. Rev. Lett. **69**, 1552 (1992).

[33] D. Wolf, Phys. Rev. Lett. **67**, 1783 (1991).

[34] J.M. Burgers, *The Nonlinear Diffusion Equation* (Riedel, Boston, 1974).

[35] M.A. Rubio, C.A. Edwards, A. Dougherty, and J.P Gollub, Phys. Rev. Lett. **63**, 1685 (1989).

[36] V.K. Horváth, F. Family, and T. Vicsek, Phys. Rev. Lett. **67**, 3207 (1991).

[37] T. Vicsek, M. Cserzö, and V.K. Horváth, Physica A **167**, 315 (1990).

[38] For other possible explanations, see ref.[30]; D. Kessler, H. Levine, and Y. Tu, Phys. Rev. A **43**, 4551 (1991).

[39] See, e.g. *Jordan Operator Algebras*, by H. Hanche-Olsen, Monographs and studies in mathematics v. 21, Pitman (1984).

[40] E. Medina, M. Kardar, Y. Shapir, and X.-R. Wang, Phys. Rev. Lett. **62**, 941 (1989); E. Medina and M. Kardar, Phys. Rev. B **46**, 9984 (1992).

[41] Similar manipulations for the KPZ equation have been discussed by Y.-C. Zhang, unpublished and private communications.

[42] U. Deker and F. Haake, Phys. Rev. A **11**, 2043 (1975).

[43] M. Schwartz and S.F. Edwards, Europhys. Lett. **20**, 301 (1992).

[44] J. P. Bouchaud and M. E. Cates, Phys. Rev. E **47**, R1455 (1993).

[45] J.G. Amar and F. Family, Phys. Rev. A **45**, 5378 (1992); B. Grossman, H. Guo and M. Grant, Phys. Rev. A **43**, 1727 (1991).

[46] R.E. Goldstein and D.M. Petrich, Phys. Rev. Lett. **67**, 3203 (1991); A. Moritan, F. Toigo, J. Koplik and J.R. Banavar, Phys. Rev. Lett. **69**, 3193 (1992).

[47] D. Ertaş and M. Kardar, Phys. Rev. Lett. **69**, 929 (1992).

[48] M. Kardar and D.R. Nelson, Phys. Rev. Lett. **58**, 2774 (1987); Phys. Rev. A **36**, 4020 (1987).

[49] M. O. Robbins, J. P. Stokes, and S. Bhattacharya, Phys. Rev. Lett. **55**, 2822 (1985).

[50] D.S. Fisher, Phys. Rev. B **31**, 1396 (1985).

[51] O. Narayan and D.S. Fisher, Phys. Rev. B **46**, 11 520 (1992).

[52] A.A. Middleton and D.S. Fisher, Phys. Rev. Lett. **66**, 92 (1991); Phys. Rev. B **47**, 3530 (1993).

[53] C.R. Myers and J.P. Sethna, Phys Rev. B **47**, 11 171 (1993); 11 194 (1993).

[54] R. Bruinsma and G. Aeppli, Phys. Rev. Lett. **52**, 1547 (1984).

[55] T. Nattermann, S. Stepanow, L.-H. Tang, and H. Leschhorn, J. Phys. II (France) **2**, 1483 (1992).

[56] O. Narayan and D.S. Fisher, Phys. Rev. B **48**, 7030 (1993).

[57] N. Martys, M. Cieplak, and M.O. Robbins, Phys. Rev. Lett. **66**, 1058 (1991); N. Martys, M.O. Robbins, and M. Cieplak, Phys. Rev. B **44**, 12294 (1991).

[58] S.V. Buldyrev, A.-L. Barabasi, S. Havlin, J. Kertesz, H.E. Stanley, and H.S. Xenias, Physica A **191**, 220 (1992); S.V. Buldyrev, A.-L. Barabasi, F. Caserta, S. Havlin, H.E. Stanley, and T. Vicsek, Phys. Rev. A **45**, R8313 (1992).

[59] H. Leschhorn, J. Phys. A, **25**, L555 (1992).

[60] D. Ertaş and M. Kardar, Phys. Rev. Lett. **73**, 1703 (1994).

[61] For example, see J. Luo *et al*, Phys. Rev. Lett. **68**, 690 (1992), and references inside.

[62] H. Sompolinsky and A. Zippelius, Phys. Rev. B **25**, 6860 (1982); A. Zippelius, Phys. Rev. B **29**, 2717 (1984).

[63] See, for example, Y. Enomoto, K. Katsumi, R. Kato, and S. Maekawa, Physica C **192**, 166 (1992).

[64] L.-H. Tang, M. Kardar, and D. Dhar, Phys. Rev. Lett. **74**, 920 (1995).

[65] See P. Ao and D.J. Thouless, Phys. Rev. Lett. **70**, 2158 (1993), and references inside.

[66] M. Tinkham, *Introduction to Superconductivity* (Mc Graw Hill, New York, 1975), p. 162.

[67] A. T. Dorsey, Phys. Rev. B **46**, 8376 (1992).

[68] C. Tang, S. Feng, and L. Golubovic, Phys. Rev. Lett. **72**, 1264 (1994).

[69] H. Leschhorn and L.-H. Tang, Phys. Rev. Lett. **70**, 2973 (1993).

[70] G. Parisi and L. Pietronero, Physica **A 179**, 16 (1991).

[71] M. Dong, M. C. Marchetti, A. A. Middleton, and V. Vinokur, Phys. Rev. Lett. **70**, 662 (1993). The identification of the exponent $\zeta = 1$ from correlation function has been questioned in Ref. [69].

[72] M.A. Rubio, C.A. Edwards, A. Dougherty, and J.P Gollub, Phys. Rev. Lett. **63**, 1685 (1989); V.K. Horváth, F. Family, and T. Vicsek, Phys. Rev. Lett. **67**, 3207 (1991); S. He, G. L. M. K. S. Kahanda, and P.-Z. Wong, Phys. Rev. Lett. **69**, 3731 (1992).

[73] S. V. Buldyrev, A.-L. Barabasi, F. Caserta, S. Havlin, H. E. Stanley, and T. Vicsek, Phys. Rev. A **45**, R8313 (1992).

[74] F. Family, K. C. B. Chan, and J. G. Amar, in *Surface Disordering: Growth, Roughening and Phase Transitions*, Les Houches Series, Nova Science Publishers, New York (1992).

[75] H. Leschhorn, Physica A **195**, 324 (1993).

[76] S. F. Edwards and D. R. Wilkinson, Proc. R. Soc. London A **381** 17 (1982).

[77] D. Ertaş and M. Kardar, Phys. Rev. E **49**, R2532 (1994).

[78] T. S. Lee *et al.*, Phys. Rev. Lett. **74**, 2796 (1995).

[79] S. J. Hagen *et al.*, Phys. Rev. B **47**, 1064 (1993).

[80] D. R. Nelson, Phys. Rev. Lett. **60**, 1973 (1988).

[81] S. Bhattacharya and M. J. Higgins, Phys. Rev. B **49**, 10 005 (1994).

[82] See Appendix B in Ref.[51].

[83] P.G. de Gennes, Rev. Mod. Phys. **57**, 827 (1985).

[84] D. Ertaş, work in progress.

[85] J. Schmittbuhl, S. Roux, J.-P. Vilotte, and K. J. Måløy, Phys. Rev. Lett. **74**, 1787 (1995).

[86] S. Kumar, D. H. Reich, and M. O. Robbins, presented at the 1995 March Meeting of the APS.

[87] J.A. Marsh and A.M. Cazabat, Phys. Rev. Lett. **71**, 2433 (1993).

[88] Y. Imry and S.-K. Ma, Phys. Rev. Lett. **35**, 1399 (1975).

[89] J.F. Joanny and M.O. Robbins, J. Chem. Phys. **92**, 3206 (1990).

[90] G. Ström, M. Fredriksson, P. Stenius, and B. Radoev, J. Colloid Interface Sci. **134**, 107 (1990).

[91] J.P. Stokes, M.J. Higgins, A.P. Kushnick, S. Bhattacharya, and M.O. Robbins, Phys. Rev. Lett. **65**, 1885 (1990).

[92] J.E. Seebergh and J.C. Berg, Chem. Eng. Sci. **47**, 4455 (1992). In their notation, $\beta = 1/B$.

[93] R.A. Hayes and J. Ralston, L. Colloid Interface Sci. **159**, 429 (1993).

About the Author

Mehmet Deniz Ertaş was born on February 4, 1969 in İzmir, Turkey. He attended Bornova Anadolu Lisesi and İzmir Fen Lisesi, graduating as valedictorian in 1986. The same year, he participated in the 17th International Physics Olympiad as a member of the Turkish team, and was awarded a Bronze Medal. He then went on to Bilkent University in Ankara, Turkey, and obtained a B.S. degree in Electrical and Electronics Engineering in 1990, along with a second major in Physics. Since then, he has been at the Massachusetts Institute of Technology as a graduate student in the Physics Department. He married Kim Louise Shively in 1993. He will be joining the Physics Department at Harvard University as a postdoctoral associate in the Fall of 1995.